International Journal of Hydrogen Energy 180 (2025) 151666

Contents lists available at ScienceDirect

International Journal of Hydrogen Energy

journal homepage: www.elsevier.com/locate/he

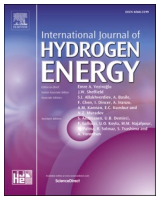

Hydrogen barrier coatings: Application and assessment

Ehsan Akbari-Kharaji [a,*], Majid Shafaie [b], Elizabeth Sackett [a], John Wood [c], Milos B. Djukic [d,**], Shirin Alexander [e]

[a] Faculty of Science and Engineering, Department of Materials Science and Engineering, Swansea University, Bay Campus, Fabian Way, Swansea, SA1 8EN, UK
[b] Department of Mechanical Engineering, Amirkabir University of Technology, Tehran, Iran
[c] AkzoNobel, Stoneygate Lane, Felling, Gateshead, NE10 0JY, UK
[d] University of Belgrade, Faculty of Mechanical Engineering, Kraljice Marije 16, Belgrade, 11120, Serbia
[e] Faculty of Science and Engineering, Department of Chemical Engineering, Swansea University, Bay Campus, Fabian Way, Swansea, SA1 8EN, UK

ARTICLE INFO

Keywords:
Hydrogen barrier coating
Hydrogen embrittlement
Hydrogen permeation
Polymer
Metal
Ceramic
Composite and multilayer

ABSTRACT

Hydrogen embrittlement (HE) threatens the structural integrity of industrial components exposed to hydrogen-rich environments. This review critically explores hydrogen barrier coatings (HBCs), polymeric, metallic, ceramic, and composite, their application and assessment, focusing on measured effectiveness in limiting hydrogen permeation and hydrogen embrittlement. Also, coating application methods and permeation assessment techniques are evaluated. Recent advances in nanostructured and hybrid coatings are emphasized, highlighting the pressing need for durable, scalable, and environmentally sustainable hydrogen barrier coatings to ensure the reliability of emerging hydrogen-based energy solutions. This comprehensive critical review further distinguishes itself by linking coating deposition methods to defect-driven transport behaviour, critically assessing permeation test approaches. It also highlights the emerging role of polymeric and hybrid multilayer coatings with direct implications for advanced and reliable hydrogen production, storage, and transport infrastructure.

1. Introduction

Hydrogen embrittlement (HE) is a formidable challenge across various industrial sectors, particularly in applications involving exposure to hydrogen-rich environments. This phenomenon significantly compromises the mechanical integrity of metals, leading to catastrophic failures. Its critical impact on material performance is acutely felt in high-pressure hydrogen storage systems, natural gas pipelines, and industries such as aerospace and automotive, where safety and reliability are paramount. Consequently, HE has been the focus of extensive research efforts [1–7].

The mechanisms governing hydrogen embrittlement (HE) are intricate and multifactorial, arising from the ingress of hydrogen into materials, which subsequently compromises their mechanical integrity. Several theories have been proposed to elucidate the interaction between hydrogen and material microstructures, including hydrogen-enhanced decohesion (HEDE), hydrogen-enhanced localized plasticity (HELP), and adsorption-induced dislocation emission (AIDE), among others [8–12]. These mechanisms often collectively and synergistically diminish the ductility and toughness of materials, heightening their HE-enhanced susceptibility to crack initiation and propagation [3]. High-strength steels and other high-strength alloys, in particular, are vulnerable to HE due to the diffusion of hydrogen atoms into their lattice structures, where they concentrate at dislocations and grain boundaries, significantly reducing fracture toughness [13–17]. These mechanisms have been widely investigated in the literature to interpret hydrogen-induced degradation phenomena; a detailed discussion falls beyond the scope of the present work and is therefore not elaborated here.

As the global transition towards hydrogen as a clean energy carrier accelerates, addressing HE has become increasingly critical. The hydrogen economy, aligned with initiatives like the UK's Climate Change Act 2008 and the goal of achieving net-zero emissions by 2050, aims to revolutionize energy storage and transportation [18–22]. However, the susceptibility of materials in hydrogen infrastructure to HE, including pipelines and storage tanks, poses significant safety and

* Corresponding author.
** Corresponding author.
E-mail addresses: ehsan.akbarikharaji@swansea.ac.uk (E. Akbari-Kharaji), mdjukic@mas.bg.ac.rs (M.B. Djukic).

https://doi.org/10.1016/j.ijhydene.2025.151666
Received 9 July 2025; Received in revised form 8 September 2025; Accepted 19 September 2025
Available online 30 September 2025

economic challenges. These challenges underscore the urgent need for the application of novel and effective HE mitigation strategies [19].

Efforts to combat HE encompass (i) material selection and altering material properties; (ii) microstructure design strategies; (iii) material design and processing optimization; (iv) environmental and stress control; and (v) limiting hydrogen ingress into material using various hydrogen barrier coatings (HBCs). The first four approaches (i)-(iv) are based on minimizing the HE susceptibility and its adverse effects on the mechanical properties, ductility, and fracture toughness of metallic materials after hydrogen infiltration into the metal. Despite ample research and enormous efforts in HE mitigation and investigation of various hydrogen-materials interactions, they are still not completely resolved, provoking HE and other hydrogen damages in most metallic materials. This is due to the extreme complexity and multifaceted nature of hydrogen-materials interactions, and still not completely resolved HE mechanisms and their synergy. Only the last approach, i.e., (v) application of HBCs using various surface engineering techniques, could completely prevent or significantly reduce the intake of hydrogen into metallic materials, thereby preventing hydrogen-materials interactions and HE [23–26]. Surface engineering techniques, particularly the application of protective hydrogen barrier coatings, so-called HBCs, have emerged as a pivotal strategy [23–26]. These coatings act as barriers to hydrogen permeation, effectively shielding the underlying substrate-metallic materials prone to HE. Among the available options, ceramic, polymeric, and metallic coatings have shown considerable potential [27–33].

Ceramic coatings, such as TiAlN and SiN, are celebrated for their high hardness, chemical stability, and low hydrogen permeability [13, 34–36]. However, other coatings, such as polymeric coatings, offer distinct advantages, including ease of application and cost-effectiveness. Notably, polymeric coatings remain relatively underexplored despite their promising hydrogen barrier properties, warranting further investigation [37–41]. The efficacy of these coatings depends on factors such as their thickness, adhesion, defect density, and deposition techniques like chemical vapour deposition (CVD) and physical vapour deposition (PVD) [42–46].

HBCs play a dual role in hydrogen infrastructure: they prevent HE while enhancing the durability and performance of components exposed to extreme conditions, such as high pressures and temperature fluctuations [47–49]. For example, automotive hydrogen storage tanks, designed to withstand pressures exceeding 700 bar and temperatures ranging from −40 °C to +100 °C, rely on these coatings to enable the safe use of high-strength steels [50].

Beyond traditional coatings, innovative materials and designs continue to emerge. Composite coatings, which integrate multiple materials, exhibit synergistic effects that enhance both mechanical and chemical resistance. Nanostructured coatings, characterized by their fine microstructure and high surface area, hold promise for achieving superior hydrogen barrier performance [51–56]. Despite these advancements, scalability and environmental considerations remain critical challenges. For instance, polymer coatings, while advantageous for their lightweight and versatile properties, raise concerns about long-term environmental impacts, including microplastic pollution and carbon emissions [57–61].

This paper provides a comprehensive review of current advancements in HBCs, with emphasis on their permeability characteristics, applied deposition techniques, and particularly the emerging role of polymer-based systems. This paper examines mechanisms of action, environmental implications, and the potential of coatings to transform hydrogen infrastructure by enabling safe and efficient operation of hydrogen technologies. Previous reviews have made valuable contributions by cataloguing barrier materials and summarising hydrogen embrittlement mechanisms; building on this foundation, this work develops a framework that links deposition techniques to the defect structures they generate and the resulting hydrogen transport behaviour. This review paper also critically assesses the strengths and limitations of gaseous and electrochemical permeation tests, highlighting the challenges of cross-comparison, and integrates the most recent advances in polymeric and hybrid multilayer coatings alongside metallic and ceramic systems. Through this approach, the review extracts design principles and research directions that are directly relevant to HBCs for pipelines, storage vessels, and the broader hydrogen economy.

2. Fundamentals of hydrogen embrittlement

Hydrogen embrittlement (HE) is a critical issue that arises when hydrogen atoms diffuse into metals and interact with either externally applied or internally generated residual stresses, leading to an irreversible significant reduction in metallic alloys' ductility and toughness, ultimately resulting in catastrophic failures [62,63]. This phenomenon is particularly problematic in high-strength alloys utilized across various critical industries. HE occurs when three critical factors, material susceptibility, stress, and environment, coincide [64–67], as illustrated in Fig. 1.

2.1. Types of hydrogen embrittlement

According to the literature, HE is generally categorized into two types: internal hydrogen embrittlement (IHE) and external hydrogen embrittlement (EHE) [68,69]. Many researchers compare results from IHE and EHE experimentally [70,71]. In the realm of experimental testing, internal hydrogen refers to specimens that have been precharged with hydrogen before testing, whereas external hydrogen involves testing specimens directly in a hydrogen gas environment. Typically, the susceptibility of materials to hydrogen-assisted fracture is assessed by evaluating their tensile ductility, such as elongation or reduction in area, under one or both of these conditions [70,71].

2.1.1. Internal hydrogen embrittlement (IHE)

Internal hydrogen embrittlement (IHE) occurs when hydrogen is introduced into the metal during manufacturing processes such as electroplating, welding, or forming. Pre-existing hydrogen atoms in the metal lattice tend to accumulate at internal defects such as dislocations and grain boundaries. This accumulation promotes the formation of localized plastic deformation zones, which subsequently facilitate the initiation and propagation of microcracks. The mechanism of IHE is

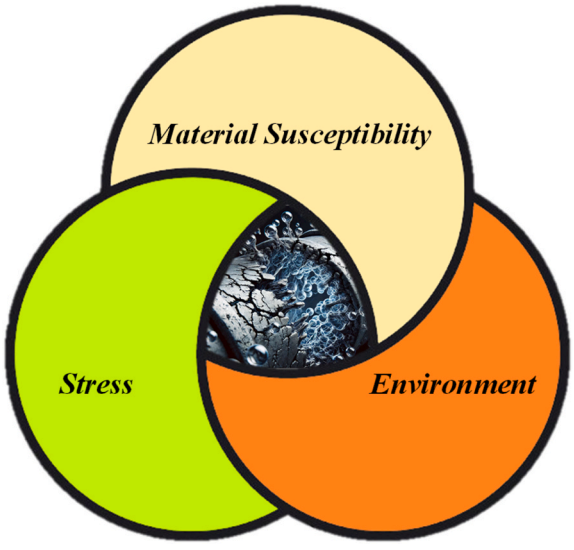

Fig. 1. Primary contributors to HE, illustrating the interplay between material susceptibility, applied or residual stress, and environmental exposure. HE commonly manifests at the intersection where all three factors coincide.

depicted in Fig. 2.

2.1.2. External hydrogen embrittlement (EHE)

External hydrogen embrittlement (EHE) takes place when hydrogen is absorbed from the external environment during service, such as in high-pressure hydrogen gas environments or acidic solutions. As shown in Fig. 3, unlike IHE, where hydrogen is already present in the material, EHE involves the ingress of hydrogen from the surrounding environment, which diffuses into the metal and leads to embrittlement.

The underlying mechanisms of HE are complex and multifaceted, primarily involving the interaction of hydrogen with the material's microstructure. Mitigating HE, whether internal or external, involves strategies aimed at reducing hydrogen ingress, controlling the environment, altering material properties, and employing surface engineering techniques.

2.2. Factors influencing hydrogen embrittlement

Hydrogen embrittlement is a multifaceted phenomenon driven by numerous factors that influence a material's vulnerability to degradation. Key factors include material properties, environmental conditions, and hydrogen concentration [1,8,64,72–78]. A thorough understanding of these factors is essential for developing effective mitigation strategies, especially for high-strength alloys that are more susceptible to HE [79,80].

2.2.1. Material properties

The intrinsic properties of materials, including their chemical composition, microstructure, mechanical characteristics, and surface condition, are critical in assessing their susceptibility to HE. The way hydrogen interacts with these material attributes greatly influences crack initiation and propagation, which can ultimately result in premature failure.

The chemical composition of a material, particularly the type and concentration of alloying elements, significantly influences its susceptibility to HE [81,82]. For instance, high-strength steels with high carbon content and low alloying elements are generally more prone to embrittlement due to the formation of brittle phases like martensite, which can trap hydrogen and facilitate crack initiation. Alloying elements such as chromium, nickel, and tungsten enhance resistance to HE by stabilizing the microstructure and reducing the solubility and diffusivity of hydrogen within the metal.

The microstructure of a material, including grain size, phase distribution, and the presence of precipitates or inclusions, is another critical factor that influences HE. Fine-grained structures, while generally improving mechanical strength, provide a higher density of grain boundaries, which serve as preferential sites for hydrogen segregation. This segregation can weaken grain boundaries, leading to intergranular cracking. Conversely, coarse-grained materials may exhibit reduced susceptibility to embrittlement due to the lower availability of grain boundary sites [83–85]. As shown by Khosravi et al. [86], this kinetic asymmetry leads to hydrogen accumulation at GBs, where detrapping is energetically less favourable. The presence of specific phases, such as martensite, bainite, or retained austenite, also affects a material's response to hydrogen. Martensitic structures, for example, are typically more susceptible to embrittlement due to their high dislocation density and tendency to trap hydrogen. In contrast, austenitic steels with stable austenite phases are generally more resistant to HE due to the reduced diffusivity of hydrogen in austenite [85,87–91].

Mechanical properties, including yield strength, tensile strength, and hardness, are strongly associated with a material's susceptibility to HE. While high-strength materials are valued for their mechanical performance, they are typically more prone to embrittlement because of their reduced ability to undergo plastic deformation. This susceptibility occurs because high-strength materials are more likely to experience strain localization, which can cause cracks to propagate quickly when hydrogen is present [15].

2.2.2. Surface condition

The condition of a material's surface, including its roughness, presence of coatings, and any surface treatments, plays a significant role in influencing hydrogen absorption and the subsequent risk of embrittlement [92]. Increased surface roughness can facilitate hydrogen entry by providing additional sites for adsorption and penetration into the metal lattice [93]. In contrast, coatings serve as protective barriers against hydrogen permeation, thereby shielding the underlying material from embrittlement. The effectiveness of these coatings is determined by factors such as their composition, thickness, and adhesion to the substrate.

2.2.3. Hydrogen concentration

The hydrogen concentration within a material plays a pivotal role in determining the severity of HE. The amount of hydrogen a material can absorb and retain depends on its solubility and diffusivity, which are affected by intrinsic material properties as well as environmental conditions [12,94].

2.2.4. Hydrogen solubility and diffusivity

Hydrogen solubility refers to the maximum amount of hydrogen that can dissolve in the metal matrix, while diffusivity describes the rate at

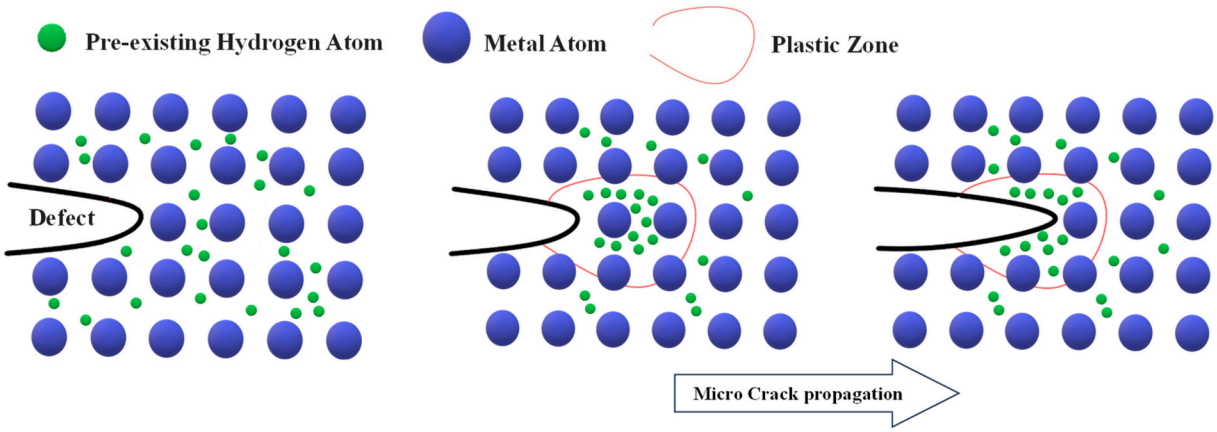

Fig. 2. Crack propagation in the presence of IHE, showing pre-existing hydrogen atoms (green) diffusion toward an initial defect, accumulating, weakening atomic bonds, promoting plastic zone development (red curved line), and accelerating micro-crack formation and crack propagation in the metal lattice (blue). (For interpretation of the references to colour in this figure legend, the reader is referred to the Web version of this article.)

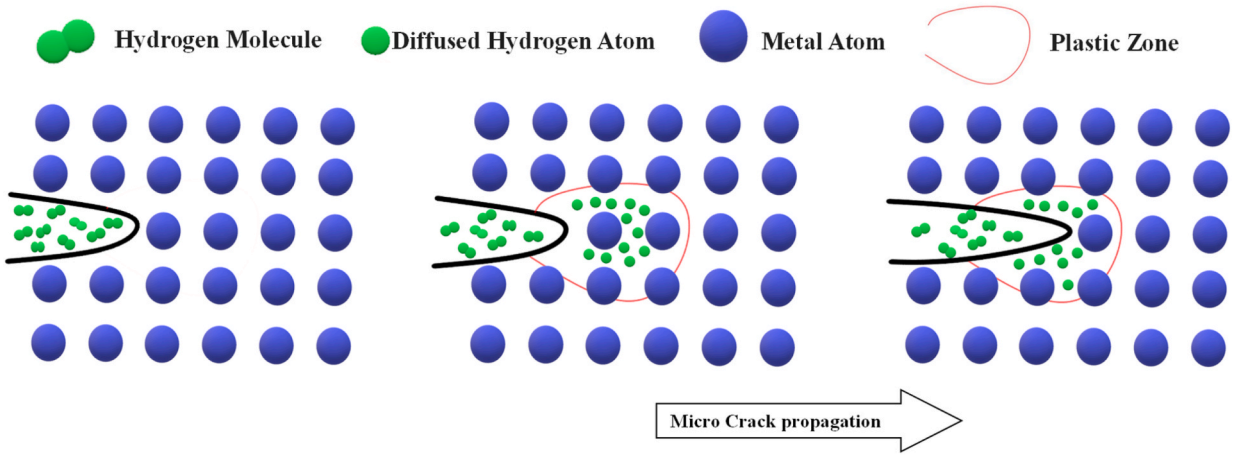

Fig. 3. Crack propagation in the presence of EHE, illustrating permeation of external hydrogen atoms (green) through initial surface defects, accumulating, weakening atomic bonds, promoting plastic zone development (red curved line), and accelerating micro-crack formation and crack propagation in the metal lattice (blue). (For interpretation of the references to colour in this figure legend, the reader is referred to the Web version of this article.)

which hydrogen atoms move through the lattice. Materials with high hydrogen solubility and diffusivity are generally more prone to embrittlement because they can absorb and transport larger amounts of hydrogen. The solubility and diffusivity of hydrogen are affected by various factors, including the alloy's composition, temperature, and the presence of microstructural traps such as dislocations, grain boundaries, and precipitates [8,95,96].

2.2.5. Hydrogen trapping

Hydrogen trapping refers to the capture of hydrogen atoms at specific locations within the material, such as dislocations, grain boundaries, or second-phase particles. Traps can either mitigate or exacerbate embrittlement, depending on their nature [97]. Beneficial traps immobilize hydrogen, preventing it from contributing to embrittlement processes, while detrimental traps accumulate hydrogen and promote localized embrittlement. The characteristics and distribution of these traps are crucial in determining a material's overall susceptibility to HE.

2.2.6. Environmental conditions

The surrounding environment has a critical impact on the HE process. Variables such as temperature, pressure, and the presence of corrosive species can modify the behavior of hydrogen within metals, thereby affecting the severity of embrittlement [20,27,98,99]. In addition, small quantities of certain gas species can either decrease, increase, or maintain the HE sensitivity at the same level [100–102].

2.2.6.1. Temperature. Temperature is a key factor that influences the solubility, diffusivity, and reactivity of hydrogen in metals. At lower temperatures, the mobility of hydrogen atoms decreases, leading to their accumulation at specific sites, such as dislocations or grain boundaries, which can increase the likelihood of crack initiation and propagation. Due to the higher diffusion barrier within grain boundaries compared to the bulk, hydrogen atoms exhibit slower mobility at these interfaces. Conversely, at higher temperatures, hydrogen atoms gain energy, enabling them to diffuse more rapidly. While this may reduce localized hydrogen concentrations, it can also elevate the risk of hydrogen attack and decarburization in steels [103–106]. Moreover, fluctuations in temperature can disrupt specific microstructural phases, resulting in the development of brittle phases like carbides or sigma phases. These brittle phases can serve as locations for hydrogen accumulation and the initiation of cracks.

2.2.6.2. Pressure. The partial pressure of hydrogen in the surrounding environment is a crucial factor influencing the degree of HE. In high-pressure settings, such as hydrogen storage and transportation systems, the driving force for hydrogen penetration into the material is significantly heightened. Higher hydrogen partial pressures lead to greater hydrogen dissolution in the metal, thereby intensifying the risk of embrittlement. This effect is particularly significant in applications involving high-pressure hydrogen gas, where pressures reach 700 bar [107–109].

2.2.6.3. Corrosive species. The presence of corrosive species, such as sulfides, chlorides, or acids, can exacerbate HE by promoting hydrogen entry into the metal [110,111]. These species can cause localized corrosion or pitting, which act as stress concentrators, facilitating hydrogen ingress. For instance, the presence of hydrogen sulfide (H_2S) in the environment can result in sulfide stress cracking (SSC), a form of HE marked by the development of brittle cracks under tensile stress and exposure to hydrogen sulfide.

2.3. Mitigation strategies

Various strategies can be implemented to reduce the impact of HE, such as applying protective coatings, utilizing specific alloying techniques, and managing environmental exposure. Coatings, including ceramic, metallic, and polymeric layers, act as barriers that prevent hydrogen from penetrating the material, thereby safeguarding the underlying metal from embrittlement. The incorporation of alloying elements can improve a material's resistance to HE by modifying its microstructure or forming stable hydrides that do not contribute to embrittlement [112,113].

Managing environmental exposure involves reducing potential sources of hydrogen, such as limiting the use of cathodic protection, avoiding acidic cleaning processes, and minimizing exposure to hydrogen-rich environments. Additionally, post-processing treatments can be used to remove hydrogen that has been absorbed into the metal lattice, thereby lowering the risk of embrittlement.

3. Permeability assessment

Evaluating permeability is likely to be highly important when studying HE. Insights into hydrogen diffusion within materials are key to assessing their vulnerability to embrittlement and guiding the development of protective coatings. On the steel surface, hydrogen molecules dissociate into atoms, which then diffuse through the steel.

When hydrogen penetrates a steel as atomic hydrogen (H) rather than as molecular hydrogen (H_2), its concentration within the metal (C_S)

adheres to Sieverts' Law, as described by Eq. (1) [114].

$$C_s = S_s\sqrt{p} \quad \text{Eq. 1}$$

Here, S_s denotes the solubility of hydrogen atoms in the steel, and p refers to the hydrogen molecule partial pressure at the measurement location. This law defines the correlation between the concentration of hydrogen dissolved in the metal and the square root of the hydrogen gas partial pressure. The hydrogen concentration in polymer film (C_f) is described by Eq. (2) [40].

$$C_f = S_f\, p \quad \text{Eq. 2}$$

Here, S_f represents the solubility coefficient of hydrogen within the polymer coating films. Unlike in steel, this law describes the relationship between the concentration of dissolved hydrogen in polymers and the hydrogen gas partial pressure, rather than its square root. It demonstrates that hydrogen solubility in polymers increases as the hydrogen gas pressure rises.

Understanding this principle is critical for analyzing hydrogen behavior in metallic materials, particularly in situations where HE or diffusion poses significant challenges.

On the other hand, the hydrogen permeability, $\mathcal{P}_f$ (through the material such as a polymer coating) is determined from the slope of the straight line $\left(\frac{dp}{dt}\right)$ measured once steady-state diffusion is achieved by Eq. (3).

$$\mathcal{P}_f = \frac{V_c d}{RTAp_h} \times \frac{dp}{dt} \quad \text{Eq. 3}$$

Where $\frac{dp}{dt}$ is the rate of pressure change during steady-state diffusion ($Pa{\cdot}s^{-1}$), V_c is the downstream chamber volume (m^3), d is the thickness of the film (m), T is the temperature of the test (K), p_h is the high gas pressure in the upstream (Pa), A equals to surface area of the specimen (m^2) and R is universal gas constant (8.314 J mol^{-1} K^{-1}).

The gas amount, q (mol), can be calculated by Eq. (4):

$$q = \frac{V_c \Delta p}{RT} \quad \text{Eq. 4}$$

where Δp represents the pressure difference in the downstream chamber measured over the duration of the test.

The diffusion coefficient D, is derived from the thickness (d) and the time lag, t', which corresponds to the point where the steady-state diffusion curve intersects the time axis shown in Fig. 4 and can be calculated by Eq. (5) [115].

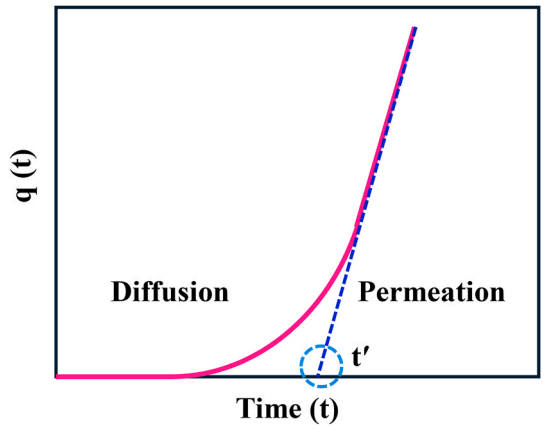

Fig. 4. Theoretical permeation curve, pink solid line, showing the total permeated amount (q) of gas over time and the time lag t′, where the extrapolated steady-state line, dashed blue line, intersects the time axis, used to determine the diffusion coefficient. (For interpretation of the references to colour in this figure legend, the reader is referred to the Web version of this article.)

The time-lag relation used here follows the classical one-dimensional Fickian diffusion for a homogeneous coating of thickness d with constant diffusivity D_f and Henry-law sorption, under a step change in upstream hydrogen pressure p_h and a perfect sink on the downstream side.

$$t' = \frac{d^2}{6D} \quad \text{Eq. 5}$$

Evaluating the permeability of coatings is a fundamental component in determining their performance, particularly in safeguarding against HE [25]. The main goal of permeability assessment is to evaluate how effectively a coating acts as a barrier to hydrogen diffusion. Preventing hydrogen penetration is critical in scenarios where hydrogen exposure could cause embrittlement and subsequent failure. This section covers the underlying principles, methodologies, and importance of permeability assessment in evaluating coating performance.

3.1. Principles of permeability assessment

Permeability assessment involves quantifying the rate at which hydrogen can pass through a coating under defined conditions. Key factors in this evaluation include hydrogen partial pressure, temperature, coating thickness, and any existing defects. A coating's permeability is influenced by its inherent material properties, such as hydrogen solubility and diffusivity, as well as its microstructural characteristics, including density and porosity. The permeability coefficient ($\mathcal{P}$) is a pivotal metric that quantifies hydrogen permeation [14].

Based on Fick's first law of diffusion, the hydrogen flux (J_S) passing through the steel sample can be determined using Eq. (6).

$$J_S = D_S\frac{dC_S}{dx} = D_S S_S \frac{\sqrt{p_o}\text{-}\sqrt{p_i}}{d_S} \quad \text{Eq. 6}$$

In this context, d_S denotes the thickness of the steel specimen, while p_o and p_i represent the hydrogen partial pressures on the high-pressure and low-pressure sides of the specimen, respectively. Hydrogen permeability through steel $\mathcal{P}_S$ ($mol.m^{-1}.s^{-1}.Pa^{-1/2}$) is expressed in Eq. (7) as the product of hydrogen solubility (S_S) and diffusivity (D_S) within the material.

$$\mathcal{P}_s = D_s S_s \quad \text{Eq. 7}$$

Hydrogen passes through polymer coatings as hydrogen molecules, and the hydrogen flux through the film (J_f) can be described by Eq. (8).

$$J_f = D_f\frac{dC_f}{dx} = D_f S_f \frac{p_o\text{-}p_i}{d_f} \quad \text{Eq. 8}$$

In this case, d_f represents the thickness of the polymer specimen, and p_o and p_i refer to the hydrogen partial pressures on the high-pressure and low-pressure sides, respectively. The hydrogen permeability through polymers $\mathcal{P}_f$ ($mol.m^{-1}.s^{-1}.Pa^{-1}$) is described by Eq. (9) as the product of the hydrogen solubility (S_f) and the diffusivity coefficient (D_f) within the coating material.

$$\mathcal{P}_f = D_f S_f \quad \text{Eq. 9}$$

A lower permeability coefficient indicates greater resistance to hydrogen permeation, enhancing the coating's effectiveness in preventing HE.

For a coated steel sample, the hydrogen flux must remain continuous across both the coating layer and the underlying steel. Since hydrogen exists as a diatomic species, the atomic flux corresponds to twice the molecular flux.

It should be noted that hydrogen transport in metals occurs as atomic hydrogen, with solubility proportional to the square root of pressure (Sieverts' law). As a result, permeability is conventionally reported in units of $mol.m^{-1}.s^{-1}.Pa^{-1/2}$. In polymeric films, hydrogen remains molecular and obeys Henry's law, giving permeability units of $mol.m^{-1}$.

$s^{-1}.Pa^{-1}$. A direct comparison of permeabilities between the two material classes is invalid, since one is governed by a linear pressure dependence, Eq. (8), while the other follows a square-root pressure dependence, Eq. (6). Meaningful comparison is only possible through the flux values (J_s and J_f) under identical upstream and downstream pressures, as expressed in Eq. (10) [40].

$$J_S = 2J_f \quad \text{Eq. 10}$$

3.2. Importance of permeability assessment

As mentioned, permeability assessment is critical for determining the effectiveness of coatings in preventing HE. The ability of the coating to block hydrogen ingress is vital in applications where hydrogen exposure could lead to catastrophic failures, such as in fuel cells and high-pressure hydrogen storage systems. By measuring the permeability coefficient, this assessment provides a quantitative evaluation of a coating's barrier properties, facilitating the selection and optimization of coatings for specific uses.

Moreover, permeability assessment is instrumental in detecting potential defects or weaknesses within the coating that could compromise its performance. Defects such as pinholes, cracks, and porosity can significantly increase a coating's permeability, diminishing its effectiveness in preventing hydrogen diffusion. Detecting and addressing these defects is crucial for maintaining the long-term durability and reliability of coatings in demanding environments.

3.3. Methods of permeability assessment

Various methods are employed to evaluate coating permeability, each with specific advantages and limitations. The method selection is influenced by factors such as the coating material, thickness, and application requirements. Common methods for permeability assessment include physical hydrogen permeation [30,116] and electrochemical hydrogen permeation setups (i-iii), see also Table 1:

i. Physical hydrogen gas permeation test using mass spectrometry

The hydrogen permeation test is a commonly employed method for evaluating the permeability of coatings. In this procedure, one side of the coated sample is exposed to a hydrogen-rich environment, while the opposite side is monitored for hydrogen permeation. As illustrated in Fig. 5, hydrogen detection is typically carried out using techniques such as mass spectrometry or electrochemical sensors. The hydrogen permeation rate is measured over time, and the permeability coefficient is calculated based on the steady-state hydrogen flux through the coating.

ii. Physical hydrogen gas permeation test using pressure gauges

The gas diffusion cell method involves the use of a sealed cell containing a hydrogen gas atmosphere, with the coated sample serving as a barrier between the hydrogen source and a detection chamber. As depicted in Fig. 6, by monitoring the pressure or hydrogen concentration in the detection chamber over time, the hydrogen diffusion rate through the coating can be assessed. This technique is particularly well-suited for high-temperature environments where exposure to hydrogen gas is a significant concern.

iii. Electrochemical hydrogen permeation test

Known as the Devanathan-Stachurski method [116], Fig. 7, the electrochemical permeation test involves a dual-cell arrangement with the coated sample serving as a membrane. Hydrogen is generated electrochemically in one cell and permeates through the coating. The permeated hydrogen is detected and oxidized in the second cell, producing a current proportional to the amount of hydrogen that has passed through the coating. This current allows for the calculation of the permeability coefficient.

Table 1 summarizes the main experimental techniques employed to evaluate hydrogen permeation through materials.

3.4. Challenges and future perspectives in permeability testing

While permeability testing is crucial for evaluating coatings, several challenges persist in obtaining accurate measurements and interpreting permeability data. A significant challenge lies in the sensitivity of current measurement techniques, especially for coatings with very low permeability.

To overcome this, researchers are deploying quadrupole online mass spectrometry to capture real-time H_2 crossover and mixed-gas time-lag in polymer films [119,120], and electrochemical hydrogen probes, notably amperometric double-electrolyte sensors and solid-state potentiometric sensors, for in-situ hydrogen permeation monitoring [121, 122].

Environmental factors, including temperature and pressure, also pose challenges, as they can significantly influence a coating's

Table 1
Comparison of hydrogen permeation measurement techniques.

Technique	Principle	Advantages	Limitations
Physical hydrogen gas permeation test using mass spectrometry	Hydrogen permeating through a permeable sample is detected in a vacuum chamber by mass spectrometry	- Highest sensitivity among gas-based methods - Quantitative permeability measurement - Applicable to ultra-low-permeability barriers	- Requires high-vacuum systems and complex calibration - High cost and limited accessibility - Thin-film leakage/sealing problems reduce reproducibility
Physical hydrogen gas permeation test using pressure gauge/detection cell	Hydrogen is applied at pressure on one side of a permeable sample; downstream accumulation/ pressure rise is measured	- Established for polymers and films (ASTM D1434, ISO 15105 [117]), though not hydrogen-specific - Applicable across a wide range of pressures and temperatures - Straightforward permeability and diffusion evaluation via time-lag analysis	- Hydrogen-specific standards absent - Lower sensitivity than mass spectrometry - Long test times for low-permeability samples - Thin-film sealing issues
Electrochemical permeation test (Devanathan–Stachurski method)	Hydrogen generated electrochemically on the charging side permeates through the specimen and is oxidized on the detection side	- Standardized by ASTM G148–97 [118] for metals to have reproducible and comparable results - Widely validated for metallic substrates - Enables real-time, in-situ monitoring - Low equipment cost - Can distinguish reversible vs. irreversible traps	- Requires conductive substrates - Signal influenced by traps, oxides, and charging efficiency - Not directly applicable to non-porous/non-conductive samples like polymers

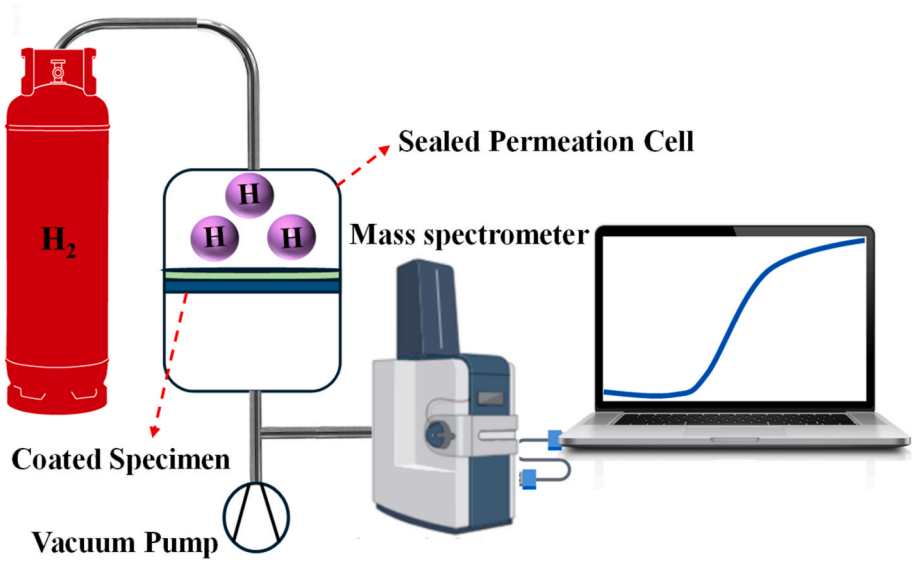

Fig. 5. Schematic of hydrogen gas (purple spheres) permeation test using mass spectrometry, where hydrogen passes through a coated specimen (green layer) and is detected on the vacuum side to determine permeability. (For interpretation of the references to colour in this figure legend, the reader is referred to the Web version of this article.)

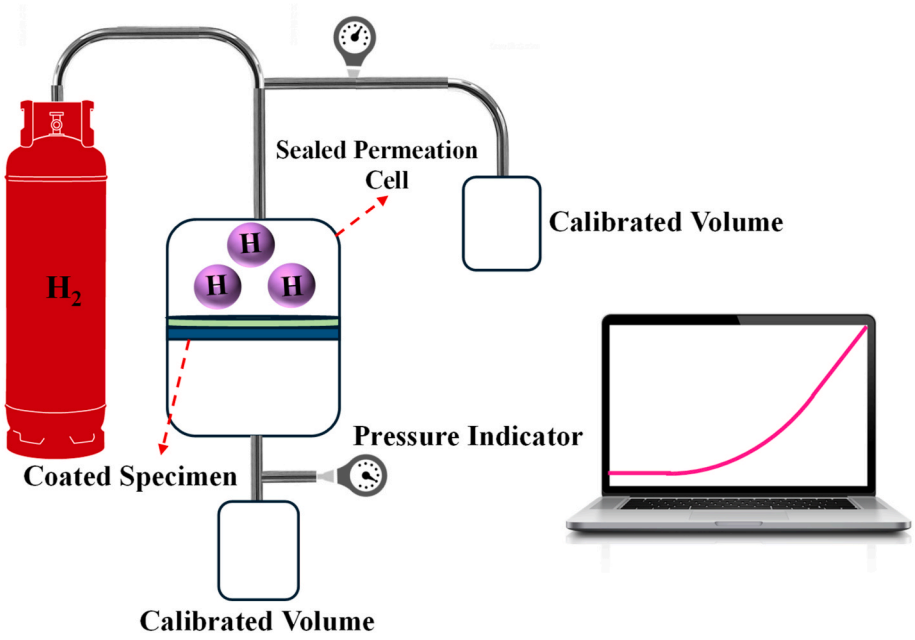

Fig. 6. Schematic of hydrogen gas (purple spheres) permeation setup using pressure gauges, where hydrogen passes through a coated specimen (green layer) in a sealed cell, and the resulting pressure change in the detection chamber is monitored to evaluate permeability. (For interpretation of the references to colour in this figure legend, the reader is referred to the Web version of this article.)

permeability. Variations in these conditions can lead to considerable changes in permeability, necessitating testing under conditions that closely mimic actual operating environments. Furthermore, the presence of multiple gases or impurities during testing can complicate data interpretation, making it necessary to employ advanced analytical methods to differentiate between various permeating species.

Future directions in permeability testing focus on creating standardized testing protocols and developing advanced analytical methods to enhance the precision and reliability of permeability measurements. The development of in-situ monitoring techniques, such as real-time electrochemical sensors and non-destructive evaluation methods, shows great potential for assessing coating permeability during operation. These advancements will offer valuable insights into coating performance in practical applications, paving the way for more effective protective solutions against HE.

In summary, permeability testing is essential for evaluating the protective performance of coatings against hydrogen embrittlement (HE). Accurate measurement and quantification of hydrogen permeation through both bare and coated materials are critical for ensuring the long-term safety and reliability of components exposed to hydrogen-rich environments. Notably, techniques capable of reliably assessing hydrogen permeability under gaseous conditions, rather than solely electrochemical methods, are particularly valuable, especially when integrated with mechanical evaluation approaches. As technological capabilities advance, the development of highly sensitive and robust testing methodologies will be pivotal in optimizing next-generation

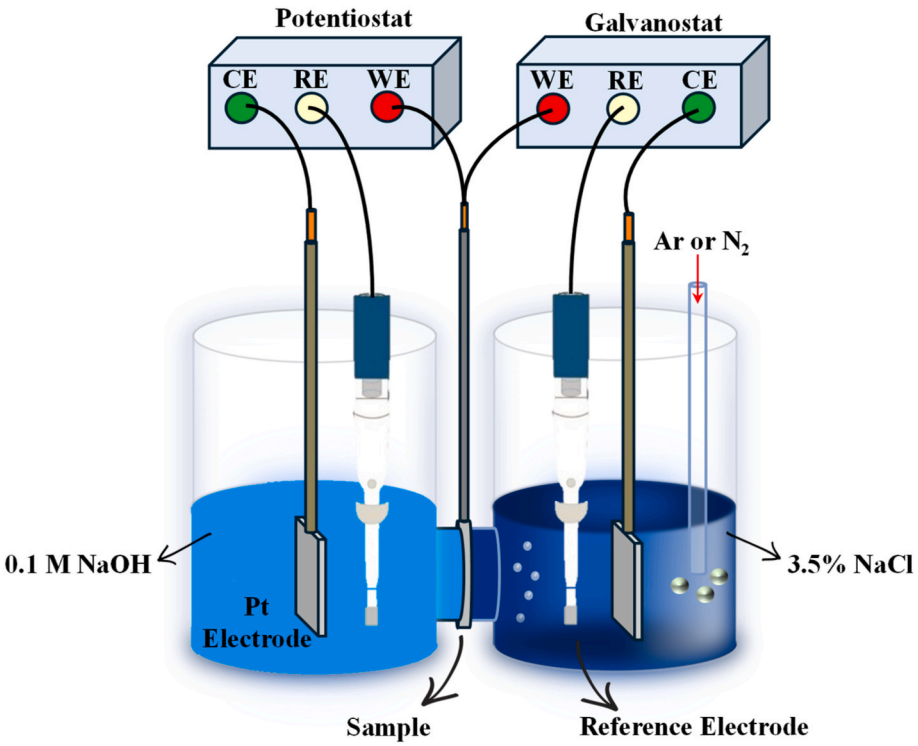

Fig. 7. Experimental setup for measuring hydrogen permeability using the Devanathan-Stachurski method where hydrogen is generated on the charging side (NaCl solution) and diffuses through the metallic sample, where it is detected on the opposite side (NaOH solution) via oxidation current measured by a potentiostat connected to the working (WE), counter (CE), and reference (RE) electrodes.

hydrogen barrier coatings across a broad spectrum of industrial applications.

4. Coating methods

Numerous techniques are available for the application of HBCs. In this section, we briefly introduce several methods employed to inhibit hydrogen permeation, along with the underlying principles of their operation. A more detailed discussion of the materials compatible with each technique is provided in the following section, as the suitability of a given method often depends on the nature of the coating material.

4.1. Physical vapour deposition (PVD)

Physical vapour deposition (PVD) encompasses a suite of vacuum-based techniques, including magnetron sputtering, evapouration, arc vapour deposition, and electron beam deposition, each tailored for specific substrate geometries and coating compositions. These methods operate by vaporizing a solid target in a low-pressure environment, followed by condensation onto the substrate to form dense, uniform films. The vacuum atmosphere minimizes contamination and enables high-purity coatings with nanometre-scale precision [123].

Among PVD methods, magnetron sputtering has emerged as a particularly advantageous technique for hydrogen prevention applications due to its ability to produce dense, defect-minimized films through energetic ion bombardment. This bombardment not only enhances adhesion but also refines grain structure, which in turn improves resistance to hydrogen diffusion and mechanical degradation [124]. One of the critical attributes of PVD coatings lies in their microstructural compactness, which impedes hydrogen ingress.

Despite their effectiveness, PVD coatings are not without limitations. Their application is often restricted to line-of-sight geometries, making uniform deposition on complex components or internal surfaces difficult [125,126]. Knowledge gaps persist in understanding the long-term degradation mechanisms of PVD coatings in operational hydrogen-rich environments. There is a need for systematic studies on crack initiation, grain boundary hydrogen diffusion pathways, and the role of interface integrity under cyclic loading and elevated temperatures.

As schematically illustrated in Fig. 8, a solid target material is vaporized via sputtering in a high-vacuum chamber and transported through an inert gas atmosphere to form a uniform thin film on an electrically conductive substrate [127,128].

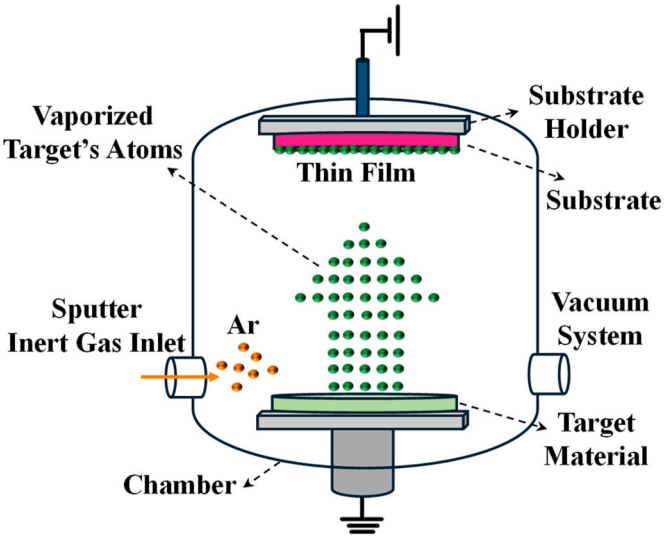

Fig. 8. Schematic illustration of the PVD process, including vapour generation, transport, and condensation onto the substrate to form thin films.

4.2. Chemical vapour deposition (CVD)

Chemical vapour deposition (CVD) is a technique where thin layers are produced through chemical reactions of vapour-phase precursors at the surface of a substrate. The process generally unfolds through four main stages: initially, reactive gases are delivered close to the substrate; next, these species attach to the surface; this is followed by surface-driven chemical transformations that lead to material deposition; and finally, volatile byproducts are released and evacuated from the surface region [129]. Unlike PVD, CVD enables the formation of conformal, pinhole-free films over complex geometries, making it a promising strategy for hydrogen barrier applications, particularly in environments where uniform coverage is critical, such as internal piping.

One of CVD's limitations lies in the high processing temperatures, which may exceed 800–1000 °C [130,131]. This restricts CVD application on thermally sensitive alloys or materials that experience phase transformation or property degradation at elevated temperatures. High vacuum CVD (HVCVD), metal-organic CVD (MOCVD), and plasma-enhanced CVD (PECVD) have emerged as alternatives to lower the thermal budget, although they often compromise film crystallinity or require more complex precursor chemistry [132].

CVD, as shown in Fig. 9, ensures precise control over thickness and microstructure, yielding high-purity coatings. The resultant films are particularly efficient in mitigating HE by reducing hydrogen ingress and enhancing surface hardness, thereby reducing microcrack propagation [133].

4.3. Thermal spraying

Thermal spraying involves propelling molten or partially molten particles at high velocity onto a substrate to form a coating layer. A broad range of materials, such as metals, ceramics, composites, and alloys, can be applied using thermal spray methods. While this method is effective in providing protective coatings, the rough finish can sometimes hinder the flow efficiency in certain applications [134,135]. The primary mechanism underlying the enhanced performance of thermally sprayed films subjected to ultra-rapid cooling is attributed to their lower defect density compared to conventionally sprayed coatings, combined with the barrier effect of passivation layers and their capacity to trap hydrogen [136].

Techniques such as plasma spraying and high-velocity oxygen fuel (HVOF) spraying are notable for producing coatings with excellent thermal and mechanical properties [97,137]. Fig. 10 depicts the thermal spray coating process schematically.

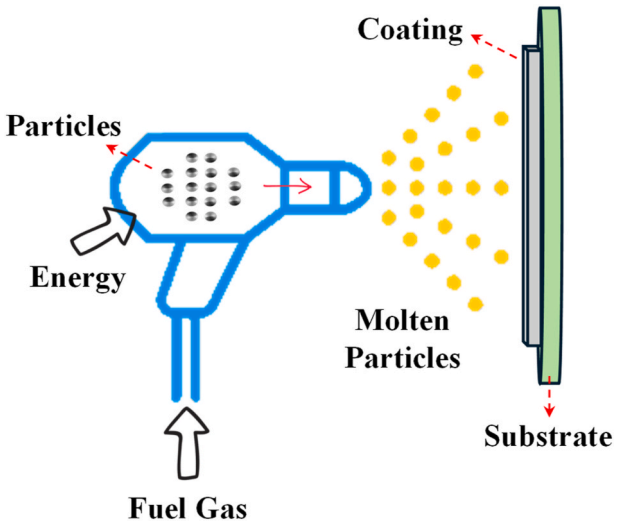

Fig. 10. Schematic representation of the thermal spray coating process, where molten or semi-molten particles are propelled onto a substrate using thermal energy and fuel gas.

4.4. Sol-gel processing

The sol-gel technique offers a low-temperature, solution-based route for fabricating ceramic coatings with tailored composition and microstructure. It involves the hydrolysis and condensation of metal alkoxide or inorganic salts to form a gel, which is then deposited and thermally treated to yield an oxide layer. While often regarded as cost-effective and chemically versatile, the sol-gel method faces several limitations in the context of hydrogen permeation resistance. This method often requires long processing times, and the coexistence of alcohol salts and water in precursor solutions can lead to shrinkage or cracking during drying and heat treatment [138]. Such defects compromise the coating's integrity and facilitate hydrogen ingress. In addition, researchers emphasize that a critical issue with sol-gel-derived coatings has been their poor adhesion to the metal surface, likely due to interfering oxide layers [139]. These inherent drawbacks highlight the need for careful optimization of processing parameters and substrate preparation when considering sol–gel coatings as hydrogen permeation barriers.

Sol-gel processing, as shown in Fig. 11, involves forming ceramic coatings from colloidal solutions through a chemical approach. This method enables the customization of coatings such as aluminum oxide (Al_2O_3), erbium oxide (Er_2O_3), and silicon dioxide (SiO_2), tailored for specific wear and corrosion resistance applications [140–143]. The

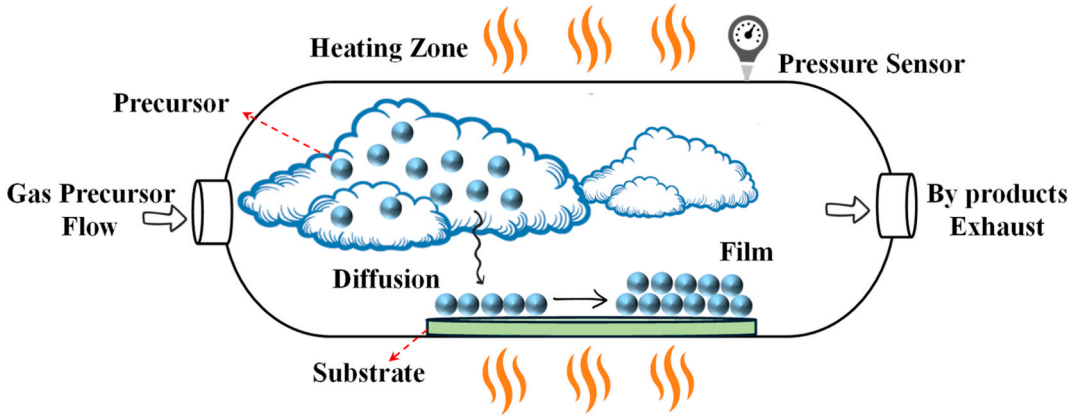

Fig. 9. Schematic of the CVD process, where vapour-phase precursors react on a heated substrate surface to form a thin film. The process involves precursor delivery, surface adsorption, chemical transformation, and byproduct removal, enabling precise control over film composition and thickness.

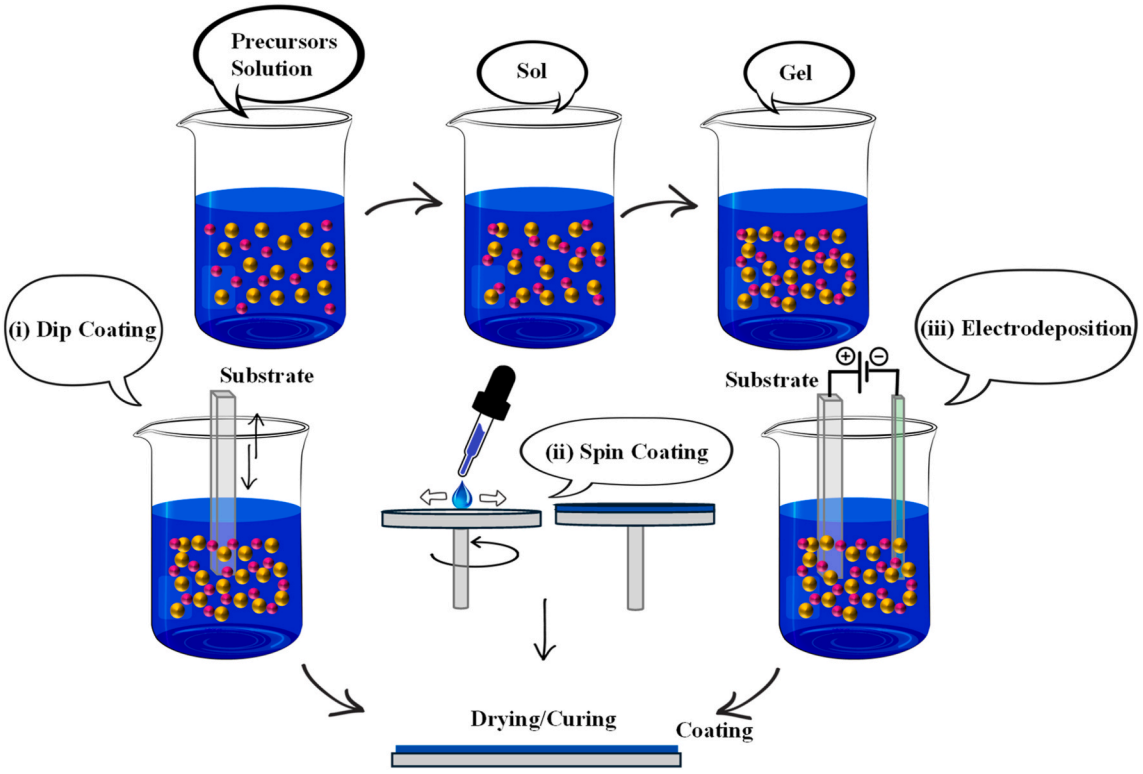

Fig. 11. Schematic of the sol-gel process for thin film coating, showing the transformation from precursor solution to sol-gel, followed by application via (i) dip coating, (ii) spin coating, or (iii) electrodeposition, and final drying/curing to form the coating.

resulting films provide dense barriers against hydrogen diffusion, improving overall performance under aggressive environments [138, 144].

4.5. Pack cementation

Pack cementation is a diffusion-based technique in which aluminides and chromides are deposited onto metal substrates. This process is carried out through a three-phase mechanism. First, volatile metal halides are produced by the reaction between a halogen-rich gas and a solid activator, and these halide vapors migrate to the substrate surface, where they undergo a chemical exchange to release reactive metal atoms. In the second phase, these atoms interact with the substrate and diffuse together, initiating the formation of a new alloy zone. Finally, a subsequent thermal treatment promotes the growth of the protective coating on top of this alloyed surface.

This method is advantageous for creating continuous and adherent protective layers, although the process can be time-consuming for complex geometries. Fig. 12 illustrates the process of pack cementation schematically.

4.6. Atomic layer deposition (ALD)

Atomic layer deposition (ALD) relies on the successive and separated introduction of two or more chemical vapours into a low-pressure environment (typically below 1 Torr). Each vapour interacts with the surface in a self-limiting reaction, meaning it only reacts with available functional groups until saturation is reached, typically depositing a submonolayer or monolayer. After each precursor exposure, inert gases such as nitrogen or argon flush the chamber to eliminate residual reactants and by-products. The subsequent reactant is then introduced, reacting with the surface species left from the first step. Repeating these

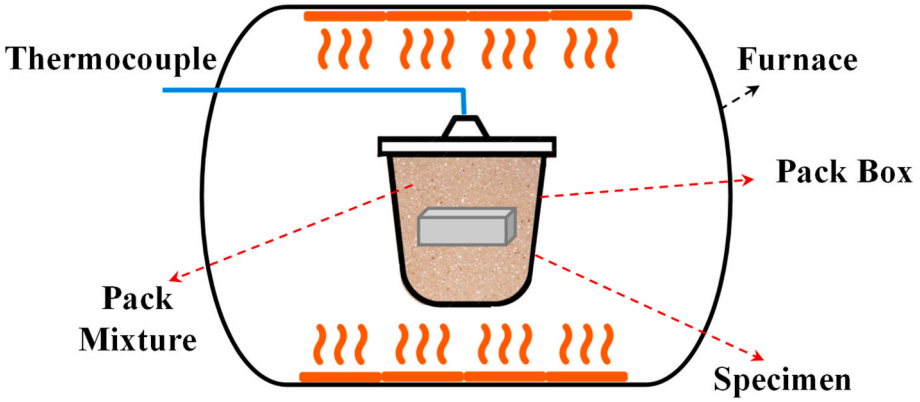

Fig. 12. Schematic representing the pack cementation process, where a specimen is embedded in a reactive powder mixture and heated in a furnace to form a layer on the sample surface through vapour-phase diffusion.

cycles builds up material layer by layer, allowing atomic-scale control over thickness and composition. ALD processes are usually carried out at moderately low temperatures, commonly under 350 °C, which makes them suitable for temperature-sensitive substrates [145].

This method has emerged as one of the most promising techniques for engineering hydrogen-resistant ceramic coatings due to its unique ability to produce ultrathin, conformal, and pinhole-free films with sub-nanometre thickness control. Unlike CVD or PVD, ALD relies on sequential, self-limiting surface reactions that ensure layer-by-layer growth with exceptional uniformity, even on high-aspect-ratio or complex geometries [146,147].

However, ALD is not without limitations. The main drawback is the slow deposition rate, which limits scalability for thick coatings. While this is acceptable for nanocoatings or precision applications, it poses challenges for industrial adoption in structural components. Additionally, the availability and cost of reactants and the equipment, especially for advanced nitrides or hybrid oxides, remain a barrier for widespread use [146].

Another concern is substrate compatibility. Despite ALD's conformality, adhesion issues can arise due to thermal expansion mismatch or inadequate surface activation. Pre-treatment strategies (e.g., plasma activation or seed layers) and applying a transition layer with a compatible thermal expansion coefficient are often necessary to ensure durable bonding, particularly when applying ALD coatings to non-oxide substrates [148]. Fig. 13 shows the illustration of the ALD process schematically.

4.7. Hot dipping

In hot-dip coating, the steel is immersed in a bath of molten zinc or aluminum, forming a protective coating on its surface [149]. Numerous investigations have explored the application of hot-dip coatings as an effective strategy to mitigate hydrogen and hydrogen isotope permeation through structural materials.

A detailed study on hot-dip aluminizing as a hydrogen isotope permeation barrier revealed that the permeation rate through bare MANET II steel could be reduced by factors of approximately 260 at 743 K and 1000 at 573 K. Despite the strong adhesion of the aluminized coating to the substrate, the comparable activation energies between coated and uncoated samples suggest that the permeation suppression arises primarily from a reduction in the effective permeation area, rather than the formation of a dense, continuous alumina barrier layer. This highlights the importance of microstructural features and intermetallic phase distribution in influencing permeation performance [150].

In another study by Zhang et al. [151], the hydrogen permeation behavior of hot-dip galvanized steel exposed to simulated marine environments was studied using a modified Devanathan–Stachurski cell, revealing a strong dependence on environmental conditions and coating integrity. The permeation current density and accumulated hydrogen content increased markedly with rising temperature and humidity, indicating enhanced hydrogen ingress under moist atmospheric exposure. Furthermore, the presence of coating defects intensified hydrogen absorption due to the cathodic protection effect provided by the surrounding zinc, which promotes electrochemical reactions on the exposed steel surface.

4.8. Dip coating

Dip coating is a commonly employed method for producing thin, uniform coatings, even on substrates with complex geometry. In this technique, as shown in Fig. 14, the substrate is immersed in a polymer solution and withdrawn at a controlled rate, allowing a uniform film to form as the solvent evaporates. The thickness of the coating can be precisely controlled by adjusting parameters such as withdrawal speed, solution viscosity, and polymer concentration. Dip coating is particularly advantageous for applications where gas barrier performance is critical, such as protective coatings for electronic components and packaging materials [152].

4.9. Casting and curing

This is another widely used method, especially for producing thick, robust films. In this process, a polymer solution is poured onto a substrate, spread to achieve the desired thickness, and subsequently cured by solvent evaporation or thermal treatment. Additives such as fillers, plasticizers, and crosslinking agents can be incorporated during the casting process to enhance mechanical strength, thermal stability, and barrier properties. This method is particularly effective for fabricating gas barrier films, including those used in food packaging [40,153].

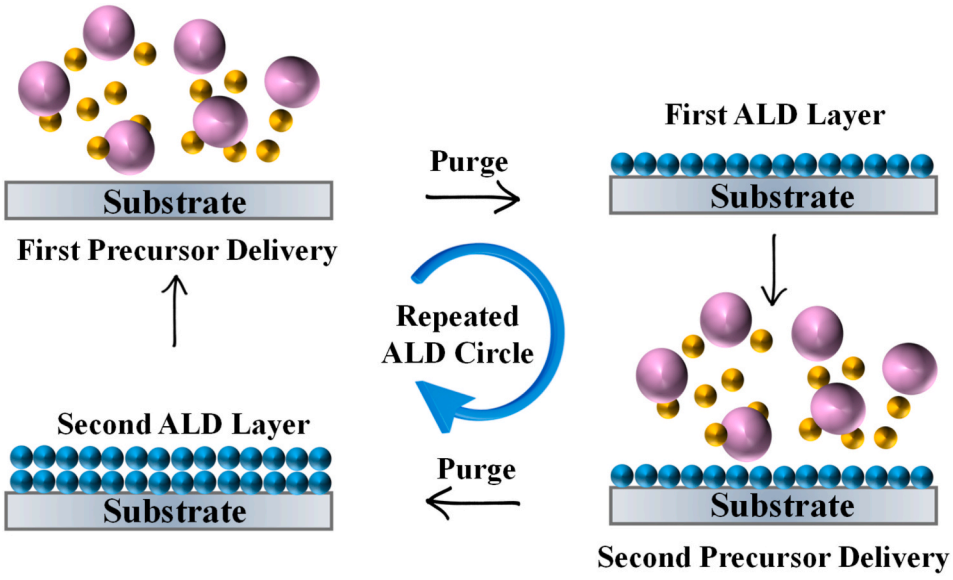

Fig. 13. Schematic of the ALD process, involving cyclic, self-limiting surface reactions of alternating precursor pulses. Each half-reaction deposits no more than a monolayer on the substrate, followed by purging with inert gas to remove excess reactants and by-products. Repetition of this sequence builds a conformal and precisely controlled thin film, typically under low pressure and moderate temperatures.

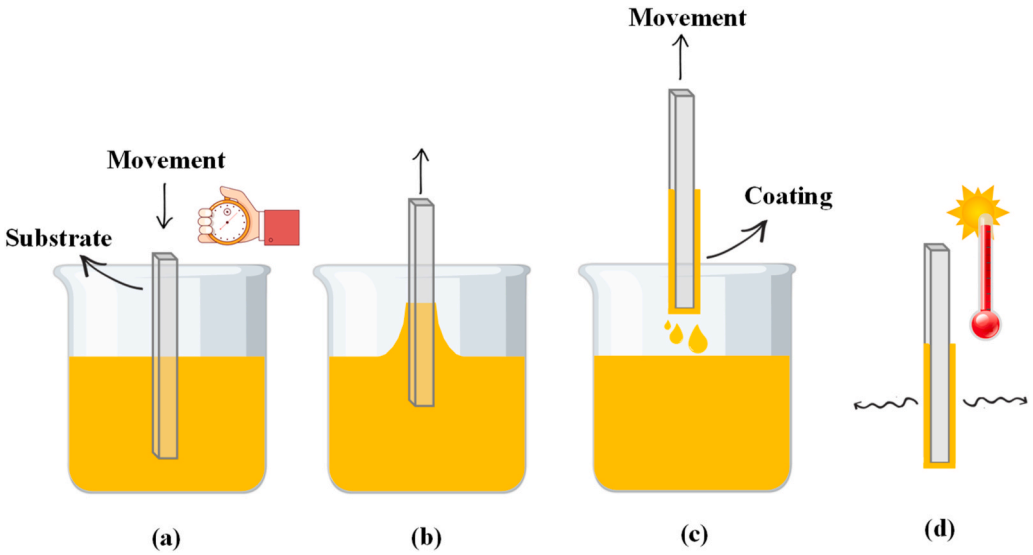

Fig. 14. Dip coating process including (a) Dipping, (b) Withdrawal, (c) Formation of coating, (d) Solvent evaporation.

4.10. Spraying

It is a versatile technique that allows for rapid and uniform deposition of polymer coatings onto substrates of varying sizes and shapes. In this method, the polymer solution or molten polymer is atomized and sprayed onto the substrate surface, forming a coating upon solvent evaporation or cooling. The spraying process can be automated, making it highly suitable for industrial-scale applications where large surfaces need to be coated efficiently. It is extensively used in the aerospace, automotive, and electronics industries, where protective and functional coatings are required [154].

4.11. Extrusion

This is predominantly employed for thermoplastic polymers, such as polyethylene, to produce continuous films, sheets, or liners. During extrusion, the molten polymer is forced through a die, and the resulting product exhibits enhanced barrier properties due to molecular chain alignment in the extrusion direction. This method is widely used in the fabrication of pipeline liners and external sheaths for hydrogen containment, where large-scale, continuous coatings are required [155, 156].

Table 2 outlines the principal coating deposition techniques used to develop hydrogen barrier layers, including metallic, ceramic, polymeric, and composite systems, and lists the advantages and disadvantages of each method in terms of process feasibility, scalability, and barrier performance.

4.12. Challenges and future perspectives in coating techniques

Despite the demonstrated hydrogen diffusion resistance of coating systems, critical challenges persist that hinder their widespread deployment in hydrogen fuel cells and energy infrastructure. Notably, the long-term mechanical reliability of these coatings, specifically their adhesion under cyclic loading, resistance to fatigue, and ability to mitigate or heal cracks under operational stresses, remains insufficiently characterized. Addressing these gaps necessitates more integrated research approaches, combining mechanical testing with in-situ hydrogen permeation analysis and environmental exposure assessments.

The incorporation of real-time, in situ diagnostic tools is critical for understanding and optimizing coating behaviour during deposition. These tools can monitor stress evolution, splat dynamics, film growth kinetics, and interfacial bonding, enabling adaptive control of process parameters to enhance adhesion and structural stability. Fig. 15 lists different coating processes employed for applying coatings.

5. Key hydrogen barrier coatings

Mitigating HE involves strategies aimed at reducing hydrogen ingress into a metallic substrate by application of various HBCs using surface engineering techniques. The mechanism of hydrogen permeation through coated metallic substrates typically follows a multistep process involving surface interactions and diffusion phenomena. Initially, molecular hydrogen (H_2) is adsorbed onto the surface of the protective coating, where it dissociates into atomic hydrogen. These hydrogen atoms then diffuse through the barrier layer and subsequently into the underlying metal substrate. Once they reach the opposite surface, the atoms recombine into molecular hydrogen and desorb from the material. An effective hydrogen permeation barrier should hinder each of these stages, particularly atomic diffusion through the coating and substrate, to minimize hydrogen uptake and transport. This conceptual framework is illustrated in Fig. 16(a) [23].

HBCs, when applied to metallic substrates through appropriate surface engineering methods, serve to impede hydrogen ingress via two principal mechanisms. Firstly, materials possessing densely packed crystal structures and strong chemical bonds, such as ionic or covalent bonds, effectively obstruct hydrogen atom diffusion by requiring substantial energy to disrupt these stable bonding interactions. This mechanism is commonly associated with metallic and ceramic coatings. In the second approach, the barrier material contains a high density of structural defects, such as dangling bonds or vacancies, which act as trap sites. These defects capture incoming hydrogen atoms and inhibit their further transport into the underlying substrate. These complementary strategies are illustrated schematically in Fig. 16(b–c) [24]. Fig. 16 (d) [26] presents a schematic representation of the hydrogen ingress mechanism in a coated metallic substrate. It highlights the sequential process starting from the adsorption and dissociation of hydrogen-containing molecules (such as H_2 or H_2O) on the coating surface. Once dissociated, atomic hydrogen enters the coating, typically through interstitial sites, and diffuses across the barrier layer. Without an effective hydrogen permeation barrier, this atomic hydrogen would continue its path, eventually reaching the metallic substrate. There, hydrogen accumulates at microstructural defects such as grain boundaries, dislocations, and vacancies, sites that facilitate hydrogen trapping and embrittlement. This figure underscores the role of coatings as diffusion barriers, where the goal is to increase both the energy barrier

Table 2
Comparison of coating deposition methods for hydrogen barrier applications.

Method	Coating material	Advantages	Disadvantages
Physical vapour deposition (PVD)	Metallic, Ceramic	- High purity and density of deposited films - Low process temperature	- Limited large-scale applicability (small chamber, high cost) - Line-of-sight, poor coverage of pores/ complex shapes
Chemical vapour deposition (CVD)	Metallic, Ceramic	- Conformal, can coat pores and complex shapes - Scalable	- High temperature required (>800 °C) - High capital and maintenance costs
Atomic layer deposition (ALD)	Ceramic, Composite	- Atomic-level thickness control - Excellent conformality, even on complex geometries	- Very slow growth rate - Expensive precursors and equipment
Electroplating	Metallic	- Simple, low-cost - Good for complex shapes	- Hydrogen uptake during deposition - Porosity reduces barrier effectiveness
Hot dipping	Metallic, Composite	- Strong adhesion - Low cost, widely available	- Non-uniformity over large areas - Brittleness and microstructural defects may increase hydrogen uptake
Thermal spraying	Metallic, Ceramic	- Thick, durable coatings - High deposition rate	- Porosity may promote hydrogen ingress - Energy-intensive, and variable adhesion
Pack cementation	Metallic	- Low cost, scalable for large production - Produces adherent diffusion coatings	- Slow process - Limited durability against hydrogen ingress
Sol–gel	Ceramic	- Low-cost, compositional flexibility - Scalable for large areas	- Porosity and cracking limit long-term effectiveness - Poor adhesion to pre-oxidized substrates
Dip coating	Polymer, Composite	- Simple, scalable, low cost - Uniform films on complex substrates	- Solvent removal may cause defects - Limited control over thickness
Casting and curing	Polymer	- Thick, robust films - Easy incorporation of fillers/ crosslinkers	- Not suitable for complex geometries - Slow drying/curing
Spraying	Polymer, Composite	- Rapid, uniform, scalable - Automated for industry	- Coating defects, if poorly controlled - Limited thickness control
Extrusion	Polymer	- Produces continuous large-scale liners/films - Chain alignment improves barrier properties	- Limited to thermoplastics - Expensive equipment
Hybrid / multilayer deposition	Composite	- Synergistic barrier + mechanical performance - Interfacial trapping reduces permeability	- Complex processing - Scale-up challenges

and diffusion length for hydrogen transport, thereby mitigating the risk of HE, stress corrosion cracking, and hydrogen blistering in structural materials.

Li et al. [25] proposed three fundamental models to describe hydrogen permeation through HBCs, as illustrated in Fig. 16(e–g). In the surface-limited model (Fig. 16 (e)), hydrogen permeation is primarily restricted by the surface of the coating, making surface reactions the rate-limiting step in the overall transport process. The areal-defect model (Fig. 16 (f)) considers the role of localized structural imperfections, such as pores, voids, or microcracks, through which hydrogen selectively permeates, with the effective permeation rate governed by the area and distribution of these defects. The third model, known as the composite barring model (Fig. 16 (g)), describes multilayer or heterogeneous coatings in which multiple permeation mechanisms as shown in Fig. 16 (h) [53] operate simultaneously, leading to improved barrier performance due to interfacial resistance and the synergistic effects of different material layers. These three models, along with a schematic of hydrogen diffusion pathway obstruction in multi-layer nanocomposite coatings, provide a conceptual framework for understanding hydrogen transport phenomena in coated systems and are widely referenced for the evaluation and design of high-performance hydrogen permeation barriers.

A variety of coatings have been developed and implemented as HBCs to mitigate the effects of HE [23–26,116,158–160]. These coatings generally fall into four main categories: metallic coatings, ceramic coatings, polymer coatings, and composite-multilayer coatings, each of which will be discussed in detail below.

5.1. Metallic coatings

This section delves into the different types of metallic coatings, their properties, application techniques, and their effectiveness in preventing HE, supported by relevant studies and research. Metallic coatings can be classified based on the metal used and their intended function.

Various strategies have been reported for applying metallic coatings; however, current strategies vary widely in their effectiveness, durability, and compatibility with different applications [161]. Metallic coatings are widely employed as protective layers that limit hydrogen uptake to prevent HE in steel [123].

5.1.1. Hydrogen permeability in metals

While metallic coatings offer significant benefits, the energy required for their application and the high cost of noble metals restrict their use to extreme service conditions where robust protection is paramount. Fig. 17 shows different metal coatings such as gold (Au) [162], chromium (Cr) [163], copper (Cu) [164], tungsten (W) [165], nickel (Ni) [166], vanadium (V) [167], and more complex alloy coatings [43,55,168] which have been applied as HBCs on susceptible substrates.

Also, Table 3 provides a comprehensive summary of hydrogen permeability data for various metallic coatings, highlighting significant variations in permeability values as a function of metallic coatings.

Materials such as vanadium (V), titanium (Ti), and niobium (Nb) demonstrate notably high hydrogen permeability, with values on the order of 10^{-8} to 10^{-9} $mol.m^{-1}.s^{-1}.Pa^{-1/2}$ at elevated temperatures (500 °C). These materials, while advantageous for hydrogen transport membranes due to their high diffusivity, are unsuitable as HBCs due to their inability to sufficiently block hydrogen ingress.

Vanadium has the highest hydrogen permeability in the table at 2.9×10^{-8} $mol.m^{-1}.s^{-1}.Pa^{-1/2}$ at 500 °C, making it the least effective hydrogen barrier coating. This high permeability likely results from Vanadium's metallic lattice structure, which allows for rapid hydrogen diffusion. Aligning the lattice constant with that of pure vanadium by co-alloying elements that contract and expand the lattice proved to be highly effective in preserving the high hydrogen diffusivity of pure vanadium [172].

Nickel (Ni) and iron (Fe) present slightly lower permeability ($\sim 10^{-10}$ $mol.m^{-1}.s^{-1}.Pa^{-1/2}$), still making them relatively permeable and hence not ideal candidates for hydrogen barrier applications. Austenitic and ferritic steels display moderate permeability in the range of 10^{-11} $mol.m^{-1}.s^{-1}.Pa^{-1/2}$, with ferritic steels demonstrating higher values ($\sim 3 \times 10^{-11}$ $mol.m^{-1}.s^{-1}.Pa^{-1/2}$), potentially due to their body-centered cubic structure, which is more accommodating to hydrogen diffusion than FCC [173].

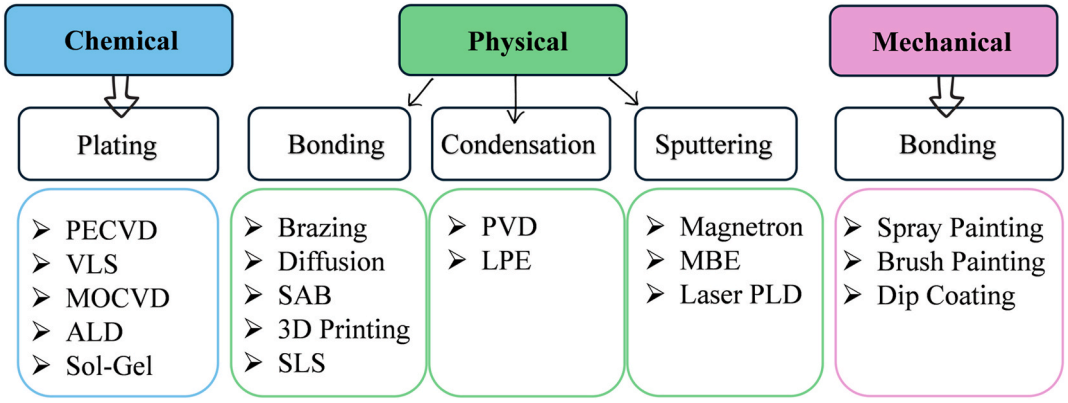

Fig. 15. Classification of coating techniques for thin film deposition based on chemical, physical, and mechanical processes [157].

At the lower end of the permeability spectrum, refractory metals such as tungsten (W) show exceptional hydrogen barrier properties with permeability values as low as 4.3×10^{-15} $mol.m^{-1}.s^{-1}.Pa^{-1/2}$. This makes it a strong candidate for high-temperature HBC applications, especially in hydrogen-intensive environments.

Inconel 600, a nickel-based superalloy, presents a moderate permeability (~2.8×10^{-11} $mol.m^{-1}.s^{-1}.Pa^{-1/2}$ at 500 °C), suggesting its viability in high-temperature environments where oxidation resistance is also a consideration.

The data for 316L stainless steel reveal a clear temperature dependence in hydrogen permeability. At 450 °C, the permeability ranges from 5.1 to 7.35×10^{-11} $mol.m^{-1}.s^{-1}.Pa^{-1/2}$, which decreases progressively to ~3.85–4.88 $\times 10^{-12}$ $mol.m^{-1}.s^{-1}.Pa^{-1/2}$ at 300 °C. This trend aligns with the Arrhenius-type behaviour of diffusion processes, highlighting the importance of operating temperature in material selection for hydrogen barriers.

Chromium (Cr) demonstrates relatively low permeability across the measured temperature range (10^{-12} to 10^{-14} $mol.m^{-1}.s^{-1}.Pa^{-1/2}$), particularly at 200 °C, where it reaches as low as 1.95×10^{-14} $mol.m^{-1}.s^{-1}.Pa^{-1/2}$.

Lightweight metals like beryllium (Be) and aluminium (Al) also exhibit very low hydrogen permeability, with Be reaching values as low as 2×10^{-15} $mol.m^{-1}.s^{-1}.Pa^{-1/2}$ at 400 °C and Al showing values down to 5.7×10^{-14} at 160 °C. These metals are promising for applications where both low weight and high hydrogen resistance are required, though considerations like toxicity and oxide film stability must be addressed.

In the context of hydrogen exposure, Abramov et al. [174] conducted a detailed investigation of deuterium diffusion and permeation through high-purity Be membranes using the gas-driven permeation method. Their work carefully decoupled surface oxide effects from bulk diffusion using multilayer analysis and reported effective diffusivities in the range of 6.7×10^{-9} to 8.0×10^{-9} $m^2.s^{-1}$, depending on purity grade. The values presented in their study were derived exclusively from high-temperature measurements, as at lower temperatures, the contribution of the oxide film becomes predominant in governing the effective diffusivity. These values, while moderate, are still significantly lower than those of uncoated structural steels.

The data suggest that W, Be, Al, and Cr are among the most promising candidates for effective HBCs due to their low hydrogen permeability. The selection of an appropriate material must balance permeability, mechanical properties, temperature conditions, and other applications (specific requirements). Further studies involving multilayer coatings and surface treatments could enhance these materials' performance in real-world applications.

5.1.2. *Various metal coatings*

Each type of coating offers unique benefits, making them suitable for specific uses. Metal coatings have been identified for their low atomic hydrogen permeability, thus providing effective protection against HE. However, not all metals are suitable for this application. For instance, lead and tin have been found to accelerate hydrogen diffusion within iron, making them ineffective as protective coatings [162].

Kim et al. [43] compared Zn–Ni, Zn–Ni–Cd, and Cd coatings and provided direct electrochemical evidence that Zn–Ni–Cd alloyed coatings offer the lowest hydrogen permeation current and highest corrosion resistance among the three. The hydrogen absorption rate was significantly suppressed due to reduced surface hydrogen coverage and a decrease in the recombination rate constant. However, serious limitations exist, as cadmium is highly toxic and subject to strict environmental regulations, which significantly restrict its application. The hard chromium coatings, though once considered viable, have demonstrated embrittlement risk in real-world applications. Araujo et al. [175] conducted a failure analysis on chromium-coated 17-4 PH steel and revealed that hydrogen-induced intergranular fracture initiated at the coating–substrate interface, worsened by gas-pitting and insufficient hydrogen baking. This case underscores the fragility of electrodeposited coatings when surface defects, residual stress, or inadequate post-treatment are present.

Zn–Co systems, while offering some sacrificial protection, showed incomplete mechanical recovery even after 48 h of post-baking at 200 °C [168]. Hillier and Robinson [168] found that only when a nickel interlayer was introduced before Zn–Co deposition was HE significantly mitigated. Furthermore, newer alloy systems such as zinc–12 %cobalt–9 %iron [168] have shown potential in reducing embrittlement through optimized interfacial behaviour and multicomponent synergies, though data on long-term mechanical cycling or real-world environmental exposure remain sparse.

A more recent and innovative approach involves magnetron-sputtered Al–Ti–W amorphous coatings, as investigated by Lakdhar et al. [55]. These coatings exhibit a dense, nanostructured morphology with no detectable porosity and excellent thermal stability up to 665 °C. Importantly, hydrogen uptake measurements under both chemical and electrochemical charging conditions demonstrated up to a 70 % reduction in absorbed hydrogen relative to uncoated steel. The performance was found to scale with W content, indicating a structure–composition–function relationship in which amorphization and atomic-scale mixing inhibit hydrogen diffusion and trapping. While the results are promising, the study lacks direct hydrogen permeation flux measurements, as well as mechanical testing under hydrogen-charged states. Additionally, corrosion resistance was noted to decrease with

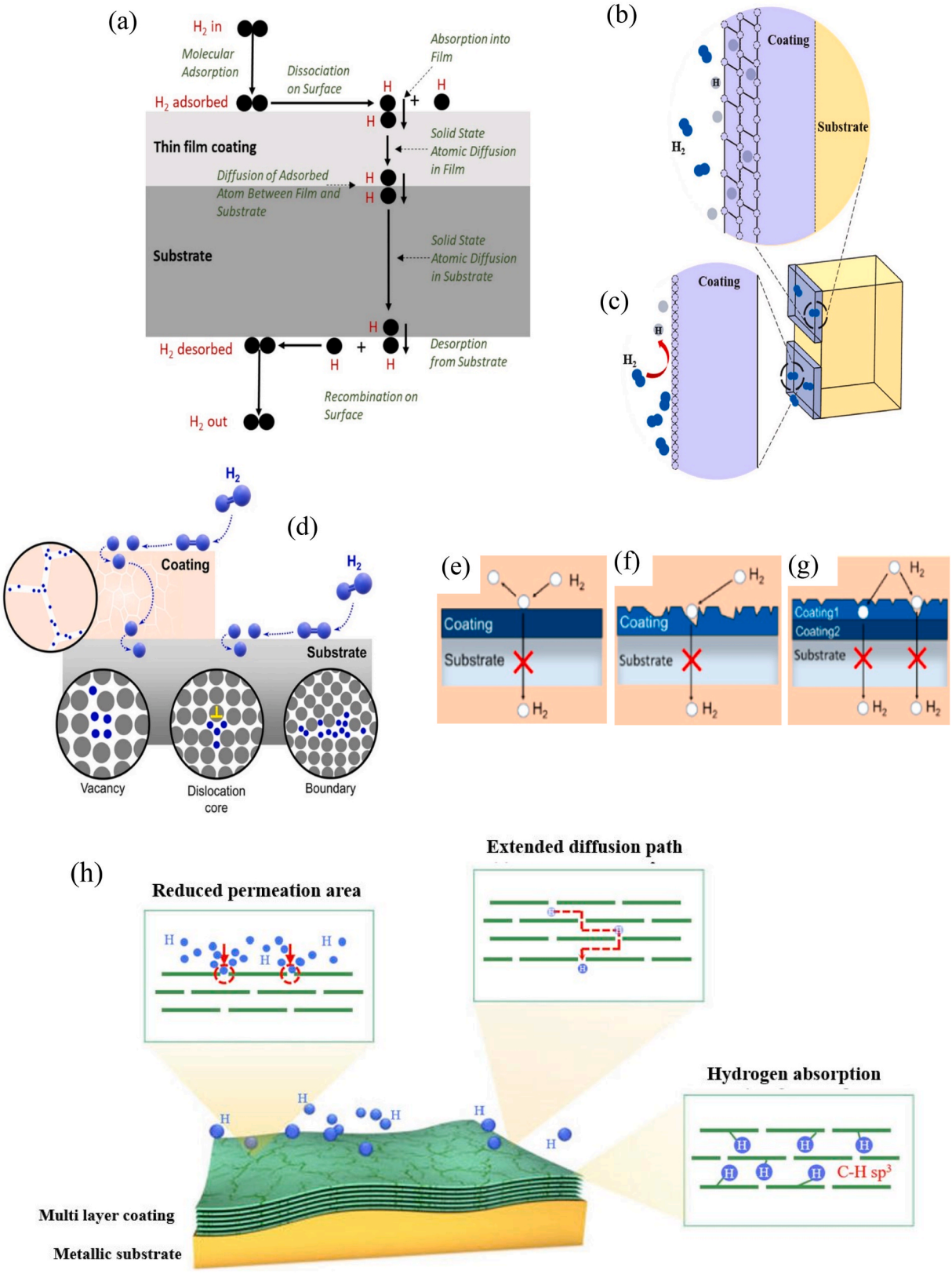

Fig. 16. (a) The multistep process of hydrogen permeation in a substrate with thin film HBC [23]; The HBC surface engineering techniques to effectively (b) trap hydrogen in HBC or (c) block the penetration of hydrogen into HBC and further into a substrate [24]; (d) HBC safeguard from excessive hydrogen entry/penetration, and distribution at various microstructural locations [26]; (e–g) Models for hydrogen barring through HBC: (e) surface limited, (f) areal-defect, and (g) composite barring [25]; (h) hydrogen diffusion pathway obstruction in multi-layer nanocomposite coatings [53].

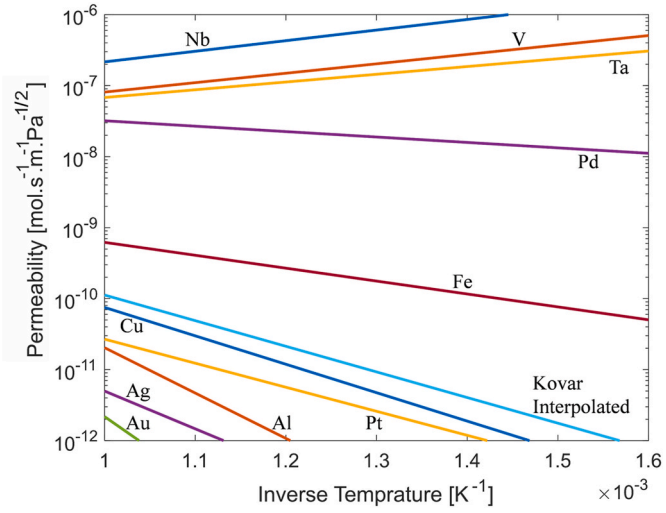

Fig. 17. Hydrogen permeability in various unoxidized metallic materials (Cu/Copper, Al/Aluminum, Pt/Platinum, Ag/Silver, Au/Gold, Kovar interpolated, Fe/Iron, Nb/Niobium, V/Vanadium, Ta/Tantalum, Pd/Palladium) [169]. (For interpretation of the references to colour in this figure legend, the reader is referred to the Web version of this article.)

Table 3
Hydrogen permeability of various metallic barrier coatings.

Metallic coatings	Hydrogen permeability ($mol.m^{-1}.s^{-1}.Pa^{-1/2}$)	T (°C)	Ref.
V	2.9×10^{-8}	500	[167]
Ti	7.5×10^{-9}		
Ni	1.2×10^{-10}		
Nb	7.5×10^{-9}		
Mo	1.2×10^{-11}		
W	4.3×10^{-15}		
Nickel-based alloy Inconel 600	2.8×10^{-11}		
Fe	1.8×10^{-10}		
Austenitic steels	$0.7 - 1.2 \times 10^{-11}$		
Ferritic steels	3×10^{-11}		
Austenitic stainless steel 316L	$5.1 - 7.35 \times 10^{-11}$	450	[170]
	$2.26 - 3.29 \times 10^{-11}$	400	
	$3.85 - 4.88 \times 10^{-12}$	300	
Cr	5.25×10^{-12}	500	[163]
	2.65×10^{-12}	400	
	3.9×10^{-13}	300	
	1.95×10^{-14}	200	
Be	2×10^{-15}	400	[25]
Al	5.7×10^{-14}	160	[171]
	1.15×10^{-13}	180	
	2.3×10^{-13}	200	

W enrichment, likely due to galvanic microcells or surface roughening, highlighting the need for careful optimization between barrier efficacy and corrosion protection.

Yamabe et al. [171] took a mechanistic approach by investigating a tri-layer aluminium-based coating (alumina/aluminium/ferro-aluminium) under high-pressure hydrogen gas. Using secondary ion mass spectrometry (SIMS), the study showed that hydrogen trapping at the aluminium–ferro-aluminium interface rather than hydrogen obstruction by alumina alone was primarily responsible for the observed reduction in hydrogen diffusivity, which was measured to be three orders of magnitude lower than in uncoated stainless steel. This is due to interfacial hydrogen trapping rather than just surface barrier effects. Notably, the coating maintained its integrity under exposure to gaseous hydrogen at 100 MPa, a highly demanding condition for hydrogen infrastructure applications. These findings suggest that coating architecture and interfacial engineering may be more critical than bulk diffusivity alone in determining effective hydrogen barrier performance.

Al–based amorphous alloys, like Al–Co–Ce, also exhibit multifunctional corrosion protection by releasing inhibitor ions and forming passive films [161]. However, aluminum coatings applied via hot-dip galvanizing or thermal spraying can suffer from brittleness and poor adhesion if not properly controlled, and their performance under cyclic hydrogen charging remains largely untested.

Refractory metals such as W and lightweight candidates are increasingly studied for use in extreme hydrogen-rich environments due to their high-temperature stability and favourable diffusion properties. Frauenfelder [165] conducted one of the earliest systematic studies on hydrogen solubility and diffusion in tungsten, reporting extremely low diffusivity and solubility values. Tungsten's high activation energy for hydrogen diffusion renders it highly resistant to hydrogen permeation, making it a strong candidate for ultra-demanding barrier applications.

Ganchenkova et al. [176], through ab initio simulations, further revealed that hydrogen prefers tetrahedral interstitial sites in Be and forms strongly bound complexes with vacancies, potentially leading to nanovoids and embrittlement. These results highlight a duality in Be's behaviour, which may slow down bulk hydrogen transport via trapping but also facilitate localized damage through void formation. Such complexity underscores the need for combining high-resolution structural studies with mechanical and hydrogen-specific testing.

Nickel-based coatings, particularly electrodeposited Ni or Ni–P systems, are highly effective at the reduction of hydrogen ingress due to their dense microstructure and inherently low hydrogen diffusivity (on the order of 10^{-10} $cm^2.s^{-1}$) [168]. They are also chemically stable and corrosion-resistant. The addition of Ni interlayers in Zn–Co systems dramatically reduces hydrogen-induced degradation in high-strength steels [168]. However, post-coating heat treatments are essential to remove absorbed hydrogen and prevent delayed cracking, which increases cost and processing complexity. Ni coatings are also susceptible to hydrogen accumulation at coating/substrate interfaces if porosity or plating defects exist.

Zinc and Zn-alloy coatings, e.g., Zn–Ni, Zn–Ni–Cd, and Zn–Co–Fe, are widely used for their sacrificial cathodic protection properties. Zn–Ni–Cd coatings, in particular, have shown superior resistance to both corrosion and hydrogen uptake compared to Cd or Zn alone, due to reduced surface hydrogen coverage and recombination rates [43]. However, their long-term hydrogen permeability is moderate, and performance can deteriorate rapidly in aggressive environments such as chloride-rich atmospheres [43,168]. Moreover, the toxicity of Cd in Zn–Ni–Cd limits its practical use. Zn–Co coatings without Ni interlayers are prone to embrittlement, and even post-baking may not fully restore mechanical integrity [168].

Tungsten possesses one of the lowest hydrogen permeabilities among metals, supported by both classical diffusion measurements [165] and recent studies on sputtered films. Its high melting point, thermal stability, and resistance to hydrogen-induced cracking make it ideal for high-temperature hydrogen systems. An experimental study has shown that a 1.5 μm tungsten coating can reduce hydrogen permeation by a factor of approximately 50 [177]. Nevertheless, the high cost of deposition, the brittleness of W films, and their susceptibility to delamination under thermal cycling limit their industrial adoption. In real-world thin film applications, grain boundary diffusion and interfacial mismatch must be carefully addressed to ensure coating effectiveness.

Cadmium coatings have traditionally been employed for their sacrificial corrosion protection and moderate hydrogen barrier performance. However, hydrogen is often introduced during electroplating, and post-coating heat treatment is required to reduce hydrogen embrittlement risk [43]. Despite these measures, HE may still occur, especially in high-strength steels, due to gas pitting, interfacial decohesion, or incomplete hydrogen outgassing. Moreover, cadmium's environmental toxicity has led to severe regulatory restrictions, making it an increasingly unattractive option. Cadmium, like nickel, is applied

through electroplating and offers lower hydrogen diffusivity compared to steel. However, similar to nickel electroplating, cadmium coatings can introduce hydrogen into the steel substrate during the plating process. To mitigate this, post-coating heat treatments are necessary to release the absorbed hydrogen, but cadmium-coated samples may still experience HE [43].

Direct permeation studies using high-purity Be membranes have shown effective diffusivities in the range of 10^{-9} $m^2.s^{-1}$, with surface oxide layers playing a critical role in limiting hydrogen flux [174]. However, Be's hydrogen response is complex: simulations reveal strong trapping at vacancies, which may localize hydrogen and cause nanovoiding or cracking under stress [176]. Be is a potential candidate for HBCs, though its effectiveness remains inconsistent. The variations in performance are likely attributed to the challenges associated with fabricating beryllium films with uniform properties. Be films are typically created through vacuum hot pressing, and their hydrogen transport properties are highly dependent on grain size [158]. Toxicity and cost also limit the widespread use of Be, but its strategic role in specific applications, such as plasma-facing walls or neutron multipliers, justifies continued research. For both W and Be, surface engineering approaches, e.g., oxide passivation, interlayers, or composite structures, are necessary to overcome brittleness and interfacial stress limitations. Furthermore, multilayer combinations involving W, Be, or refractory-based amorphous alloys may yield hybrid coatings that combine exceptionally low hydrogen permeability with structural resilience.

Overall, metallic coatings show diverse strategies for reducing hydrogen uptake, ranging from sacrificial layers such as zinc and cadmium to barrier-type systems including nickel, tungsten, and multilayer architectures. The effectiveness of these coatings is closely tied to their microstructure, density, and interfacial integrity. For example, Ni and Ni–P films can act as hydrogen traps but require careful post-treatments, while W layers achieve very low permeability, though their brittleness and processing challenges remain limiting. Al- and Ti-based multilayers, as well as Al/Fe–Al tri-layer systems, highlight the potential of engineered architectures to disrupt diffusion pathways. Collectively, the studies emphasize that coating performance is not determined by composition alone but by the ability to minimize defects, control porosity, and stabilize interfaces, which together dictate long-term resistance to hydrogen embrittlement.

While the role of metallic coatings in mitigating HE remains relatively underexplored and context-dependent, certain metallic systems, such as tungsten, have demonstrated significantly lower hydrogen permeabilities in comparison to other HBCs, highlighting their potential in specific applications. Their effectiveness as hydrogen barriers depends significantly on factors such as hydrogen permeability, coating thickness, application methods, and post-coating treatments. High-temperature annealing, for instance, is often employed to reduce metallurgical imperfections and enhance barrier performance. Each metallic system presents distinct trade-offs in terms of performance, cost, and environmental suitability. While materials like beryllium and tungsten exhibit excellent hydrogen barrier properties, they are costly and sensitive to process variables. Aluminum-based coatings offer promising multi-functional capabilities but require further validation under hydrogen service conditions. Nickel, zinc, and cadmium provide more cost-effective alternatives, though they come with limitations such as dependency on processing parameters. Beryllium's complex behavior also comes with environmental concerns and warrants more research before it can be widely adopted. Moving forward, the development of advanced metallic coatings should focus on alloy tailoring, microstructural refinement, and interfacial engineering to maximize hydrogen barrier performance without compromising mechanical integrity or environmental sustainability.

5.1.3. Techniques for applying metal coatings

The development of metallic coatings as hydrogen barriers demands an integrated understanding of deposition technique, microstructural architecture, and service-environment compatibility. Electroplating, cladding, and thermal spraying offer distinct advantages in controlling coating thickness, adhesion, and hydrogen diffusivity, yet differ markedly in scalability, defect tolerance, and process-induced stresses. As demonstrated across recent studies, the effectiveness of these coatings is governed not only by their intrinsic material properties but also by interfacial stability, defect management, and structural coherence under hydrogen-rich and cyclic loading conditions.

Thermally sprayed coatings, particularly those based on nickel- and chromium-rich alloys, represent a promising protective strategy against hydrogen attack in petrochemical structures and equipment. These coatings offer substantial resistance to hydrogen-induced embrittlement. However, their effectiveness can be limited by inherent porosity, which may promote excessive hydrogen trapping and recombination within the coating microstructure [178].

The findings indicated that the niobium coating applied by the thermal spray technique effectively served as a barrier against hydrogen ingress, thereby mitigating the detrimental impact of hydrogen on the mechanical properties of API 5CT P110 steel. Quantitative hydrogen analysis revealed that the coating exhibited a hydrogen trapping capacity approximately 7.5 times greater than that of the uncoated steel [97].

Electroplated coatings are low-cost and easy to apply, but their performance is extremely sensitive to process control, defect density, and post-deposition treatment. Their hydrogen permeability varies widely depending on porosity and microstructure, and they often lack robust adhesion and environmental durability, especially under cyclic thermal and mechanical loads.

Electrodeposited copper (ED-Cu) coatings have been evaluated by Williams et al. [164]. They studied strain rate sensitivity, and the embrittlement was exacerbated at a lower strain rate. Their SSRT-based study revealed that ED-Cu is highly sensitive to deposition chemistry and hydrogen content. Specimens deposited from acidic baths (~26 ppm H) exhibited significant embrittlement and intergranular cracking, while those from alkaline baths (~5 ppm H) remained ductile. Microstructural analysis showed void formation, dislocation networks, and impurity clustering as the primary features associated with embrittlement. While the study did not measure hydrogen permeation directly, it demonstrated that the choice of electrolyte and post-processing significantly impacts hydrogen susceptibility. Thus, ED-Cu coatings can be engineered to be hydrogen-tolerant, but only with tight control over processing parameters and hydrogen source mitigation.

Collectively, these alloy systems demonstrate that the hydrogen barrier capability of metallic coatings is not solely a function of elemental composition but is critically influenced by microstructural uniformity, deposition method, and interfacial chemistry. Future work should prioritize the integration of in situ hydrogen permeation testing with mechanical and microstructural analyses to assess coating performance under conditions mimicking service exposure. Additionally, alloying strategies that promote beneficial hydrogen trapping, such as at coherent phase interfaces, could lead to next-generation multifunctional barrier systems without compromising mechanical stability.

Plating, which includes both electrochemical and chemical deposition methods, is commonly used to apply a thin, uniform metal layer onto the steel surface. Electroplating typically produces a smooth finish, which is desirable in many applications, while electroless plating can be used for more intricate geometries. However, both methods can introduce hydrogen into the substrate during electrochemical reactions, requiring post-coating heat treatment to mitigate potential HE [168, 179]. Electroplated coatings, such as Zn–Ni–Cd and Zn–Co–Fe [43,168], demonstrate good initial hydrogen barrier performance and cathodic protection but suffer from high process sensitivity, coating porosity, and in some cases, toxicity or environmental incompatibility (Cd and Cr). Their mechanical stability under cyclic load and long-term adhesion is often compromised without meticulous post-treatment, such as baking or interlayer deposition.

PVD coatings, including Al–Ti–W amorphous systems [55,123], offer superior hardness, microstructural density, and thermal resistance. These coatings generally achieve lower hydrogen diffusivity due to their fine columnar or amorphous microstructures. However, they are limited by substrate compatibility, deposition cost, and challenges related to internal stresses and scalability. Architectural control, particularly in multi-layer systems, has emerged as a key design factor [171].

The Dip coating method to apply coatings such Al–Mg–Si and Al–Si is used to produce barrier coating against hydrogen permeation. Kyo et al. [180] studied the hydrogen entry behaviour of hot-dip Al–Mg–Si coated steel and demonstrated the successful fabrication of a ternary Al–Mg–Si coating on a steel substrate via hot-dip processing, yielding a microstructure characterized by a fine quasi-eutectic mixture of aluminum and Mg_2Si phases. This unique microstructural configuration was shown to play a crucial role in mitigating hydrogen ingress. In comparison to conventional zinc coatings, the Al–Mg–Si-coated steel exhibited a substantially lower hydrogen uptake—less than one-sixth—under equivalent exposure conditions. This remarkable reduction in hydrogen entry is attributed to the moderate galvanic corrosion potential of the Al–Mg–Si coating, which likely results in diminished cathodic hydrogen evolution. The findings highlight the potential of hot-dip Al–Mg–Si coatings as a promising sacrificial layer for protecting high-strength steels, offering a notable advantage in reducing the susceptibility to HE while maintaining corrosion resistance. Han et al. [181] reported that hot-dip aluminizing of steel in an Al–Si melt significantly improved the quality and uniformity of the coating compared to pure aluminum baths, reducing the intermetallic layer thickness from 80 μm to about 10 μm. This refinement is attributed to the formation of Al–Fe–Cr–Si crystalline phases, which slow aluminum diffusion into the steel, leading to more controlled growth of the coating. Upon subsequent heat treatment, a well-bonded, pore-free duplex layer consisting of ductile FeAl and α-Fe (Al) phases formed, enhancing its potential as an effective hydrogen or tritium permeation barrier, especially since even the thin oxide layer (0.8 μm g-Al_2O_3 at 900 °C) remains within functional limits for such applications.

Each of these techniques has its trade-offs, and the choice of method depends on the specific requirements of the application, including coating thickness, surface finish, and the need for post-coating treatments.

5.2. Ceramic coatings

Ceramic coatings have emerged as a pivotal technology in materials engineering, particularly for applications requiring robust protection against HE. Renowned for their high hardness, chemical stability, and minimal hydrogen permeability, these coatings are ideal for environments where metals are vulnerable to hydrogen exposure. This section provides an in-depth exploration of ceramic coatings, focusing on their unique properties, application methods, and efficacy in preventing hydrogen ingress. Ceramics possess a suite of characteristics, such as high melting points, chemical inertness, and exceptional wear resistance, that make them excellent candidates for protective layers. However, their inherent brittleness poses challenges related to adhesion and fracture toughness. Despite these limitations, ceramics remain invaluable in applications demanding thermal stability and resistance to chemical attack.

Ceramic coatings, categorized into nitrides, carbides, and oxides, are promising barriers against hydrogen permeation. Their dense microstructures and low gas permeability surpass those of polymeric and metallic coatings [40]. High-quality ceramic coatings are primarily produced through chemical or PVD under vacuum, yielding smooth surfaces that minimize flow friction. While thermal spray methods are favored for large-scale industrial applications, they may introduce defects that act as pathways for hydrogen permeation [40].

5.2.1. Hydrogen permeability of ceramics

Despite their advantages, ceramics face limitations due to their brittleness, which can lead to cracking during deposition and compromise their efficacy. Performance is heavily influenced by operational conditions, with metal surface defects and localized stresses exacerbating degradation risks. Although ceramics excel at mitigating HE at elevated temperatures (with data reported for 400 °C [158]), limited studies exist on their performance under ambient conditions, where extrapolated data often fill the gaps.

Table 4 Presents an extensive dataset on hydrogen permeability values for a range of ceramic materials, grouped into nitrides, carbides, oxides, and mixed compositions, measured at various temperatures, typically between 300 °C and 800 °C.

A comparative evaluation of the data reveals a significant disparity in hydrogen permeation behaviour across different ceramic materials and even within individual classes. Among all tested ceramics, nitrides emerge as the most effective barrier against hydrogen permeation. Particularly, titanium carbide (TiC) and zirconium nitride (ZrN) demonstrate the lowest hydrogen permeability values in the entire dataset, measured at 3.62×10^{-18} and 7.9×10^{-18} $mol.m^{-1}.s^{-1}.Pa^{-1/2}$ at 300 °C and 400 °C, respectively. These exceptionally low values indicate their outstanding resistance to hydrogen diffusion, positioning them as prime candidates for high-performance applications where low hydrogen permeability is critical. Similarly, silicon nitride (SiN) performs impressively, with a permeability on the order of 10^{-17} $mol.m^{-1}.s^{-1}.Pa^{-1/2}$ at 400 °C, showcasing its excellent capability to resist hydrogen infiltration across a moderately wide temperature range.

Titanium aluminium nitride (TiAlN) also features prominently among the best-performing materials, with a permeability of 2.9×10^{-17} $mol.m^{-1}.s^{-1}.Pa^{-1/2}$ at 400 °C. This compound, like ZrN and SiN, belongs to the nitride class, which collectively shows a trend of superior hydrogen barrier characteristics. The trend is further substantiated by other nitrides such as CrN and AlCrN, which exhibit similarly low permeation rates in the range of 10^{-16} to 10^{-17} $mol.m^{-1}.s^{-1}.Pa^{-1/2}$.

While nitrides generally outperform other classes, certain carbides also demonstrate excellent hydrogen barrier properties under specific conditions. Titanium carbide (TiC), for example, presents a remarkably low hydrogen permeability of 3.62×10^{-18} $mol.m^{-1}.s^{-1}.Pa^{-1/2}$ at 300 °C, which is comparable to the best nitrides. However, the performance of TiC varies considerably across temperatures and sources, indicating that processing methods, microstructure, and measurement conditions may significantly influence its effectiveness. In contrast, silicon carbide (SiC), another well-known carbide, displays relatively poor performance, with permeabilities as high as 8.5×10^{-13} $mol.m^{-1}.s^{-1}.Pa^{-1/2}$ at 500 °C, thus making it less suitable for demanding hydrogen barrier applications.

Oxide ceramics, as a group, exhibit the broadest range of hydrogen permeabilities. On one end of the spectrum, silicon dioxide (SiO_2) provides high resistance, with values ranging from 2×10^{-17} to 4×10^{-16} $mol.m^{-1}.s^{-1}.Pa^{-1/2}$ over a wide temperature interval of 100–650 °C. Erbium oxide (Er_2O_3) also displays strong hydrogen barrier capability, particularly at mid-range temperatures, with permeabilities in the 2 to 4.1×10^{-16} range. However, many other oxides fall short in performance. Iron oxide in the form of FeO exhibits the highest hydrogen permeability observed in the dataset, at 4.3×10^{-11} $mol.m^{-1}.s^{-1}.Pa^{-1/2}$ at 800 °C. Similarly, Fe_3O_4 and Cr_2O_3 also show poor hydrogen resistance, with values reaching into the 10^{-12} $mol.m^{-1}.s^{-1}.Pa^{-1/2}$ range at elevated temperatures. These results suggest that while some oxides are highly effective, others may be wholly inadequate for hydrogen-rich environments.

Mixed ceramic compositions offer a complex picture. Some combinations yield superior results; for instance, the TiN–TiC composite achieves a permeability as low as 7.9×10^{-18} $mol.m^{-1}.s^{-1}.Pa^{-1/2}$ at 300 °C, indicating synergistic effects between its constituent phases. In contrast, other mixed materials such as the Al_2O_3–TiN–TiC system perform poorly, with permeabilities up to 1.4×10^{-11} $mol.m^{-1}.s^{-1}$.

Table 4
Hydrogen permeability of various ceramic barrier coatings.

	Ceramic coatings	Hydrogen permeability ($mol.m^{-1}.s^{-1}.Pa^{-1/2}$)	T (°C)	Ref.
Nitrides	BN	7.5×10^{-14}	500	[35]
		3×10^{-14}	400	
		1.2×10^{-14}	300	
	TiN	2.21×10^{-14}	500	[133]
		7.58×10^{-15}	400	
		2.12×10^{-15}	300	
		9×10^{-14}	500	[35]
		2.1×10^{-14}	400	
		5.5×10^{-15}	300	
	TiAlN / TiMoN	10^{-14}	500	[182,183]
		2.2×10^{-15}	400	
		7×10^{-16}	300	
	WN	1.57×10^{-15}	400	[184]
	CrWN	1.14×10^{-15}		
	CrN	5.76×10^{-16}		
	ZrN	7.9×10^{-18}		
	AlCrN	3.33×10^{-16}		
	Cr_2N	2.41×10^{-16}		
	TiAlN	2.9×10^{-17}	400	[185]
		4.5×10^{-16}	550	
		$2–5 \times 10^{-16}$	600	
		10^{-13}	500	[182,183]
		2.5×10^{-14}	400	
		7×10^{-15}	300	
	SiN	10^{-17}	400	[186]
Carbides	SiC	8.5×10^{-13}	500	[35]
		2×10^{-13}	400	
		4×10^{-14}	300	
	TiC	4.87×10^{-16}	400	[187]
		2.16×10^{-12}	500	[184]
		2.37×10^{-13}	400	
		1.14×10^{-14}	300	
		7.59×10^{-15}	500	[170]
		1.88×10^{-15}	450	
		3.66×10^{-17}	400	
		3.62×10^{-18}	300	
Oxides	Cr_2O_3	2.54×10^{-12}	700	[125]
		9.2×10^{-13}	650	
		4.1×10^{-13}	600	
		1.19×10^{-13}	550	
	Fe_3O_4	1.6×10^{-12}	600	[188]
	FeO	4.3×10^{-11}	800	
	Y_2O_3	2×10^{-13}	600	[189]
	SiO_2	2×10^{-17} - 4×10^{-16}	100–650	[190]
	Er_2O_3	4.1×10^{-16}	600	[185]
	Al_2O_3	2×10^{-16}	600	
		4×10^{-17}	400	
		6.3×10^{-13}	700	[125]
		2.9×10^{-13}	650	
		1.3×10^{-13}	600	
		5.5×10^{-14}	550	
		1.18×10^{-13}	500	[184]
		7.49×10^{-14}	400	
		7.59×10^{-14}	300	
	Cr_2O_3– Al_2O_3	2.6×10^{-13}	700	[125]
		1.15×10^{-13}	650	
		5.62×10^{-14}	600	
		2.57×10^{-14}	550	
Mixed (carbide, nitride, oxide)	Al_2O_3– TiN–TiC	1.4×10^{-11}	450	[170]
		5.75×10^{-12}	400	
		1.8×10^{-12}	370	
		1.6×10^{-12}	325	
		3 to 7 $\times 10^{-13}$	280	
	TiN–TiC	3.24×10^{-16}	400	[191]
		5.27×10^{-16}	500	[170]
		2.23×10^{-17}	450	
		1.84×10^{-17}	400	
		7.9×10^{-18}	300	

$Pa^{-1/2}$ at 450 °C. These findings highlight the critical role of phase composition and interface structure in determining hydrogen transport behaviour in composite ceramics.

In conclusion, the data decisively indicate that nitrides, especially ZrN, SiN, and TiAlN, along with TiC, exhibit the most promising characteristics for use as hydrogen barriers, combining low permeation rates with temperature resilience. Selecting some carbides and oxides can also perform well, but their effectiveness is more variable and often dependent on specific conditions. Conversely, certain oxides like FeO and mixed compositions such as Al_2O_3–TiN–TiC are demonstrably poor choices for hydrogen containment, due to their high permeability values. The comprehensive comparison provided by this table thus offers a valuable foundation for informed material selection in hydrogen-critical technologies.

5.2.2. Various ceramics coatings

Ceramics' exceptional resistance to heat and corrosion stems from their strong covalent bonding and stable crystalline or amorphous structures, which reduce hydrogen solubility and diffusion rates compared to metals or polymers. These coatings are particularly attractive for components exposed to high-temperature, high-pressure hydrogen environments, including hydrogen pipelines and aerospace systems.

The nitrides group exhibits the broadest range of permeation values, with titanium aluminum nitride (TiAlN) emerging as one of the most effective barriers. This performance is attributed to its dense columnar microstructure, high hardness, and strong covalent-metallic bonding nature, which together suppress hydrogen transport and provide mechanical resilience [170,182,192]. In contrast, boron nitride (BN), relatively open and layered hexagonal structure may explain the poor performance compared to more compact transition metal nitrides. Similarly, although certain nitrides such as ZrN and CrN exhibit relatively low hydrogen permeation rates, their barrier performance is highly dependent on the quality of the deposition process and their stability under irradiation and mechanical stress. Among the coatings investigated, ZrN delivered the most promising overall performance, while Cr_2N exhibited superior adhesion to the substrate. WN demonstrated the lowest residual strain, indicating favourable mechanical compatibility, whereas AlCrN and Cr_2N showed the highest coefficients of thermal expansion (CTE), which may influence thermal mismatch behaviour during service [184].

Hybrid TiN–TiC multilayers, such as those studied in [191], achieve improved performance by combining the toughness of TiC with the low hydrogen diffusivity of TiN. This suggests that multilayer designs can enhance hydrogen barrier effectiveness through the introduction of multiple interfaces and controlled phase stacking. Nitrides are generally unsuitable for use as plasma-facing materials due to their tendency to generate NH_x radicals upon interaction with hydrogen plasma. Furthermore, the potential for nitrogen transmutation into radioactive [186] under irradiation presents additional concerns [193]. Conversely, while titanium carbide (TiC) coatings possess exceptionally high mechanical properties, exceeding 30 GPa in hardness and reaching Young's modulus of approximately 450 GPa, they are prone to adhesion failures when applied to steel substrates [194]. This is primarily attributed to the significant mechanical mismatch with steel, which typically exhibits a hardness in the range of 8–10 GPa and a Young's modulus of around 250 GPa. To address this incompatibility, introducing a titanium nitride (TiN) interlayer has proven effective in mitigating adhesion issues. TiN exhibits a hardness of about 20 GPa, which is more comparable to that of steel, and also offers a thermal expansion coefficient that falls between those of steel ($12.15 \times 10^{-6}\ K^{-1}$) and TiC ($7.4 \times 10^{-6}\ K^{-1}$), specifically $9.4 \times 10^{-6}\ K^{-1}$ for TiN. Additionally, nitrides generally possess a lower Young's modulus than carbides, further contributing to improved mechanical compatibility [195]. WC-based systems, although less frequently reported in permeation studies, show great promise due to their compatibility with tungsten substrates and their ability to form stable interfaces that trap hydrogen species [196].

The oxides category displays the most diverse permeability range, reflecting the heterogeneous nature of oxide structures and their sensitivity to phase purity, porosity, and deposition technique. The hydrogen permeability of iron oxide scales was evaluated, revealing a value of 1.6×10^{-12} $mol.m^{-1}.s^{-1}.Pa^{-1/2}$ at 823 K for scales predominantly composed of Fe_3O_4, and 4.3×10^{-11} $mol.m^{-1}.s^{-1}.Pa^{-1/2}$ at 1073 K for those primarily consisting of wustite (FeO). These findings indicate that the hydrogen permeation through iron oxide layers is approximately one to two orders of magnitude lower than that observed in pure iron. [188]. These elevated values are likely due to their non-dense, defect-rich microstructures and inherent reducibility under hydrogen-rich atmospheres. Oxides like black oxide coatings form a magnetite (FeO) layer when components are immersed in alkaline salt solutions at 130–150 °C. This chemical integration with the substrate produces a layer about 1–2 μm thick [197]. Vitreous coatings applied through induction heating or furnaces protect against corrosion and erosion, offering scalability for hydrogen-related industries [198,199].

Researchers showed oxide materials such as ZrO_2 exhibit excellent chemical inertness and thermal stability, and when processed via controlled techniques such as pulsed laser deposition, can form dense, crack-free coatings with long-term hydrogen resistance [200].

Among oxide composites, the Al–Cr–O system developed by Levchuk et al. [201] reported 2–3.5 times better hydrogen barrier performance at 700 °C compared with Al_2O_3, due to its reduced porosity, improved adhesion, and synergistic phase interactions. The silica-based coating, with a reported permeability in the range of approximately 2×10^{-17} to 4×10^{-16} $mol.m^{-1}.s^{-1}.Pa^{-1/2}$ [190], also demonstrates strong potential, especially when integrated into composite or amorphous oxide systems to enhance barrier uniformity. Overall, while oxides tend to have higher permeability than optimized nitrides, their excellent environmental stability and compatibility with various deposition techniques make them attractive for long-duration or corrosive applications.

From a comparative standpoint, TiAlN from the nitrides group currently ranks among the top-performing ceramic coatings, combining extremely low hydrogen permeability with mechanical durability. However, the best overall performance is increasingly being achieved through multilayer or composite approaches that combine the strengths of multiple ceramic chemistries. These approaches warrant further exploration, especially in scenarios requiring both high-temperature stability and hydrogen resistance.

While many of these coatings perform adequately as single layers, increasing evidence supports the superiority of multilayered and composite architectures, which leverage interfacial effects and structural complexity to enhance hydrogen barrier properties [182,183,187].

TiN combination with TiC in multilayer systems offers an effective approach to mitigating such issues by distributing strain and interrupting continuous diffusion paths [191].

In multi-layered coatings, as crystal grain boundaries become hydrogen diffusion barriers, the interfaces of the films may also serve as effective hydrogen diffusion barriers. Among these, TiAlN continues to show outstanding performance due to its nanocomposite-like structure, where multiple phases such as TiN and AlN enhance both barrier function and mechanical stability. Furthermore, multi-layered TiAlN/TiMoN systems demonstrate reduced permeability and improved fracture resistance in addition to the introduction of interfaces that block diffusion and suppress crack propagation [182]. Also, experimental results demonstrated that coatings with fine-grained microstructures exhibit strong resistance to hydrogen permeation, and this protective effect is further enhanced when multiple coating layers are employed. In such multilayered systems, both the grain boundaries within the crystalline structure and the interfaces between individual layers can act as sites for hydrogen trapping [183].

Among the widely used materials, titanium carbide (TiC) [170], silicon nitride (SiN) [186], and titanium aluminum nitride (TiAlN) [185] have demonstrated notable resistance to hydrogen transport,

provided the coatings are deposited with high structural integrity and minimal porosity. Alumina and chromium oxide excel at blocking hydrogen permeation in high-performance steels but are prone to spalling and cracking at ambient temperatures, as research showed that AISI 304 stainless steel coated with these oxides exhibited flaking and embrittlement under stress tests, compromising their integrity [202].

In conclusion, ceramic coatings hold tremendous potential in mitigating hydrogen-induced damage in metallic systems. With the appropriate combination of material chemistry, deposition precision, and structural engineering, these coatings can play a critical role in advancing safe and durable hydrogen technologies. While many ceramic coatings perform well at elevated temperatures [158,184], there is still a scarcity of systematic data under ambient or cyclic conditions. Extrapolation of high-temperature behavior to room-temperature performance is often unreliable due to the nonlinear and material-specific nature of hydrogen diffusion kinetics. Additionally, variability in experimental procedures and limited long-term testing under service-like conditions hinder the direct comparison of coating systems.

5.2.3. Techniques for applying ceramic coatings

The application of ceramic coatings can be achieved through various techniques. PVD coatings provide continuous, low-permeability layers that act as hydrogen diffusion barriers, while their improved surface hardness helps mitigate microcrack formation.

According to studies, sputtered coatings of materials such as various nitride ceramics are frequently utilized in corrosive and hydrogen-prone environments, offering exceptional hardness, thermal stability, and resistance to HE [133,184].

Low-pressure chemical vapour deposition (LPCVD)-deposited silicon nitride films are typically stoichiometric and contain relatively low concentrations of hydrogen. In contrast, plasma-enhanced chemical vapour (PECVD) silicon nitride films are generally non-stoichiometric and incorporate significantly higher hydrogen content. It is important to note that the CVD nitride layers were deposited on a thinner underlying oxide. This further substantiates the conclusion regarding the superior stability of CVD nitride, as the thinner oxide would facilitate more rapid hydrogen diffusion compared to the thicker oxide typically used with PECVD nitride [203].

However, CVD techniques face significant challenges. One key limitation is the residual tensile stress generated during deposition due to thermal gradients and lattice mismatches between the Al_2O_3 coating and steel substrate. These stresses can induce microcracks upon cooling or thermal cycling, acting as hydrogen entry points [125]. Advanced solutions, such as tailoring precursor ratios or introducing stress-relief buffer layers, can be proposed. However, it requires further validation across different substrates and environments.

LPCVD is particularly effective for silicon nitride coatings, where hydrogen is trapped in deeper layers, maximizing the barrier's efficiency [203]. Applications include TiN, SiC, CrN, and diamond-like carbon (DLC) coatings, which excel in environments prone to corrosion, especially those involving chloride ions [132,204,205].

Mittra et al. [200] emphasized the importance of deposition quality, showing that pulsed laser deposited (PLD) ZrO_2 coatings exhibited significantly better hydrogen resistance than naturally grown oxide layers on zirconium alloys. Their dense and amorphous microstructure effectively blocked hydrogen transport, reducing absorption by more than an order of magnitude.

Plasma spraying yields dense coatings, such as titanium carbide (TiC) and zirconium dioxide (ZrO_2), that are highly suitable for high-temperature applications. Advances in high-velocity oxygen fuel (HVOF) and high-velocity air fuel (HVAF) spraying have minimized porosity and microcracks, leading to more compact and hydrogen-resistant coatings [206]. However, achieving uniform coverage and eliminating residual porosity remain challenges, especially for large-scale applications.

To develop high-performance tritium permeation barriers for ferritic steels, conducted by Zhang et al. [144], a combined approach, utilizing sol–gel and electrolytic deposition techniques, was explored. Initially, a 50 nm-thick ZrO_2 thin film was deposited on SS430 ferritic steel using the sol–gel dip-coating method. This process enabled the formation of a nanostructured oxide layer; however, the inherent porosity of sol-gel-derived coatings presented a challenge for achieving optimal barrier integrity. To address this, an electrolytic deposition step was subsequently applied as an innovative sealing strategy, whereby open pores in the sol–gel film were infiltrated and sealed with either ZrO_2 or Al_2O_3. This secondary treatment increased the overall coating thickness to approximately 100 nm and substantially improved the film's continuity and density. Hydrogen permeation tests conducted at 300–600 °C revealed that the initial sol–gel-derived ZrO_2 layer provided modest barrier performance, with a permeation reduction factor (PRF) in the range of 6–100. The PRF is defined as the ratio of hydrogen permeation flux (J) through an uncoated substrate to that through a coated substrate under identical conditions, which can be calculated by Eq. (11) [207]:

$$PRF = \frac{J_{uncoated}}{J_{coated}} \quad \text{Eq. 11}$$

In contrast, after electrolytic sealing, the PRF increased significantly to values between 100 and 1000, demonstrating a marked enhancement in resistance to hydrogen permeation. These results highlight the effectiveness of the electrolytic deposition process in mitigating microstructural defects such as open pores, which act as fast diffusion pathways. Furthermore, the study underscores the importance of optimizing key process parameters, particularly current density and post-deposition heat treatment temperature, to achieve consistently high barrier performance. The synergy between sol–gel deposition for uniform coating formation and electrolytic deposition for defect sealing offers a promising route toward engineered multilayer ceramic coatings with superior hydrogen isotope barrier properties.

In another study [138], ZrO_2 coatings approximately 180 nm in thickness were synthesized on ferritic steel substrates using sol-gel-based wet-chemical techniques, specifically dip coating and electrolytic deposition. The sol-gel process enabled the formation of uniform, adherent, and nanostructured ceramic layers with controlled microstructural features. These coatings exhibited excellent hydrogen permeation resistance across the temperature range of 300–550 °C, as evidenced by PRFs consistently exceeding 1000. Notably, the barrier performance achieved here was significantly superior, by approximately an order of magnitude, to that reported in earlier work for thinner ZrO_2 coatings (100 nm) at temperatures up to 400 °C, despite only a modest increase in thickness. This substantial enhancement is attributed not only to the increased coating thickness but also to the improved microstructural quality imparted by the sol-gel route, which effectively reduces interconnected defect pathways. Moreover, upon exposure to deuterium–tritium gas at 300 °C, the sol-gel-derived ZrO_2 coatings exhibited markedly higher tritium retention compared to dense, bulk yttria-stabilized zirconia (YSZ) in both single-crystalline and polycrystalline forms. These findings underscore the critical role of microstructural imperfections, particularly grain boundaries and residual porosity, in dictating hydrogen isotope transport and trapping behaviour. The superior barrier characteristics of the thicker sol-gel-derived coatings are likely a result of the suppression of through-thickness defects, thereby hindering direct diffusion pathways from the surface to the coating–substrate interface.

To improve hydrogen isotope barrier performance in structural steels, a titanium carbide (TiC) coating was developed using the pack cementation method followed by heat treatment [208]. This process yielded a bilayer structure: an outer titanium nitride (TiN) layer and an inner titanium-enriched diffusion zone within the steel. This titanized coating significantly reduced the hydrogen permeation current density from 19 $\mu A.cm^{-2}$ (uncoated steel) to 2.22 $\mu A.cm^{-2}$.

Further enhancement was achieved through post-titanizing surface treatments. Specifically, the TiC-coated steel underwent nitridation in

flowing ammonia at 760 °C for 1 h, followed by oxidation in air under the same conditions. This process produced a dense, three-layer nitridation–oxidation coating (NOC), consisting of a rutile TiO_2 outer layer, a Ti–N middle layer, and a Ti–C inner layer. Microstructural analysis revealed that this configuration effectively eliminated intergranular porosity and achieved superior surface densification. Consequently, the hydrogen permeation current density was dramatically reduced to 0.13 $\mu A.cm^{-2}$, marking a significant improvement in barrier performance.

In contrast, direct oxidation of the TiC coating (without prior nitridation) led to a structurally inferior oxidized coating (OC). This OC showed surface coarsening, delamination, and high porosity, which compromised mechanical integrity and resulted in a higher hydrogen permeation current density of 1.14 $\mu A.cm^{-2}$. These results highlight the essential role of nitridation in forming a compact, stable microstructure that enhances the hydrogen barrier performance of ceramic coatings.

In a detailed investigation, FeAl-based multilayer HBCs were successfully developed on 316L stainless steel using a combination of pack cementation and sol–gel techniques [209]. Two distinct systems were synthesized: a bilayer $FeAl/Al_2O_3$ and a trilayer $FeAl/Al_2O_3/TiO_2$ coating. The sol–gel method enabled the formation of a dense, stable α-Al_2O_3 intermediate layer approximately 1 μm thick. For the trilayer system, the addition of a TiO_2 top layer increased the total thickness to about 1.5 μm. Microscopic examinations confirmed that the trilayer coating possessed a compact, crack-free, and well-adhered structure, indicating high microstructural integrity.

Mechanical performance assessments, carried out via scratch testing, showed that the trilayer $FeAl/Al_2O_3/TiO_2$ coating achieved a higher critical load of 55.8 N before delamination, compared to 51.2 N for the bilayer $FeAl/Al_2O_3$ system. This enhanced interfacial bonding was accompanied by improved toughness and ductility, highlighting the mechanical reinforcement provided by the TiO_2 layer. More importantly, hydrogen permeation tests revealed that the trilayer coating was markedly more effective at suppressing hydrogen ingress at room temperature. In terms of normalized current density reduction after hydrogen exposure, the trend followed a significant order of magnitude: uncoated 316L steel:$FeAl/Al_2O_3$:$FeAl/Al_2O_3/TiO_2$ = 1:26:120. This substantial improvement underscores the critical role of the TiO_2 top layer in elevating hydrogen barrier performance, positioning the $FeAl/Al_2O_3/TiO_2$ system as a highly effective candidate for hydrogen-resistant applications in harsh environments.

A composite Al_2O_3/Cr_2O_3 coating was developed on steel using a hybrid method combining pack cementation and sol–gel processes, synchronized with heat treatment to preserve the steel's mechanical integrity [210]. The resulting multilayer coating featured an outer α-/θ-Al_2O_3 layer, a transitional Al_2O_3–Cr_2O_3 mixed layer, and an inner Cr–Fe diffusion layer. The Microstructural analysis confirmed a dense, crack-free structure with strong adhesion, while XRD revealed the formation of stable α-Al_2O_3 and Cr_2O_3 phases, likely stabilized by their mutual interaction.

Hydrogen permeation tests showed a substantial performance enhancement, with current density dropping from 17.1 $\mu A.cm^{-2}$ (uncoated) to 0.27 $\mu A.cm^{-2}$. This dramatic reduction highlights the coating's effectiveness as a tritium barrier, making it a promising solution for high-temperature applications.

The precision of ALD techniques enables the deposition of dense barrier films such as Al_2O_3, Cr_2O_3, BN, TiO_2, and multilayer oxides, e.g., Cr_2O_3/Al_2O_3, which exhibit excellent performance in resisting hydrogen permeation and HE. ALD-grown Al_2O_3, in particular, has been extensively studied and demonstrates low gas permeability, high dielectric strength, and mechanical integrity under thermal and chemical exposure [146,148].

A study by Bull et al. [147] has shown that ALD-grown BN films act as highly effective hydrogen barriers at temperatures up to 1770 K, even outperforming high hydrogen barrier traditional tungsten coatings due to BN's combination of chemical inertness and high activation energy for hydrogen diffusion. The smoothness and grain-boundary-free microstructure of ALD-BN effectively suppresses hydrogen ingress, while their thermal stability and nitrogen retention are superior even in reducing environments.

Another significant advancement is the development of Cr_2O_3/Al_2O_3 bilayer coatings, as demonstrated by Zhang et al. [148]. These bipolar oxide films utilize a p-n junction interface between Cr_2O_3 (p-type) and Al_2O_3 (n-type), which generates an internal electric field that further impedes hydrogen diffusion. Moreover, these ALD coatings on stainless steel substrates yield structurally robust and thermally compatible layers with significantly reduced hydrogen permeability, validated under plasma discharge conditions.

The dip coating method has been reported to deposit nanocrystalline cerium oxide (CeO_2) particles on the surface of a SiC membrane, resulting in a uniformly porous microstructure. This pressureless fabrication method enabled the formation of CeO_2 at both the surface and cross-section of the membrane, which significantly influenced its gas permeation behavior. By adjusting the dip-coating parameters, the porosity and density of the membrane could be finely controlled, offering a tunable approach to optimize gas transport properties for advanced separation or barrier applications [211].

Advances in deposition techniques and multi-layer coating strategies continue to enhance their effectiveness, paving the way for broader adoption in hydrogen-related applications.

5.3. Polymer coatings

To date, research on the use of polymers and polymer composite coatings as HBCs has been reported, but it has not been comprehensively explored. Therefore, this study focuses more on the application of organic coatings and innovative strategies for combating HE.

5.3.1. Hydrogen permeability of polymers

The permeability of polymers to hydrogen is one of the critical properties influencing their effectiveness as HBCs. Although no polymeric coating is entirely impermeable to hydrogen molecules, various polymer properties and characteristics impact gaseous permeability. Factors such as polymer type, crystallinity, density, molecular alignment, and the inclusion of crosslinking or fillers significantly affect hydrogen diffusion rates [156,212,213]. Zhang et al. [214] present a detailed explanation of the mechanisms behind hydrogen permeation in polymers, particularly high-density polyethylene (HDPE) and ethylene-vinyl alcohol (EVOH). The hydrogen permeation process involves two primary stages: adsorption and diffusion. In the adsorption stage, hydrogen molecules preferentially accumulate in regions of the polymer matrix with low potential energy, creating non-uniform distributions or clusters. This is more pronounced in HDPE, which offers more adsorption sites due to its weaker intermolecular forces. EVOH, on the other hand, forms strong hydrogen bonds between its hydroxyl groups, resulting in less available space for hydrogen adsorption and a lower overall adsorption density.

During the diffusion stage, hydrogen molecules exhibit localized vibrational motion interspersed with occasional long-range jumps between voids or "holes" in the polymer matrix. In HDPE, these transitions occur more frequently and over larger distances due to its higher free volume and weaker internal bonding, allowing hydrogen molecules to move more actively. In contrast, the tight structure of EVOH, reinforced by strong hydrogen bonding, significantly restricts molecular motion, leading to reduced diffusion.

5.3.1.1. Key factors influencing permeability

5.3.1.1.1. Polymer type and crystallinity. Permeability generally decreases with increasing crystallinity due to reduced free volume. Fujiwara et al. [155] observed that materials with higher degrees of crystallinity, such as HDPE and especially HDPE (PE100), exhibit significantly lower hydrogen permeability and less structural damage

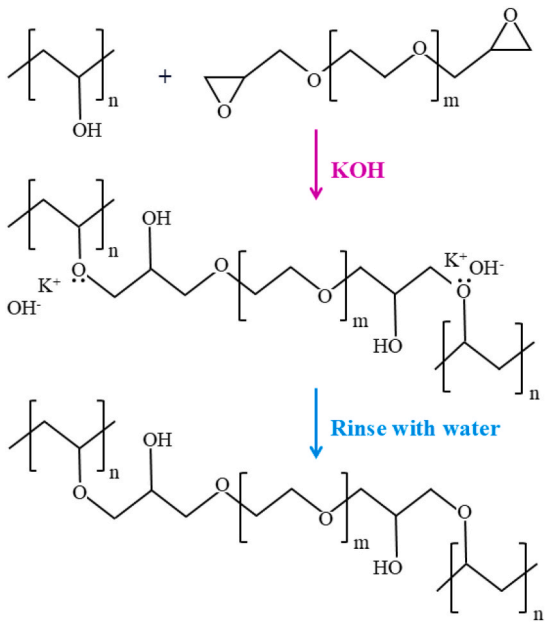

Fig. 18. The crosslinking reaction between PVA and PEGDGE. In this process, crosslinking reaction occurs through the nucleophilic attack of the hydroxyl groups on PVA molecules, which target the carbon atom of the terminal epoxide rings in PEGDGE, leading to ring-opening and subsequent crosslink formation [41].

when exposed to hydrogen pressures up to 90 MPa. This behaviour is largely attributed to the reduced free volume in crystalline regions, which limits hydrogen diffusion. Conversely, materials with lower crystallinity, such as low-density polyethylene (LDPE) and linear low-density polyethylene (LLDPE), showed higher permeation rates and pronounced structural damage (e.g., blistering and void formation) upon hydrogen exposure. These materials allow more hydrogen to penetrate due to their larger amorphous regions and higher free volume, which also increases the likelihood of mechanical failure during decompression. Additionally, the study demonstrates that under hydrostatic pressure, polyethylene's crystallinity slightly increases due to the compaction of the amorphous phase, further reducing hydrogen solubility and diffusion. However, this pressure-induced increase in crystallinity is reversible and modest in magnitude. Notably, the solubility of hydrogen remains confined to amorphous regions, reinforcing the conclusion that higher crystallinity enhances resistance to hydrogen permeation. This suggests that optimizing polymer crystallinity could be a promising strategy for designing low-permeability coatings for hydrogen storage and transport applications, although their long-term durability under operational conditions remains to be fully established.

Takeuchi et al. [215] highlight that hydrogen molecules tend to reside in the polymer matrix or at the interface between polymer and water domains, rather than fully in water-rich regions. Moreover, polymer crystallinity and equivalent weight (EW) critically affect permeation. High-EW membranes tend to develop local semicrystalline structures that reduce void space and restrict hydrogen diffusion through tightly packed polymer chains, lowering both solubility and diffusivity. Conversely, low-EW membranes contain fewer PTFE regions and exhibit highly tortuous aqueous domains, which hinder hydrogen diffusion and reduce solubility.

5.3.1.1.2. Density. The effect of polymer density on hydrogen permeation in polymers is closely linked to the material's ability to impede molecular transport, which is critical for preventing HE in steel pipelines. Lei et al. [40] studied a range of polymeric materials, including poly(vinyl alcohol) (PVA), poly(vinyl chloride) (PVC), and epoxy resins, that were evaluated for hydrogen permeability. It was found that polymers with higher density and more compact molecular structures demonstrated lower hydrogen permeability. Notably, crosslinked PVA, which forms a denser network through glutaraldehyde crosslinking, achieved the lowest hydrogen permeability in their study. This is attributed to the increased density from intra- and intermolecular hydrogen bonding that limits free volume and diffusivity paths for hydrogen molecules. Higher-density polymers reduce both solubility and diffusivity of hydrogen, the two main components that govern permeation.

According to another study [216], there is a clear inverse correlation between polymer density and hydrogen permeability. Lower-density polymers tend to exhibit higher hydrogen flux, indicating a more open polymer matrix that facilitates the diffusion of small molecules like hydrogen. This trend is attributed to the fact that lower density often implies greater free volume within the polymer structure, which enhances gas diffusivity. For instance, polystyrene, which has relatively low density, demonstrated both high hydrogen permeability and favourable selectivity over carbon dioxide in pure gas tests. However, this relationship is nuanced by the presence of crystallinity and solubility effects. Highly crystalline regions in a polymer can act as barriers with very low permeability, effectively reducing the overall hydrogen permeability regardless of polymer density.

5.3.1.1.3. Crosslinking. The effect of crosslinking on the permeability of polymers like PVA varies depending on the type of crosslinking agent used. In some cases, crosslinking leads to a reduction in permeability due to the formation of a denser molecular network, as observed in glutaraldehyde-crosslinked PVA. However, other crosslinking systems, such as those utilizing diepoxy-based crosslinkers, e.g., poly (ethylene glycol) diglycidyl ether, PEGDGE, have been reported to increase permeability. This increase is attributed to a reduction in polymer crystallinity, which enhances free volume and facilitates gas diffusion. Therefore, the impact of crosslinking on the polymer's permeability is not universal and must be evaluated based on the specific crosslinking chemistry employed [217]. Fig. 18 illustrates the crosslinking reaction between PVA and PEGDGE [41].

In another study, Saha et al. [218] demonstrated that crosslinking significantly reduces hydrogen permeation in polymers by limiting

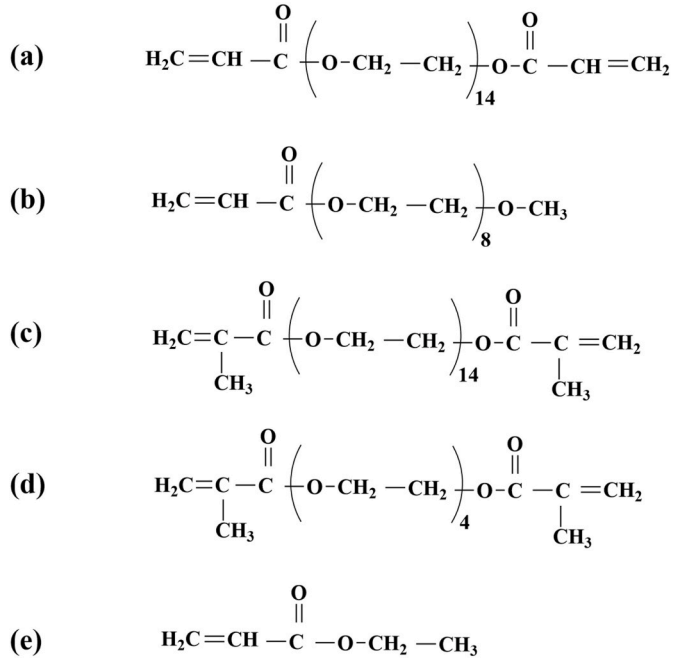

Fig. 19. Structures of some monomers and cross-linkers [219]: (a) Poly (ethylene glycol) diacrylate (PEGDA), (b) Poly(ethylene glycol) methyl ether acrylate (PEGMEA), (c) Poly(ethylene glycol) dimethacrylate (PEGDMA), (d) Tetra(ethylene glycol) dimethacrylate (TEGDMA), (e) Ethylacrylate (EA).

chain mobility and decreasing free volume within the matrix. Specifically, the authors developed a semi-interpenetrating network (S-IPN) composed of thermoplastic polyurethane (TPU) and epoxy, where epoxy forms a crosslinked structure entangled with TPU chains. This architecture not only improved the mechanical strength and thermal stability of the coating but also dramatically suppressed hydrogen gas transmission. For example, a 40 wt% epoxy-based S-IPN (S-IPN2) showed a 62 % reduction in hydrogen gas transmission rate (H_2GTR) compared to uncoated nylon 6 at room temperature.

H_2GTR quantifies the rate at which molecular hydrogen permeates through a material under controlled conditions of temperature and pressure. It is typically measured using a gas permeability apparatus that monitors the pressure change across a test membrane. According to Eq. (12), the transmission rate is calculated using parameters such as the pressure differential across the sample, the test chamber volume, the exposed surface area, and the temperature, with corrections for gas constants [218].

$$\mathrm{GTR} = \frac{\ln\left(\frac{p_{n+1}-p_n}{p_n-p_\infty}+1\right)V}{dtaTR_m} \qquad \text{Eq. 12}$$

In this analysis, p_n represents the pressure on the bottom side (test chamber) of the sample at a specific time n, while p_∞ corresponds to the pressure on the top side, where hydrogen gas is introduced. The test chamber volume is denoted by V (cm^3), and dt indicates the time difference between n and n+1, expressed in days. The exposed sample area is given as a (m^2), and the test temperature T is in Kelvin. The term R represents the universal gas constant normalized by the molar volume ($V_m = 0.00371$ bar·K^{-1}), under standard conditions.

The study by Lin et al. [219] investigated the influence of cross-linking on hydrogen and other gas permeation in poly (ethylene glycol) diacrylate (PEGDA) networks. Their results showed that hydrogen permeability, along with solubility and diffusivity, is largely independent of cross-link density across a series of cross-linked PEGDA polymers when water is used to modulate the cross-link density. Despite varying the amount of cross-linking by adjusting the water content in prepolymer solutions, the polymers maintained constant density, fractional free volume, and glass transition temperatures. This indicates that, contrary to many assumptions in the literature, cross-linking alone does not necessarily restrict gas transport or significantly alter the polymer's physical structure in rubbery network polymers like XLPEGDA. Moreover, their analysis suggested that attributing changes in gas permeation behaviour purely to cross-link density can be misleading if other structural or chemical variables, such as chain end group concentration or crystallinity, are not properly controlled. Specifically for hydrogen, which is a small penetrant, its diffusion and permeability appear unaffected by the degree of cross-linking, likely due to the retention of similar free volume and chain flexibility across the series. Thus, in such network polymers, cross-linking might not be a dominant factor in controlling hydrogen permeation unless accompanied by other concurrent changes in polymer microstructure. Fig. 19 illustrates structures of relevant monomers and cross-linkers.

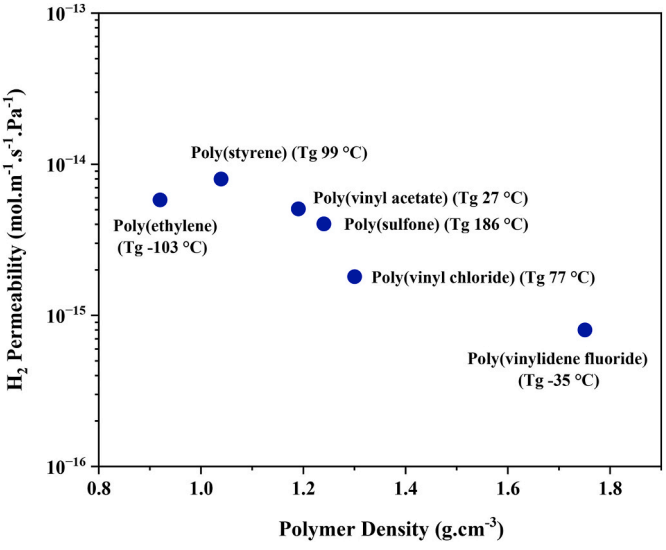

Fig. 20. Plot of polymers density against hydrogen permeability [216].

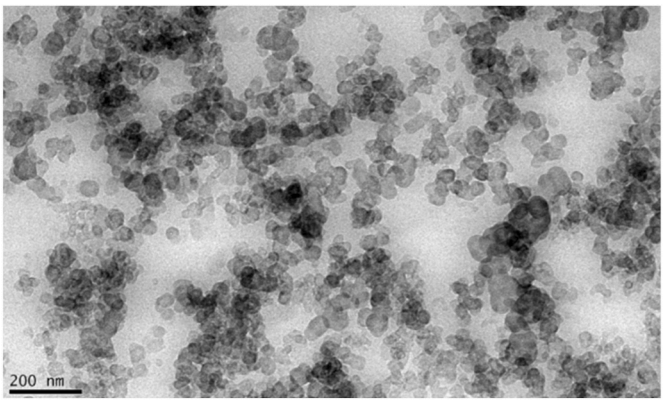

Fig. 21. TEM observation showing CB particles (appearing as black or gray spheres) embedded within a peroxide-crosslinked EPDM composite [221].

5.3.1.1.4. Glass transition temperature (Tg). Above the glass transition temperature (*Tg*), polymer chains become more mobile, increasing permeability. Below the *Tg*, the polymer exists in a glassy state characterized by rigid and less mobile polymer chains, limiting diffusion [213]. Deckers et al. [220] showed that *Tg* significantly influences hydrogen permeation in polymers such as isotactic polypropylene (IPP). This results in a reduced free volume and lower segmental motion, thereby restricting the diffusion pathways available for small penetrant molecules like hydrogen (H_2). Above *Tg*, the polymer enters a rubbery state, where increased chain mobility and segmental dynamics lead to enhanced free volume and molecular motion, thereby facilitating higher diffusivity.

Orme et al. [216] reported the effect of the *Tg* on hydrogen permeation in polymers indirectly through polymer density and structure-related permeability characteristics. Polymers with lower density, which generally correlate with a more amorphous and flexible structure (often associated with temperatures above *Tg*), tend to demonstrate higher hydrogen permeability. For instance, polystyrene, which has a relatively low density and a *Tg* above room temperature, exhibits both high hydrogen permeability and good selectivity over carbon dioxide. This implies that when a polymer is tested below its *Tg*, it behaves in a more glassy and rigid manner, restricting the motion of polymer chains and limiting gas diffusion. Conversely, polymers that are above or near their *Tg* under test conditions exhibit more segmental mobility, facilitating gas transport. Fig. 20 shows the obtained permeability of different polymers with various densities and *Tg*.

5.3.1.1.5. Additives and fillers. Inorganic fillers, such as silica and clay, create physical barriers to gas diffusion, decreasing permeability depending on filler type, shape, and interaction with the polymer [212].

Jung et al. [221] reported that the addition of fillers significantly influences hydrogen permeation behaviour in ethylene propylene diene monomer (EPDM) polymers. According to the study, carbon black (CB) fillers, due to their porous nature, introduced dual-mode sorption mechanisms comprising Henry's absorption into the polymer matrix and Langmuir adsorption at the filler interface. This dual sorption resulted in higher hydrogen uptake with increasing CB content. In contrast, silica-filled and neat EPDM followed single-mode sorption governed by Henry's law, indicating that silica does not significantly interact with

Table 5
Hydrogen permeability of various polymer barrier coatings.

Polymer material	H_2 permeability (mol.$m^{-1}.s^{-1}.Pa^{-1}$)	Ref.
PVA + glutaraldehyde (PVA + GA)	2.81×10^{-18}	[40]
PVA + poly(ethylene glycol) diglycidyl ether (PEGDGE)	3.35×10^{-18}	[41]
Poly(vinyl alcohol) (PVA)	5.02×10^{-18}	[40]
Poly(vinylidene chloride) (PVDC)	1.60×10^{-17}	[135]
Ethylene–vinyl alcohol copolymer (EVAL)	1.67×10^{-16}	[216]
Poly(vinyl fluoride) (PVF)	1.80×10^{-16}	[224]
Diglycidyl ether of bisphenol A/ polyetheramine (DGEBA/D400)	$4.99–5.06 \times 10^{-16}$	[40]
Polyamide 11 (PA 11)	$3.22–7.04 \times 10^{-16}$	[225]
Kynar® (poly(vinylidene fluoride), PVDF)	8.04×10^{-16}	[216]
Poly(vinyl chloride) (PVC)	8.17×10^{-16}	[40]
Chloro-isobutene–isoprene rubber (CIIR)	8.57×10^{-16}	[224]
High-density polyethylene (HDPE)	$4.93–9.25 \times 10^{-16}$	[155,225, 226]
Medium-density polyethylene (MDPE)	$5.96–10.62 \times 10^{-16}$	[155]
Ultra-high-molecular-weight polyethylene (UHMWPE)	$8.84–14.57 \times 10^{-16}$	[155,226]
Poly(methyl methacrylate) (PMMA)	$0.124–8.04 \times 10^{-16}$	[216,224]
Cross-linked poly(ethylene oxide) (XLPEGD)	$1.69–1.77 \times 10^{-15}$	[219]
Linear low-density polyethylene (LLDPE)	$1.18–2.20 \times 10^{-15}$	[155]
Isobutene–isoprene rubber (IIR)	2.42×10^{-15}	[224]
Acrylonitrile–isoprene rubber (NIR)	2.49×10^{-15}	
Poly(styrene-co-butadiene)	2.65×10^{-15}	[216]
Styrene–butadiene rubber (SBR)	2.98×10^{-15}	[224]
Polytetrafluoroethylene (PTFE)	3.20×10^{-15}	
Poly(benzyl methacrylate) (PBMA)	3.68×10^{-15}	[216]
Chloro-sulfonyl polyethylene (CSM)	$1.31–3.68 \times 10^{-15}$	[224]
Polysulfone (PSU)	4.05×10^{-15}	[216]
Natural rubber (NR)	4.09×10^{-15}	[224]
Chloroprene rubber (CR)	$2.23–4.55 \times 10^{-15}$	
Poly(vinyl acetate) (PVAc)	5.06×10^{-15}	[216]
Low-density polyethylene (LDPE)	$1.33–5.79 \times 10^{-15}$	[155,216, 225–227]
Polyurethane (PU)	$0.663–6.06 \times 10^{-15}$	[135]
Ethylene–propylene–diene terpolymer (EPDM)	6.96×10^{-15}	[228]
Fluoroelastomer (FKM)	$3.50–7.32 \times 10^{-15}$	[224]
Biaxially oriented polypropylene (BOPP)	7.81×10^{-15}	[227]
Polystyrene (PS)	$7.58 - 7.97 \times 10^{-15}$	[216,224]
Acrylonitrile–butadiene rubber (NBR)	$1.45–8.43 \times 10^{-15}$	[224,228]
Poly(propylene glycol) (PPG)	$1.28–19.7 \times 10^{-15}$	[229]
Fluorinated polyimide (FPI)	$1.60–36.2 \times 10^{-15}$	[135]
Polypropylene (PP)	1.38×10^{-14}	[224]
Polybutadiene (BR)	1.41×10^{-14}	
Poly(phenylmethyl siloxane) (PMPS)	3.85×10^{-14}	[230]
Poly(methylsilylene-co-phenylsilylene) (PMSPS)	8.71×10^{-14}	
Silicone rubber (VMQ)	1×10^{-13}	[224]
Polydimethylsiloxane (PDMS)	$1.25 - 2.17 \times 10^{-13}$	[216,227, 230]
Poly(trimethylsilylpropyne) (PTMSP)	5.52×10^{-12}	[231]

hydrogen at the filler interface. Furthermore, the type and concentration of filler affected hydrogen diffusivity differently. In silica-filled EPDM, diffusivity decreased linearly with filler content, attributed to the extended tortuous diffusion path. However, CB-filled EPDM showed an exponential decline in diffusivity due to the combined effects of increased tortuosity, stronger polymer-filler interactions, and hydrogen adsorption at CB surfaces. These changes in diffusivity were the dominant factor affecting permeability, more so than solubility. Notably, permeability correlated exponentially with physical properties like density and hardness in CB-filled composites, a trend explained by the reduced fractional free volume caused by filler-induced densification of the polymer matrix. Fig. 21 depicts a TEM image of a CB-filled EPDM composite.

In another study [222], they investigated how CB and silica fillers influence hydrogen permeation in peroxide-crosslinked EPDM composites. It was found that adding CB fillers significantly increased hydrogen solubility due to both absorption into the polymer matrix and physical adsorption at the CB filler interfaces. In contrast, silica-filled EPDM composites displayed hydrogen solubility nearly identical to that of neat EPDM, indicating minimal interaction between silica and hydrogen molecules.

Yamabe and Nishimura [223] reported the effect of fillers, carbon black (CB) and silica (SC), on hydrogen permeation in ethylene–propylene rubber and nitrile–butadiene rubber (NBR) composites, which are used in O-rings for high-pressure hydrogen applications. It was found that hydrogen permeation follows Henry's law across all samples, indicating molecular hydrogen solubility is linearly related to pressure. However, the type of filler significantly influences the hydrogen uptake and subsequent material performance. CB-containing composites demonstrated higher hydrogen content than those with SC or no fillers. This increase is attributed to both the intrinsic trapping capability of CB and an enhancement in hydrogen solubility within the polymer matrix, suggesting a dual contribution to the elevated hydrogen uptake. The elevated hydrogen content in CB-filled composites correlated with increased blister formation and severity following decompression. In contrast, SC-filled composites showed minimal blistering despite comparable or superior mechanical reinforcement. This discrepancy is due to SC's negligible hydrogen trapping and the favourable mechanical properties it imparts, such as higher elastic modulus and fracture resistance. Thus, while CB enhances mechanical strength, it compromises hydrogen resistance due to its affinity for hydrogen retention. The study concludes that selecting fillers like silica, which do not promote hydrogen trapping yet reinforce the material, is critical for developing hydrogen-compatible rubber components.

5.3.1.1.6. Hydrogen permeability data. The hydrogen permeability values of various polymers, as extracted from studies, are summarized in Table 5.

These values reflect hydrogen gas permeability through polymers, which is crucial for applications like gas storage, piping systems, packaging, and hydrogen fuel infrastructure. A detailed scientific analysis reveals that hydrogen permeability among polymers spans a wide range, from as low as 10^{-18} to as high as 10^{-12} mol.$m^{-1}.s^{-1}.Pa^{-1}$, indicating significant differences in performance depending on molecular structure, polarity, crystallinity, and free volume.

Among the tested materials, the best hydrogen barrier is polyvinyl alcohol (PVA) modified with glutaraldehyde (PVA+GA), which exhibits an exceptionally low permeability of 2.81×10^{-18} mol.$m^{-1}.s^{-1}.Pa^{-1}$. The second-best candidate is polyvinyl alcohol (PVA) crosslinked with poly (ethylene glycol) diglycidyl ether (PEGDGE), exhibiting a hydrogen permeability of 3.35×10^{-18} mol.$m^{-1}.s^{-1}.Pa^{-1}$. While this value is lower than that of unmodified PVA with a lower molecular weight, which stands at 5.02×10^{-18} mol.$m^{-1}.s^{-1}.Pa^{-1}$, the reduction is primarily attributed to the use of higher molecular weight PVA, rather than the crosslinking itself. In fact, the Lei et al. [41] study shows that PEGDGE crosslinking generally increases permeability due to reduced polymer crystallinity. Therefore, while PEGDGE enhances the rheological properties necessary for coating applications, it does not improve, and can slightly compromise, the barrier properties of PVA films. Closely following these are polyvinylidene chloride (PVDC) with a permeability of 1.60×10^{-17} mol.$m^{-1}.s^{-1}.Pa^{-1}$ and polyamide 11 (PA 11), which ranges from 3.22 to 7.04×10^{-16} mol.$m^{-1}.s^{-1}.Pa^{-1}$. These materials are all characterized by a high degree of polarity and often semi-crystalline structures that tightly pack polymer chains, minimizing the diffusion pathways for hydrogen molecules.

In contrast, the worst performers in terms of hydrogen permeability are materials such as poly(trimethylsilyl propyne) (PTMSP), which demonstrates a staggering permeability of 5.52×10^{-12} mol.$m^{-1}.s^{-1}.Pa^{-1}$. This makes PTMSP the most permeable material in the list and therefore the least suitable for hydrogen containment applications. PTMSP's poor performance can be attributed to its highly porous

structure and unusually high free volume, traits that are advantageous for other uses such as gas separation membranes but disadvantageous for containment. Other high-permeability materials include polydimethylsiloxane (PDMS) with a permeability of 1.25–2.17 × 10^{-13} mol.m^{-1}.s^{-1}.Pa^{-1} and silicone rubber (VMQ), which has a similarly high value of 1 × 10^{-13} mol.m^{-1}.s^{-1}.Pa^{-1}. These siloxane-based materials are known for their high flexibility and low glass transition temperatures, features that facilitate gas diffusion and result in poor barrier performance. Poly phenylmethyl siloxane (PMPS), another siloxane variant, also falls into the group of poor barriers, with a permeability of 3.85 × 10^{-14} mol.m^{-1}.s^{-1}.Pa^{-1}. Rubber materials such as polybutadiene (BR) and polypropylene (PP) also display high permeability values: 1.41 × 10^{-14} mol.m^{-1}.s^{-1}.Pa^{-1} and 1.38 × 10^{-14} mol.m^{-1}.s^{-1}.Pa^{-1}, respectively, due to their nonpolar and amorphous molecular structure that lacks hydrogen barrier performance.

Several polymers fall into an intermediate range, offering moderate hydrogen barrier properties. These include common polyethylenes such as high-density polyethylene (HDPE), which ranges from 4.93 to 9.25 × 10^{-16} mol.m^{-1}.s^{-1}.Pa^{-1} and is the best among the polyethylene variants due to its high crystallinity. Medium-density polyethylene (MDPE) and ultra-high molecular weight polyethylene (UHMWPE) perform slightly worse, with values reaching as high as 14.57 × 10^{-16} mol.m^{-1}.s^{-1}.Pa^{-1}. Low-density polyethylene (LDPE) and linear low-density polyethylene (LLDPE) are less effective still, with permeability ranges of 1.33–2.84 × 10^{-15} mol.m^{-1}.s^{-1}.Pa^{-1} and 1.18–2.20 × 10^{-15} mol.m^{-1}.s^{-1}.Pa^{-1}, respectively. This hierarchy correlates with the general trend that increasing crystallinity and molecular weight reduce gas permeability. Among elastomers, chloro-isobutene-isoprene rubber (CIIR) performs comparatively well with a permeability of 8.57 × 10^{-16} mol.m^{-1}.s^{-1}.Pa^{-1}, making it the best among the rubber-based materials. Other rubbers such as acrylonitrile-butadiene rubber (NBR), natural rubber (NR), styrene-butadiene rubber (SBR), and isobutene-isoprene rubber (IIR) show values in the range of 1.45–4.09 × 10^{-15} mol.m^{-1}.s^{-1}.Pa^{-1}, which is moderately permeable but may be acceptable in less critical applications or where flexibility is a higher priority.

Materials such as polystyrene (PS) and its biaxially oriented form (BOPP) have permeability values of 7.58–7.97 × 10^{-15} and 7.81 × 10^{-15} mol.m^{-1}.s^{-1}.Pa^{-1}, respectively, indicating moderate performance that could be sufficient for packaging or insulation in less hydrogen-sensitive environments. Engineering plastics such as polymethyl methacrylate (PMMA) and fluorinated polyimide (FPI) show intermediate values as well, with PMMA [224] having a permeability of 1.24 × 10^{-15} mol.m^{-1}.s^{-1}.Pa^{-1} and FPI ranging from 1.60 to 36.2 × 10^{-15} mol.m^{-1}.s^{-1}.Pa^{-1}, suggesting potential use in layered or composite barrier systems. Finally, an epoxy matrix made from diglycidyl ether of bisphenol A and polyetheramine (DGEBA/D400) performed well, with a permeability range of 4.99–5.06 × 10^{-16} mol.m^{-1}.s^{-1}.Pa^{-1}.

Overall, the best hydrogen barrier material from the dataset is the PVA + GA combination, offering the lowest permeability measured. Among thermoplastics, polyamide 11 stands out as a top performer. For elastomers, CIIR offers the best balance of barrier properties and mechanical flexibility. On the opposite end, PTMSP is the worst barrier, with extremely high permeability, followed by PDMS and VMQ, which are also unsuitable for applications needing hydrogen containment. These findings highlight the critical importance of material selection based on specific gas barrier requirements, as differences in molecular architecture can lead to several orders of magnitude variations in performance.

5.3.2. *Various polymers coatings*

Polymers are the most widely used coating and liner material in the pipeline industry, owing to advantages such as ease of processing, cost-effectiveness, corrosion resistance, and mechanical characteristics. Various polymer types have been tested for hydrogen permeation [40,41,155,156,224,232,233], as summarized in subsequent sections.

Polymeric materials have emerged as promising candidates for HBCs due to their low density, ease of processing, tunable molecular architecture, and, in certain cases, inherent resistance to hydrogen permeation. However, the effectiveness of polymers as hydrogen barriers varies significantly depending on their molecular structure, degree of crystallinity, crosslinking, free volume characteristics, and interaction with water and other gases. Early studies identified that polymers may leverage their segmental motion suppression and cohesive energy density to impede hydrogen diffusion, particularly when properly modified or reinforced with fillers and additives [50].

Hydrogen permeation in polymers is governed by the solution-diffusion mechanism. Thus, both free volume and chemical affinity of the polymer to hydrogen critically influence its performance. Polymers with low hydrogen solubility and reduced chain mobility, such as crosslinked or semicrystalline systems, tend to show enhanced resistance to hydrogen permeation [229]. Nonetheless, this performance is rarely absolute. Low-temperature performance and leakage after the cyclic testing due to plasticization or microcracking under cyclic hydrogen charging remain limitations that hinder broader application, particularly in structural or high-pressure hydrogen storage contexts [228].

Crystallinity plays a pivotal role in determining barrier performance. Studies have shown that hydrogen diffusion rates decrease significantly with increasing polymer crystallinity, as crystalline regions exhibit very low permeability and hinder hydrogen from migrating through the less ordered amorphous domains [40,41,218].

Crosslinking is another critical strategy to enhance hydrogen barrier properties. Highly crosslinked poly(propylene glycol) (PPG) networks exhibited a monotonic decrease in hydrogen and CO permeabilities with increasing crosslink density, attributed to the suppression of cooperative molecular motions and reduced chain segmental mobility [229]. Yet, excessive crosslinking can result in brittle films or poor interfacial adhesion to substrates, highlighting the need for optimization tailored to application-specific mechanical constraints.

Importantly, polymers such as poly(1- (trimethylsilyl) - 1 -propyne) (PTMSP) exhibit unusually high hydrogen permeability due to their high fractional free volume and microporosity, making them fundamentally unsuitable for barrier applications despite their advantageous processing properties [231]. This demonstrates the trade-off between transport efficiency, e.g., in separation membranes, and barrier function. Thus, for HE protection, polymers must be critically selected or engineered with specific performance trade-offs in mind.

Moreover, polymeric systems often exhibit time-dependent degradation under hydrogen exposure, including swelling, softening, or plasticization effects that can alter barrier efficiency over time. This dynamic behavior is further complicated when polymers are used in conjunction with metal substrates, where interfacial diffusion, delamination, or galvanic effects may emerge under cycling or humid conditions [228]. Therefore, standalone hydrogen permeability values are insufficient. The comprehensive assessments must account for mechanical stability, adhesion, and environmental resistance.

Poly(propylene glycol) networks represent another class of promising hydrogen barrier materials. As shown in the seminal study by Andradý and Sefcik, increasing crosslink density in PPG networks drastically reduces hydrogen and CO permeation [229]. The authors attributed these results to constrained segmental dynamics and reduced free volume. Importantly, they demonstrated that hydrogen diffusivity is inversely related to the average molecular weight between crosslinks, reinforcing the utility of precise network design in barrier optimization.

Elastomeric materials such as nitrile butadiene rubber (NBR), ethylene propylene diene monomer (EPDM), and fluoroelastomer (FKM) are often used in sealing applications. Recent thermal desorption analysis coupled with gas chromatography revealed dual diffusion behaviour in NBR and EPDM due to the heterogeneous distribution of carbon black fillers, which create separate fast and slow hydrogen diffusion pathways [228]. FKM, in contrast, displayed a single, slower hydrogen diffusion process, indicating a more homogeneous barrier network.

Notably, the presence of fillers increased hydrogen solubility while reducing diffusivity, suggesting a complex trade-off between mechanical reinforcement and permeation performance.

Conversely, poly(1-(trimethylsilyl)-1-propyne) (PTMSP) exhibits exceptionally high hydrogen permeability, over four orders of magnitude greater than polysulfone, making it fundamentally unsuitable for use as a hydrogen barrier [231]. This anomalous behaviour stems from its ultra-high fractional free volume (~25 vol%) and interchain microvoids, which facilitate fast gas transport through surface diffusion and competitive adsorption effects. While PTMSP has been extensively explored in gas separation membranes, its structural characteristics render it more akin to a molecular sieve than a barrier material. Moreover, its permeability increases with decreasing temperature, contrary to classical polymer behaviour, due to enhanced free volume connectivity at low thermal energy, further highlighting its incompatibility for embrittlement mitigation [231].

Silicone rubber, while occasionally used for its thermal and oxidative stability, exhibits one of the highest permeabilities to hydrogen and other small gases due to its flexible, low-density siloxane backbone [230]. Replacing Si–O bonds with the stiffer Si–C bonds within the backbone chains significantly reduces permeability.

In light of these multifaceted considerations, growing interest has emerged in hybrid strategies, such as polymer-inorganic nanocomposites or dual-layer coatings, that aim to synergistically combine the favourable properties of different material classes. While these approaches offer promise in addressing some intrinsic limitations of conventional polymers, such as high hydrogen permeability, they also introduce new challenges related to interfacial stability, scalability, and long-term performance. Given the relative paucity of studies on polymeric systems, no single approach currently dominates the field, and further research is essential to establish robust, scalable hydrogen barrier solutions.

5.3.3. Techniques for applying polymer coatings

The fabrication of polymer coatings as hydrogen barriers involves various techniques, each offering unique advantages depending on the required coating properties, substrate characteristics, and intended applications. These methods include dip coating, casting and curing, spraying, and extrusion, all of which are widely utilized in industrial and research environments. In a study by Kargari et al. [234], PDMS coatings were applied to polyetherimide (PEI) membranes using dip coating, film casting, and pouring methods, with dip coating yielding the highest H_2 selectivity due to enhanced penetration of the polymer into surface pinholes and better coating uniformity.

In a study, the permeation behavior of epoxy resin was quantitatively evaluated using the cylinder method, revealing no significant influence of curing temperature on hydrogen permeability within the examined range [235]. The experimentally derived permeability values were applied to model hydrogen loss rates in high-pressure storage systems comprising epoxy resin-coated glass capillaries and modular arrays. Notably, despite initial assumptions, adhesive joint losses were found to be minimal, supporting the feasibility of such systems and indicating that strategic design, such as increasing glass wall thickness slightly and minimizing adhesive gaps, can effectively reduce pressure drops and overall hydrogen loss without substantial weight penalties.

Spraying is another technique employed by Lei et al. [41] to apply a novel internal polymeric coating composed of crosslinked polyvinyl alcohol (PVA) and poly(ethylene glycol) diglycidyl ether (PEGDGE) was engineered specifically for application via spray techniques onto steel pipelines and similar infrastructure intended for high-pressure hydrogen environments. The formulation was optimized to maintain the rheological characteristics essential for efficient and uniform spray application, while simultaneously achieving an exceptionally low hydrogen permeability of just 3.35×10^{-18} mol.m^{-1}.s^{-1}.Pa^{-1}. This dual performance underscores its potential as a practical and scalable solution for enhancing hydrogen containment in industrial systems.

Extruded polyether ether ketone (PEEK) films were thoroughly evaluated by Monson et al. [236] for their gas permeation behavior and compared with polycarbonate (PC) and polyether imide (PEI), two polymers commonly used in semiconductor microenvironments. The extrusion method was critical in producing specimens with well-aligned polymer chains and moderate levels of crystallinity, which strongly influenced the diffusion characteristics of hydrogen, nitrogen, and oxygen gases. Compared to PC and PEI, extruded PEEK exhibited significantly lower gas permeation rates, up to five times lower, due to its inherently higher crystallinity and more compact molecular structure, which serve as effective barriers to gas transport.

The selection of a suitable coating technique depends on several factors, including the desired coating thickness, substrate geometry, mechanical requirements, and cost considerations. For applications requiring thin, precise coatings, dip coating and spraying offer significant advantages due to their uniformity and scalability. In contrast, casting is preferred for producing thicker coatings with enhanced mechanical robustness, while extrusion remains the method of choice for large-area applications involving thermoplastic polymers.

The choice of coating technique depends on factors such as desired coating thickness, substrate geometry, and environmental resistance. Table 6 summarizes the main characteristics of these methods.

Future advancements may focus on improving coating performance through automated deposition systems, hybrid coatings, and the incorporation of nanofillers [40,154]. These innovations will optimize barrier properties, environmental resistance, and scalability for industrial applications.

In addition to laboratory studies, polymer coatings have also been adopted in practical applications. Type IV high-pressure hydrogen storage tanks, for instance, employ polymer liners such as HDPE and PA6 within carbon-fiber reinforced composites to reduce hydrogen permeation in fuel-cell vehicles. Epoxy- and polyurethane-based coatings have further been applied as protective linings in pipelines and storage vessels, underscoring the translational potential of polymers in hydrogen infrastructure [237].

A critical consideration for polymeric barriers lies in their environmental durability. Long-term exposure to humidity, temperature cycling, and UV radiation can induce swelling, microcracking, and plasticization of polymer matrices, leading to degradation of hydrogen barrier performance. Accelerated aging studies confirm that cyclic thermal and moisture conditions significantly reduce durability over time [238]. While these effects are well recognized in polymer barrier applications generally, systematic long-term evaluations under hydrogen service conditions remain sparse, highlighting an important research gap.

From an economic perspective, polymer coatings are attractive due to their low cost, lightweight nature, and scalability in large-area deposition processes, including spray or extrusion techniques [239]. However, their limited environmental stability may offset these advantages in demanding hydrogen-rich environments [240,241]. Hybrid strategies, particularly polymer–inorganic nanocomposites and multilayer architectures, represent promising directions to balance affordability with long-term functional stability [242].

Table 6
Comparison of polymer coating techniques.

Technique	Advantages	Applications
Dip coating	Uniform thin coatings; and precision control	Gas barriers, electronics, and packaging
Casting and curing	Thick; robust coatings; and performance tuning	Films for food packaging, and gas barriers
Spraying	Quick; versatile; and industrial adaptability	Aerospace, automotive, and electronics
Extrusion	Continuous coatings; and molecular alignment	Pipeline liners

5.4. Composite and multilayer coatings

Composite and multilayer coatings have garnered significant attention as barrier systems against hydrogen permeation due to their potential to synergistically combine the desirable traits of individual components, such as high mechanical stability, low hydrogen diffusivity, and robust adhesion. Among the most promising designs are those involving graphene-based nanocomposites, polymer-layered structures, and ceramic-polymer hybrids, which exhibit unique diffusion-blocking mechanisms owing to their tortuous path effects and interfacial control. However, despite the diversity of strategies, a comprehensive understanding of their performance limitations, interfacial failure mechanisms, and processing challenges remains insufficient.

Composite coatings incorporate phases with very low hydrogen permeability, such as ceramics, nanomaterials, or inorganic fillers, into a polymer matrix. These inclusions act as physical barriers to hydrogen diffusion, creating tortuous pathways that impede molecular transport. For example, the addition of graphene or MXene nanomaterials has been shown to significantly enhance the hydrogen barrier properties of polymer coatings. Graphene-based composites, in particular, exhibit exceptionally low hydrogen permeability due to their two-dimensional structure, which effectively blocks hydrogen molecules [157,243,244]. Similarly, the incorporation of ceramic fillers, such as alumina or silica, improves both the mechanical strength and hydrogen resistance of polymer matrices [245,246]. However, challenges related to achieving uniform filler distribution and strong interfacial adhesion between the polymer and filler must be addressed to optimize performance.

Multilayer coatings offer another promising approach for enhancing hydrogen barrier properties. These coatings are composed of alternating layers of polymers and functional materials, each contributing specific attributes such as mechanical reinforcement, low hydrogen permeability, or environmental resistance. Recent works have emphasized the importance of multilayer configurations formed via layer-by-layer (LbL) assembly or dip-coating techniques, where nanomaterials such as graphene oxide (GO) or MXenes are interleaved with polymers or ceramics to form 'brick-and-mortar' structures. For instance, Yang et al. demonstrated that PEI/PAA multilayers assembled at optimized pH values exhibited oxygen permeability as low as 3.2×10^{-21} cm^3(STP)·cm. cm^{-2}·s^{-1}·Pa^{-1}, attributed to their uniform morphology and controlled interdiffusion barrier formation [247]. However, their sensitivity to humidity and limited thermal stability highlight the need for chemically crosslinked or hybrid solutions.

In this context, graphene-enhanced systems have emerged as leading candidates due to graphene's exceptional low-permeability and mechanical resilience. Nevertheless, pristine graphene remains impractical for large-scale coating applications due to poor dispersion and interfacial adhesion. To overcome these, several studies introduced functionalized or reduced GO (rGO) variants embedded in polymer matrices such as polyurethane or polyethyleneimine. The work of Bandyopadhyay et al. [248] showed that incorporating 43.3 wt% of hexylamine-functionalized reduced graphene oxide (RGO-HA) in a PU matrix on nylon film reduced the hydrogen gas transmission rate by 82 %. The enhancement was primarily attributed to the excellent dispersion and exfoliation of RGO-HA, which introduced tortuous paths for hydrogen permeation. They reported that the enhanced barrier properties of the composite-coated nylon film suggest promising potential for their application in hydrogen storage containers for fuel cell vehicles in the near future.

More advanced architectures, such as covalently bonded graphene oxide-polymer multilayers, show promise in addressing interfacial debonding at polymer-substrate boundaries and GO aggregation. Li et al. [249] developed a reactive LbL film comprising modified GO and PEI, achieving a 78.8 % reduction in H_2 transmission through covalent bonding that enhanced chemical resistance across pH and thermal ranges. Consequently, to enhance the stability of the film's hydrogen barrier performance across diverse environments, it is imperative to employ covalent bonds in the self-assembly process in place of non-covalent interactions. Still, covalent systems often require stringent processing conditions, e.g., pH control, crosslinking agents, raising concerns for scalability and compatibility with temperature-sensitive substrates.

Table 7
Examples of composite and multilayer polymer coatings.

Type of coating	Composition	Key features	Ref.
Composite coating	Polymer + ceramic fillers	Improved barrier performance, and high toughness	[245, 246]
Graphene-based coating	Graphene + polymer matrix	Exceptional barrier properties	[157, 243]
MXene-based coating	MXene nanomaterials +polymer	Enhanced hydrogen resistance	[244]
Multilayer coating	PEI/PAA layers	Dramatic reduction in gas permeability	[247]
Graphene oxide multilayer	PET + graphene oxide	78.8 % reduction in hydrogen permeation	[249]

Similarly, multilayer designs combining ceramic and polymeric phases offer another viable strategy. Liu et al. [250] constructed a GO-reinforced $AlPO_4/Cr_2O_3$ double coating via dip-coating, which exhibited not only a deuterium permeation reduction factor (PRF) above 100 in the 450–550 °C range but also superior mechanical strength (21.5 MPa bonding strength) and corrosion resistance. The synergy between Cr_2O_3's stable oxide network and GO's tortuous path function led to a dense, defect-free coating. However, thermal stability becomes compromised beyond 600 °C due to the Cr_2O_3 phase transition, and optimization of GO content is critical to avoid embrittlement.

Despite these advances, current composite and multilayer coatings often lack uniform adhesion at the metal interface, a factor critically governed by surface chemistry and microstructure. Bahlakeh et al. [251] used molecular dynamics and quantum mechanics simulations to show that adhesion strength between epoxy and various iron oxide surfaces (FeO, Fe_2O_3, and Fe_3O_4) is strongly dependent on hydroxyl group coverage and oxide type, with ferric oxide (Fe_2O_3) showing the strongest binding via electrostatic and hydrogen bonding. This insight is vital for tailoring surface treatments and selecting compatible polymers that form robust interfacial chemistries. Nevertheless, such computational insights need to be validated across multiple substrate chemistries and environmental conditions, which remain underexplored in the literature.

Graphene oxide-polyurethane composite coatings have demonstrated improved barrier properties when functionalization and dispersion are optimized. Upcoming research should focus on developing multifunctional coating systems with hierarchically engineered structures. High tortuosity nanofillers, such as functionalized graphene oxide (GO) or MXene, are employed to enhance diffusion resistance by creating elongated and tortuous pathways for hydrogen transport. Simultaneously, chemically crosslinked polymer matrices provide essential mechanical compliance and long-term environmental stability. Tailoring the interface through controlled surface pretreatment, for instance, Fe_2O_3 surface enrichment [251] or covalent anchoring strategies [249], further optimizes adhesion and structural integration. To enable industrial scalability, fabrication methods like modified layer-by-layer (LbL) assembly, spray-casting, and hybrid sol–gel techniques are increasingly adopted, offering a balance between performance and manufacturability. In addition, standardized testing protocols for hydrogen permeation under thermal/mechanical cycling and long-term humidity exposure are urgently needed to assess coating reliability beyond short-term lab-scale metrics.

The fabrication of composite and multilayer coatings often involves complex and time-consuming processes, such as layer-by-layer assembly or solution casting, which may limit scalability for industrial applications. Additionally, ensuring uniform thickness, consistent filler

distribution, and strong interlayer adhesion is critical to achieving reliable performance. Although new coating technologies, particularly for coatings incorporating advanced nanomaterials, have been introduced, many of these advancements still pose a considerable obstacle to their widespread adoption [135].

Future research in composite and multilayer coatings should focus on addressing these challenges through process optimization, material innovation, and cost reduction. Advanced deposition techniques, such as cold spraying, laser cladding, and automated layer-by-layer assembly, hold promise for improving the scalability and uniformity of these coatings. Furthermore, the development of hybrid systems that combine polymers with nanomaterials, ceramics, and other functional phases will enable the creation of coatings with superior hydrogen resistance and mechanical properties. Innovations in smart coatings, including self-healing and environmentally responsive systems, will further enhance the reliability and adaptability of composite and multilayer coatings in dynamic environments.

Table 7 summarizes notable developments in composite and multilayer coatings for hydrogen barrier applications.

While in the realm of composite coatings, challenges remain, continued advancements will pave the way for broader industrial adoption in sectors such as aerospace, automotive, energy, and pipeline infrastructure. Studies showed that some crosslinked polymers with certain crosslinking agents emerged as effective hydrogen barriers due to their dense molecular structure. For example, polyvinyl alcohol (PVA), particularly when crosslinked with glutaraldehyde, achieves exceptional hydrogen resistance by forming a compact network with very low hydrogen permeability. Studies have shown that PVA and some crosslinked PVA exhibit lower hydrogen permeability compared to the majority of other polymer coatings, which makes it a promising material for preventing hydrogen ingress [40,217]. Similarly, epoxy-based coatings offer excellent adhesion to metal substrates, strong mechanical properties, and good hydrogen barrier performance, making them widely applicable in industrial environments where a balance of adhesion, durability, and hydrogen resistance is required [251]. They may also be regarded as suitable candidates for the fabrication of composite coatings.

While these materials show significant promise, challenges remain in their widespread implementation. Achieving uniform coatings, particularly for composite and multilayer systems, requires precise control over processing conditions to ensure homogeneity in thickness and filler distribution. Irregularities in coating properties can compromise hydrogen resistance, especially in large-scale applications [245,246]. Additionally, environmental conditions such as mechanical stress, thermal cycling, and humidity pose durability concerns for polymer coatings. Maintaining long-term performance under such conditions necessitates further investigation into material stability and degradation mechanisms.

The performance of composite and multilayer hydrogen barrier coatings is strongly influenced by the quality of the coating/substrate interface [252]. Optimizing the coating/substrate interface through surface engineering enhances adhesion and long-term stability. Strategies include promoting chemical bonding between functional groups of the coating matrix and substrate surface [253], as well as designing surface roughness to achieve mechanical interlocking [254]. Such approaches improve load transfer across the interface and minimize delamination under hydrogen-rich environments.

The incorporation of supplementary nanofillers such as graphene and MXenes [255–258] has been explored to reduce hydrogen permeability and reinforce the coating structure. However, their uniform dispersion within polymer matrices remains a challenge due to strong van der Waals interactions and agglomeration tendencies. Poor dispersion not only compromises barrier continuity but also introduces stress-concentration sites that accelerate coating failure. To overcome these issues, techniques such as surface functionalization of nanofillers, non-covalent modification [259–261], the use of agents [262], and controlled defect formation [263] methods have been proposed. These methods improve interfacial compatibility between nanofillers and the polymer matrix, thereby enhancing hydrogen barrier performance while maintaining mechanical integrity.

High production costs represent another obstacle, particularly for advanced systems incorporating nanomaterials like MXenes. These materials involve complex synthesis and processing methods, limiting their large-scale application. Moreover, adhesion challenges, particularly with ceramic phases like alumina, often arise due to thermal expansion mismatches with metal substrates. Addressing these issues is crucial for achieving robust and reliable coatings for industrial use [148,250].

In summary, composite and multilayer coatings represent a pivotal advancement in the development of hydrogen barrier technologies, offering enhanced resistance through the synergistic integration of polymers, nanomaterials, and functional fillers. These engineered systems combine tailored molecular architectures with optimized interfacial properties to significantly improve durability and permeability performance under demanding conditions. However, the successful deployment of such coatings will require a convergent strategy that bridges molecular design, advanced processing techniques, and systems-level engineering. Addressing these interdisciplinary challenges is crucial for enabling reliable, cost-effective solutions in hydrogen-critical sectors such as energy storage and transportation, and fuel cell components, where precise hydrogen control directly impacts operational performance and safety. Continued innovation in material formulation and scalable fabrication methods will be key to supporting their widespread adoption across diverse industrial applications.

5.5. Challenges and future perspectives in HBCs

1. ***Recent innovations in smart coatings*** mark a significant step forward in addressing the persistent challenges associated with HBCs. Notably, self-healing systems can autonomously repair microcracks, thereby restoring their barrier properties and extending service lifetimes. Environmentally responsive coatings that adapt to external stimuli, such as changes in temperature or hydrogen concentration, offer further potential for application in dynamic environments. The integration of sensors within coating matrices enables real-time monitoring of operational conditions, providing valuable feedback for timely maintenance and system optimization [245,246].
2. ***The continued evolution of HBCs*** demands targeted improvements in material composition, coating architectures, and deposition techniques. Cold spraying, laser cladding, and automation-based approaches are expected to facilitate uniform coating deposition while reducing production costs [248]. The development of multilayered systems that combine polymers with functional materials presents a promising avenue for enhancing hydrogen barrier properties and mechanical resilience [247,249]. Simultaneously, environmental sustainability considerations are pushing for coatings formulated with non-toxic solvents, recyclable ingredients, and energy-efficient processing methods.
3. ***A critical bottleneck in current HBCs research*** is the lack of standardized hydrogen permeability testing protocols. Variations in reported values stem from inconsistent conditions regarding temperature, pressure, and sample thickness, hindering meaningful comparisons across studies. Essential metrics such as solubility, diffusivity coefficients, and permeation reduction factors (PRFs) are often reported selectively and under differing conditions. Furthermore, comprehensive long-term data, particularly under cyclic loading, high-pressure hydrogen exposure, and other complex service scenarios, remain limited, thereby constraining predictive reliability. Incorporating real-time diagnostics, such as electrochemical permeation monitoring or in-situ spectroscopic techniques, may provide crucial insights into coating degradation and failure mechanisms during operation. These tools serve to bridge the gap between

fundamental materials characterization and actual service performance, an especially important consideration for critical applications in hydrogen pipelines, containment vessels, and energy infrastructure.

4. ***Application-specific coating design*** will be pivotal for future developments. Advanced architectures such as gradient interfaces, functionally graded systems, and atomically engineered multilayers [53,153,264,265] offer pathways to improve interfacial bonding and mitigate thermal expansion mismatches. The strategic implementation of in situ diagnostics, first-principles simulations, and machine learning-guided material screening [266–268] is anticipated to accelerate the optimization of coatings for both performance and manufacturability. The deliberate selection of materials with matched thermal expansion coefficients for multilayer systems, especially in the inner layers, followed by an outer material with very low hydrogen permeability, provides a rational design approach. Additionally, coating hardness may play a role in hydrogen resistance and could be considered as a supplementary parameter in future coating design strategies, pending further experimental validation.
5. ***In the realm of metallic HBCs coatings***, the absence of a universal solution necessitates careful trade-offs among permeability resistance, mechanical performance, adhesion, and environmental durability. Current findings underscore that no single coating excels universally, and suitability must be judged by application-specific requirements. Despite notable progress, critical gaps persist. Moreover, few investigations connect microstructural features, like grain boundaries, amorphicity, or interfacial chemistry, to transport behavior and fracture resistance. Multilayer coatings with engineered hydrogen trap sites and self-healing interfaces, such as those reported in aluminum-based high-pressure systems [171], represent a promising yet underdeveloped frontier.
6. ***Ceramics' fundamental limitation*** lies in the intrinsic brittleness of ceramics, which often leads to cracking, spallation, or delamination. Such defects not only compromise the structural integrity but also create pathways for hydrogen ingress, undermining the barrier function. Furthermore, achieving consistent coating quality across complex geometries remains difficult, particularly with techniques like thermal spraying, which may introduce porosity and microcracks. The dependency of coating performance on processing parameters and substrate compatibility also adds complexity to scale-up efforts. From a testing standpoint, the scarcity of standardized, long-term, and in-situ permeability evaluations under cyclic, ambient, or combined stress-hydrogen environments limits the ability to predict service life accurately. Looking ahead, future development should prioritize the design of multilayer and hybrid ceramic architectures that combine phases with complementary thermal expansion, toughness, and hydrogen diffusivity.
7. ***Among polymer coatings***, crosslinked networks such as those based on polyvinyl alcohol (PVA) and epoxy composites exhibit significant promise due to their favourable barrier characteristics. The incorporation of nanomaterials and the emergence of smart coating technologies are expected to further enhance permeability resistance, durability, and scalability. Future advances in material processing, sustainability, and structural optimization will be crucial to enabling widespread industrial implementation. These strategies are fundamental for ensuring HE protection and maintaining the integrity of hydrogen-exposed infrastructure.
8. ***Emerging strategies*** offer promising alternatives. Polymer–inorganic nanocomposites, for example, leverage the very low permeability of metal oxides or layered silicates embedded within polymer matrices to significantly reduce gas transport through tortuous diffusion pathways. However, achieving uniform nanofiller dispersion and maintaining robust interfaces under stress remain an active challenge. Layered architectures combining a soft adhesion-promoting primer with a rigid topcoat have also demonstrated improved interface stability without sacrificing hydrogen barrier performance [226]. The field is also witnessing developments in bioinspired and molecularly engineered polymers, tailored to modulate free volume, chain packing density, and hydrogen bonding characteristics. These efforts are likely to yield novel coatings with enhanced resistance to hydrogen ingress and greater mechanical flexibility.
9. ***Next-generation HBCs*** will be characterized not only by composition but by their engineered interfacial properties, mechanical compatibility, and scalable processing tailored to distinct hydrogen technologies. Future studies could include: (i) implementing in situ permeation, thermal desorption spectroscopy (TDS), and slow strain rate testing under realistic hydrogen service conditions; (ii) quantifying trapping energies and diffusivity in correlation with structural attributes and processing history; (iii) explore gradient or hybrid architectures integrating dense barriers with sacrificial outer layers to endure dynamic hydrogen exposure; and (iv) develop unified testing methodologies that allow rigorous comparative evaluations across coating systems under consistent environmental and mechanical loads.

6. Conclusions and outlook

This review provides a comprehensive examination of hydrogen permeability across diverse materials and coating systems, highlighting their pivotal role in mitigating hydrogen embrittlement (HE). A rigorous synthesis of theoretical frameworks, experimental methodologies, and material-specific performance data underscores the centrality of permeability assessment as a foundational parameter in the design and selection of hydrogen barrier coatings (HBCs). Among the various strategies explored to reduce HE susceptibility, the application of surface modifications, particularly through advanced coating deposition, emerges as the most effective means of impeding hydrogen ingress. These surface-functionalized barriers not only minimize hydrogen diffusion but also enhance structural resilience under aggressive service conditions.

- ***Among metallic coatings*** evaluated for hydrogen permeation resistance, beryllium (Be) exhibits the lowest hydrogen permeability reported, reaching values as low as 2×10^{-15} $mol.m^{-1}.s^{-1}.Pa^{-1/2}$ at 400 °C. This positions Be as the best performer in terms of absolute permeability. However, its practical use is severely constrained by several factors: high toxicity, which poses serious health risks during handling and processing; brittleness, leading to potential cracking under stress; and complex hydrogen trapping behaviours that may induce nano voiding or embrittlement over time. In contrast, tungsten (W), with a slightly higher but still exceptionally low permeability of 4.3×10^{-15} $mol.m^{-1}.s^{-1}.Pa^{-1/2}$, is widely regarded as the most practical and robust metallic hydrogen barrier. It combines exceptionally low hydrogen permeability with superior thermal stability, mechanical strength, and environmental safety, making it a preferred choice for high-temperature and hydrogen-intensive applications. At the other end of the spectrum, vanadium (V) demonstrates the highest hydrogen permeability among metals studied, at 2.9×10^{-8} $mol.m^{-1}.s^{-1}.Pa^{-1/2}$ at 500 °C, more than three orders of magnitude higher than W or Be. This makes it the least effective hydrogen barrier, despite its usefulness in hydrogen-selective membranes due to high diffusivity.
- ***Ceramic coatings***, in particular, demonstrate outstanding potential due to their inherently low hydrogen permeability and excellent thermomechanical stability. However, the ultimate effectiveness of these coatings is profoundly dependent on the deposition technique employed, with precision-driven methods such as the differential pressure approach offering the most reliable and accurate quantification of hydrogen permeability. Together, these insights reinforce the critical importance of integrating materials science, coating engineering, and accurate permeability measurement in the

development of robust HBCs. Hydrogen permeation, governed by a confluence of thermodynamic laws, diffusivity, and solubility behaviours, is profoundly influenced by both intrinsic material properties and extrinsic factors such as microstructure, coating method, and environmental conditions. By dissecting the hydrogen transport mechanisms in metals, polymers, and ceramics, the study elucidates how materials' structure, grain boundaries, and defect structures modulate permeation kinetics. This understanding is particularly vital for materials deployed in hydrogen-intensive technologies, where even trace ingress can compromise structural integrity. Among ceramic coatings, titanium carbide (TiC) and zirconium nitride (ZrN) demonstrated the most outstanding hydrogen barrier performance, with an exceptionally low permeability of 3.62×10^{-18} at 300 °C and 7.9×10^{-18} $mol.m^{-1}.s^{-1}.Pa^{-1/2}$ at 400 °C, respectively. This positions them as the most effective ceramic materials for hydrogen containment applications, particularly in high-temperature environments. In contrast, iron oxide (FeO) exhibited the highest hydrogen permeability among ceramics, reaching 4.3×10^{-11} $mol.m^{-1}.s^{-1}.Pa^{-1/2}$ at 800 °C, making it the least suitable ceramic coating for use in hydrogen-rich conditions. This stark contrast underscores the importance of careful material selection based on both permeability performance and environmental operating conditions.

- ***Among polymeric coatings***, the best hydrogen barrier performance was achieved by polyvinyl alcohol (PVA) crosslinked with glutaraldehyde (PVA + GA), which exhibited an exceptionally low permeability of 2.81×10^{-18} $mol.m^{-1}.s^{-1}.Pa^{-1}$. This was closely followed by other modified PVA systems, including those crosslinked with PEGDGE, confirming that crosslinking significantly enhances hydrogen barrier properties by reducing molecular free volume. In contrast, the worst performer was poly (trimethylsilyl propyne) (PTMSP), with a permeability of 5.52×10^{-12} $mol.m^{-1}.s^{-1}.Pa^{-1}$, approximately six orders of magnitude higher. PTMSP's highly porous structure and large free volume, while beneficial for gas separation membranes, make it unsuitable for hydrogen containment applications. This stark disparity underscores the critical influence of polymer structure on gas barrier performance and highlights the importance of selecting materials tailored to the demands of hydrogen-sensitive environments.
- ***In the context of polymer liners*** used in high-pressure hydrogen storage systems, despite significant advances in the development of hydrogen permeation barriers, several critical challenges persist. These liners offer substantial benefits, including reduced container weight and enhanced volumetric efficiency; however, they are vulnerable to hydrogen ingress under dynamic service conditions. One prominent issue arises during rapid decompression, where the buildup of internal hydrogen concentration leads to structural damage caused by large pressure differentials, thereby accelerating permeation and compromising the liner's integrity. To address these limitations, the integration of reinforced polymer liners within metallic containment systems has been proposed as a promising mitigation strategy against hydrogen embrittlement.
- ***Composite and multilayer coatings*** represent a transformative approach in the development of hydrogen barrier systems, offering enhanced mechanical resilience, reduced gas permeability, and improved environmental stability through the synergistic integration of polymers, nanomaterials, and ceramics. Advances in functional filler dispersion, interfacial chemistry, and scalable deposition techniques have significantly improved the barrier performance of these coatings. However, challenges such as processing complexity, interfacial adhesion, and long-term durability under thermal and mechanical stresses remain critical hurdles. Future efforts should prioritize the design of multifunctional architectures with hierarchically structured fillers, chemically crosslinked matrices, and tailored interfaces, while also establishing standardized testing protocols to validate long-term reliability. Bridging materials innovation with scalable manufacturing will be pivotal in enabling the widespread adoption of these coatings in demanding applications such as hydrogen storage, energy infrastructure, and aerospace systems.
- ***Beyond polymer-specific coating challenges***, broader technical obstacles remain in the evaluation and deployment of HBCs. A major limitation lies in the absence of standardized, high-resolution permeability testing methods capable of accurately capturing ultra-low fluxes under realistic thermal and pressure conditions. Moreover, the long-term reliability of these barriers is influenced by factors such as coating defects, exposure to environmental contaminants, and the effects of mechanical fatigue, parameters that are often underexplored in current studies. Importantly, the interplay between interfacial bonding, coating architecture, and hydrogen trapping behaviour warrants deeper investigation, particularly through the development of in-situ diagnostic tools and real-time monitoring systems. Such approaches would not only illuminate degradation mechanisms but also inform the rational design of next-generation barrier systems for demanding hydrogen-related applications.
- ***The selection of coating materials*** must also be tailored to the specific environmental conditions in which they will be used. Polymer composites offer several benefits, including lower costs, greater plasticity, and suitability for large-scale manufacturing. However, they are not suitable for high-temperature environments due to their lower melting points compared to metal substrates, and their degradation rate accelerates at elevated temperatures. For applications such as hydrogen storage tanks that are transported at room temperature, lightweight polymers and their composite coatings are preferable. These materials are likely to be widely adopted in everyday applications, such as hydrogen-powered vehicles and hydrogen transport pipelines. In contrast, extreme environments, such as those found in industries, require more robust materials, including metals, dielectrics, and their composites. In corrosive and toxic environments, materials such as carbides, nitrides, and graphene should be considered. The ideal coating for gaseous hydrogen storage and transport would be cost-effective, possess a high hydrogen permeation barrier, and be easy to manufacture. Nevertheless, challenges such as the formation of pores and cracks during the coating process remain difficult to overcome. Layer-by-layer polymer coatings, which are recognized for their excellent surface uniformity, present a promising solution. Due to the plasticity and ease of fabrication of polymer molecules, these coatings show considerable potential for use in hydrogen storage and transportation. However, most research on polymer coatings has traditionally focused on blocking macromolecular gases such as oxygen and carbon dioxide. The application of these coatings to inhibit the permeation of smaller molecules, such as hydrogen and helium, is still under investigation, and the commercialization of polymer-based HBCs remains a long-term objective.
- ***Equally important is the incorporation of smart functionalization coating strategies***, extending beyond barrier properties to include adaptive and responsive functionalities. For instance, self-healing mechanisms [269] based on reversible chemical bonds or microcapsule release systems can restore barrier integrity, while embedded sensor technologies enable real-time monitoring of hydrogen ingress and coating degradation [270,271]. Incorporating such multifunctionality into structural materials, through functionally graded structures [272], synergistic chemical blends [40,41], or nanostructured additives [273,274], offers the potential to significantly enhance the coating's barrier performance. Although certain standardization efforts for gas permeation have been undertaken [117,275], further progress in this field requires the establishment of harmonized testing and benchmarking protocols, developed within standardized frameworks specifically tailored to hydrogen permeation to ensure comparability across studies. Alongside these, advanced in-situ analytical tools for real-time gas permeation

monitoring, will remain indispensable for uncovering degradation pathways and validating smart-coating performance during service.

- ***Looking ahead***, the convergence of computational materials science, precision nanofabrication, and advanced characterization techniques presents a transformative pathway for the rational design of next-generation HBCs. Future progress in this field will rely on strategically integrating multiple innovations to enhance both the performance and durability of coatings while ensuring environmental and economic sustainability. A key direction lies in the development of multilayer and functionally graded coatings that utilize interfacial engineering and tailored hydrogen trapping mechanisms without compromising mechanical cohesion. These architectures not only enhance barrier performance but also allow for adaptive responses to complex service environments.
- ***Finally, future research of HBSs*** should increasingly prioritize environmental sustainability by minimizing the use of hazardous elements and exploring low-energy fabrication routes, without compromising performance. Balancing such goals with the functional complexity of multilayer coatings remains an important challenge. Together, these multidisciplinary advancements will underpin the next generation of HBCs, enabling more reliable protection against HE across a diverse range of applications. In conclusion, as hydrogen energy systems move toward broader deployment, the engineering of advanced HBCs is poised to play a pivotal role in enabling safe, efficient, and durable infrastructure. The insights gleaned from this work contribute to the foundational understanding and future trajectory of material solutions aimed at addressing the pervasive challenge of HE.

CRediT authorship contribution statement

Ehsan Akbari-Kharaji: Writing – review & editing, Writing – original draft, Visualization, Validation, Methodology, Investigation, Formal analysis, Conceptualization. **Majid Shafaie:** Writing – review & editing, Writing – original draft, Visualization, Validation, Investigation, Formal analysis. **Elizabeth Sackett:** Supervision, Project administration. **John Wood:** Writing – review & editing, Supervision, Project administration. **Milos B. Djukic:** Writing – review & editing. **Shirin Alexander:** Writing – review & editing.

Ethical approval

Not applicable.

Availability of data and materials

Not applicable.

Declaration of competing interest

The authors declare that they have no known competing financial interests or personal relationships that could have appeared to influence the work reported in this paper.

Acknowledgment

The authors would like to thank the COATED M2A CDT at Swansea University, supported by the Engineering and Physical Sciences Research Council (EP/S02252X/1). Also, the authors would like to express their sincere gratitude to AkzoNobel for their valuable support and collaboration in this research. Their expertise, resources, and insightful discussions have been instrumental in the progress of this work.

References

[1] Nagumo M. Fundamentals of hydrogen embrittlement. Springer; 2016.
[2] Chen Y, Zhao S, Ma H, Wang H, Hua L, Fu S. Analysis of hydrogen embrittlement on aluminum alloys for vehicle-mounted hydrogen storage tanks: a review. Metals 2021;11:1303. https://doi.org/10.3390/met11081303.
[3] Djukic MB, Bakic GM, Zeravcic VS, Sedmak A, Rajicic B. The synergistic action and interplay of hydrogen embrittlement mechanisms in steels and iron: localized plasticity and decohesion. Eng Fract Mech 2019;216:106528. https://doi.org/10.1016/j.engfracmech.2019.106528.
[4] Ilyushechkin A, Schoeman L, Carter L, Hla SS. Material challenges and hydrogen embrittlement assessment for hydrogen utilisation in industrial scale. Hydro 2023;4:599–619. https://doi.org/10.3390/hydrogen4030039.
[5] Chen Y-S, Huang C, Liu P-Y, Yen H-W, Niu R, Burr P, et al. Hydrogen trapping and embrittlement in metals–A review. Int J Hydrogen Energy 2024. https://doi.org/10.1016/j.ijhydene.2024.04.076.
[6] Ahad MT, Bhuiyan MMH, Sakib AN, Becerril Corral A, Siddique Z. An overview of challenges for the future of hydrogen. Materials 2023;16:6680. https://doi.org/10.3390/ma16206680.
[7] Wang Z, Lu Q, Cao Z, Chen H, Huang M, Wang J. Review on hydrogen embrittlement of press-hardened steels for automotive applications. Acta Metall Sin 2023;36:1123–43. https://doi.org/10.1007/s40195-022-01408-4.
[8] Li X, Ma X, Zhang J, Akiyama E, Wang Y, Song X. Review of hydrogen embrittlement in metals: hydrogen diffusion, hydrogen characterization, hydrogen embrittlement mechanism and prevention. Acta Metall Sin 2020;33:759–73. https://doi.org/10.1007/s40195-020-01039-7.
[9] Sun B, Wang D, Lu X, Wan D, Ponge D, Zhang X. Current challenges and opportunities toward understanding hydrogen embrittlement mechanisms in advanced high-strength steels: a review. Acta Metall Sin 2021;34:741–54. https://doi.org/10.1007/s40195-021-01233-1.
[10] Walter R, Jewett R, Chandler W. On the mechanism of hydrogen-environment embrittlement of iron-and nickel-base alloys. Mater Sci Eng 1970;5:99–110. https://doi.org/10.1016/0025-5416(70)90039-X.
[11] Lynch S. Hydrogen embrittlement phenomena and mechanisms. Corrosion Rev 2012;30:105–23. https://doi.org/10.1515/corrrev-2012-0502.
[12] Robertson IM, Sofronis P, Nagao A, Martin ML, Wang S, Gross D, Nygren K. Hydrogen embrittlement understood. Metall Mater Trans 2015;46:2323–41. https://doi.org/10.1007/s11661-015-2836-1.
[13] Dwivedi SK, Vishwakarma M. Hydrogen embrittlement prevention in high strength steels by application of various surface coatings-A review. International conference on advanced production and industrial engineering. Springer; 2019. p. 673–83. https://doi.org/10.1007/978-981-15-8542-5_58.
[14] Dwivedi SK, Vishwakarma M. Hydrogen embrittlement in different materials: a review. Int J Hydrogen Energy 2018;43:21603–16. https://doi.org/10.1016/j.ijhydene.2018.09.201.
[15] Gong P, Turk A, Nutter J, Yu F, Wynne B, Rivera-Diaz-del-Castillo P, Rainforth WM. Hydrogen embrittlement mechanisms in advanced high strength steel. Acta Mater 2022;223:117488. https://doi.org/10.1016/j.actamat.2021.117488.
[16] Lovicu G, Bottazzi M, D'aiuto F, De Sanctis M, Dimatteo A, Santus C, Valentini R. Hydrogen embrittlement of automotive advanced high-strength steels. Metall Mater Trans 2012;43:4075–87. https://doi.org/10.1007/s11661-012-1280-8.
[17] Venezuela J, Liu Q, Zhang M, Zhou Q, Atrens A. A review of hydrogen embrittlement of martensitic advanced high-strength steels. Corrosion Rev 2016;34:153–86. https://doi.org/10.1515/corrrev-2016-0006.
[18] Valentini R, Bacchi L, Biagini F, Mastroianni M. Application of laboratory and on field techniques to determine the risk of hydrogen embrittlement in gaseous hydrogen and relative mixtures transport and storage. Matériaux Tech 2023;111:202. https://doi.org/10.1051/mattech/2023010.
[19] Meda US, Bhat N, Pandey A, Subramanya K, Raj MLA. Challenges associated with hydrogen storage systems due to the hydrogen embrittlement of high strength steels. Int J Hydrogen Energy 2023;48:17894–913. https://doi.org/10.1016/j.ijhydene.2023.01.292.
[20] Sun B, Zhao H, Dong X, Teng C, Zhang A, Kong S, et al. Current challenges in the utilization of hydrogen energy-a focused review on the issue of hydrogen-induced damage and embrittlement. Adv Appl Energy 2024:100168. https://doi.org/10.1016/j.adapen.2024.100168.
[21] Yu H, Díaz A, Lu X, Sun B, Ding Y, Koyama M, et al. Hydrogen embrittlement as a conspicuous material challenge—comprehensive review and future directions. Chem Rev 2024. https://doi.org/10.1021/acs.chemrev.3c00624.
[22] Hendry D, Castle J. A strategy for achieving net-zero emissions by 2050. EGU general Assembly conference Abstracts2021. p. EGU21-4688.10.5194/egusphere-egu21-4688.
[23] Rönnebro EC, Oelrich RL, Gates RO. Recent advances and prospects in design of hydrogen permeation barrier materials for energy Applications—a review. Molecules 2022;27:6528. https://doi.org/10.3390/molecules27196528.
[24] Liu J, Guo Y, Xing X, Zhang X, Yang Y, Cui G. A comprehensive review on hydrogen permeation barrier in the hydrogen transportation pipeline: mechanism, application, preparation, and recent advances. Int J Hydrogen Energy 2025;101:504–28. https://doi.org/10.1016/j.ijhydene.2024.12.379.
[25] Li Y, Barzagli F, Liu P, Zhang X, Yang Z, Xiao M, et al. Mechanism and evaluation of hydrogen permeation barriers: a critical review. Ind Eng Chem Res 2023;62:15752–73. https://doi.org/10.1021/acs.iecr.3c02259.
[26] He Q, Liu D, Zhou Y, Sun T-Y, Huang L-F. Nitride coatings for environmental barriers: the key microscopic mechanisms and momentous applications of first-principles calculations. Surface Sci Technol 2024;2:24. https://doi.org/10.1007/s44251-024-00053-6.
[27] Barrera O, Bombac D, Chen Y, Daff T, Galindo-Nava E, Gong P, et al. Understanding and mitigating hydrogen embrittlement of steels: a review of

experimental, modelling and design progress from atomistic to continuum. J Mater Sci 2018;53:6251–90. https://doi.org/10.1007/s10853-017-1978-5.
[28] Gaude-Fugarolas D. A comprehensive study of hydrogen redistribution and embrittlement prevention in ferrous alloys. Frontiers in materials processing, applications, research and technology: select proceedings of FiMPART 2015. Springer; 2018. p. 203–19. https://doi.org/10.1007/978-981-10-4819-7_18.
[29] Sun B, Dong X, Wen J, Zhang XC, Tu ST. Microstructure design strategies to mitigate hydrogen embrittlement in metallic materials. Fatig Fract Eng Mater Struct 2023;46:3060–76. https://doi.org/10.1111/ffe.14074.
[30] Wetegrove M, Duarte MJ, Taube K, Rohloff M, Gopalan H, Scheu C, et al. Preventing hydrogen embrittlement: the role of barrier coatings for the hydrogen economy. Hydrogen, vol. 4; 2023. p. 307–22. https://doi.org/10.3390/hydrogen4020022.
[31] Abiru Y, Nishiguchi H, Maekawa M, Nagata T, Itaya T, Koga M, Nishi T. Hydrogen embrittlement detection technology using nondestructive testing for realizing a hydrogen society. Materials 2024;17:4237. https://doi.org/10.3390/ma17174237.
[32] Choudhary S, Vishwakarma M, Dwivedi SK. Evaluation and prevention of hydrogen embrittlement by NDT methods: a review. Mater Proceed 2021;6:18. https://doi.org/10.3390/CMDWC2021-10044.
[33] Lee JA, Woods S. Hydrog Embrittl 2016.
[34] Stöver D, Buchkremer H, Hecker R. Hydrogen and deuterium permeation through metallic and surface-oxidized chromium. Surf Coating Technol 1986;28:281–90. https://doi.org/10.1016/0257-8972(86)90085-X.
[35] Tamura M, Noma M, Yamashita M. Characteristic change of hydrogen permeation in stainless steel plate by BN coating. Surf Coating Technol 2014;260:148–54. https://doi.org/10.1016/j.surfcoat.2014.09.041.
[36] Liu D-G, Yang T-T, Liu Y-L, Luo L-M, Wu Y-C. Thermal shock and tritium resistance of SiO2 coating on the inner wall of 316L stainless steel pipeline. Vacuum 2021;185:110032. https://doi.org/10.1016/j.vacuum.2020.110032.
[37] Menon NC, Kruizenga AM, Alvine KJ, San Marchi C, Nissen A, Brooks K. Behaviour of polymers in high pressure environments as applicable to the hydrogen infrastructure. Pressure vessels and piping conference. American Society of Mechanical Engineers; 2016. https://doi.org/10.1115/PVP2016-63713. V06BTA037.
[38] Hwang J-S, Kim J-H, Kim S-K, Lee J-M. Effect of PTFE coating on enhancing hydrogen embrittlement resistance of stainless steel 304 for liquefied hydrogen storage system application. Int J Hydrogen Energy 2020;45:9149–61. https://doi.org/10.1016/j.ijhydene.2020.01.104.
[39] Jung JK, Kim IG, Kim K. Evaluation of hydrogen permeation characteristics in rubbery polymers. Curr Appl Phys 2021;21:43–9. https://doi.org/10.1016/j.cap.2020.10.003.
[40] Lei Y, Hosseini E, Liu L, Scholes C, Kentish S. Internal polymeric coating materials for preventing pipeline hydrogen embrittlement and a theoretical model of hydrogen diffusion through coated steel. Int J Hydrogen Energy 2022;47:31409–19. https://doi.org/10.1016/j.ijhydene.2022.07.034.
[41] Lei Y, Liu L, Scholes CA, Kentish SE. Crosslinked PVA based polymer coatings with shear-thinning behaviour and ultralow hydrogen permeability to prevent hydrogen embrittlement. Int J Hydrogen Energy 2024;54:947–54. https://doi.org/10.1016/j.ijhydene.2023.11.151.
[42] Zhao J, Jiang Z, Lee CS. Effects of tungsten on the hydrogen embrittlement behaviour of microalloyed steels. Corros Sci 2014;82:380–91. https://doi.org/10.1016/j.corsci.2014.01.042.
[43] Kim H, Popov BN, Chen KS. Comparison of corrosion-resistance and hydrogen permeation properties of Zn–Ni, Zn–Ni–Cd and Cd coatings on low-carbon steel. Corros Sci 2003;45:1505–21. https://doi.org/10.1016/S0010-938X(02)00228-7.
[44] Samanta S, Vishwanath K, Mondal K, Dutta M, Singh SB. Electroless amorphous NiP coatings over API X70 steel: resistance to wear and hydrogen embrittlement. Met Mater Int 2022:1–15. https://doi.org/10.1007/s12540-021-01102-7.
[45] Sadananda K, Yang JH, Iyyer N, Phan N, Rahman A. Sacrificial Zn–Ni coatings by electroplating and hydrogen embrittlement of high-strength steels. Corrosion Rev 2021;39:487–517. https://doi.org/10.1515/corrrev-2021-0038.
[46] Holmberg K, Matthews A. Coatings tribology: properties, mechanisms, techniques and applications in surface engineering. Elsevier; 2009.
[47] Dwivedi SK, Vishwakarma M, Ahmed S. Experimental investigation of hydrogen embrittlement during coating process and effect on mechanical properties of high strength steel used for fasteners. Mater Today Proc 2018;5:18707–15. https://doi.org/10.1016/j.matpr.2018.06.217.
[48] Magliano A, Perez Carrera C, Pappalardo CM, Guida D, Berardi VP. A comprehensive literature review on hydrogen tanks: storage, safety, and structural integrity. Appl Sci 2024;14:9348. https://doi.org/10.3390/app14209348.
[49] Sofian M, Haq MB, Al Shehri D, Rahman MM, Muhammed NS. A review on hydrogen blending in gas network: insight into safety, corrosion, embrittlement, coatings and liners, and bibliometric analysis. Int J Hydrogen Energy 2024;60:867–89. https://doi.org/10.1016/j.ijhydene.2024.02.166.
[50] Okonkwo PC, Belgacem IB, Mansir IB, Aliyu M, Emori W, Uzoma PC, et al. A focused review of the hydrogen storage tank embrittlement mechanism process. Int J Hydrogen Energy 2023;48:12935–48. https://doi.org/10.1016/j.ijhydene.2022.12.252.
[51] Behera P, Rajagopalan SK, Brahimi S, Venturella CA, Gaydos SP, Straw RJ, Yue S. Effect of brush plating process variables on the microstructures of Cd and ZnNi coatings and hydrogen embrittlement. Surf Coating Technol 2021;417:127181. https://doi.org/10.1016/j.surfcoat.2021.127181.
[52] Michler T, Naumann J. Coatings to reduce hydrogen environment embrittlement of 304 austenitic stainless steel. Surf Coating Technol 2009;203:1819–28. https://doi.org/10.1016/j.surfcoat.2009.01.013.
[53] Shi K, Xiao S, Ruan Q, Wu H, Chen G, Zhou C, et al. Hydrogen permeation behavior and mechanism of multi-layered graphene coatings and mitigation of hydrogen embrittlement of pipe steel. Appl Surf Sci 2022;573:151529. https://doi.org/10.1016/j.apsusc.2021.151529.
[54] Croll S. Stress and embrittlement in organic coatings during general weathering exposure: a review. Prog Org Coating 2022;172:107085. https://doi.org/10.1016/j.porgcoat.2022.107085.
[55] Lakdhar I, Alhussein A, Capelle J, Creus J. Al-Ti-W alloys deposited by magnetron sputtering: effective barrier to prevent steel hydrogen embrittlement. Appl Surf Sci 2021;567:150786. https://doi.org/10.1016/j.apsusc.2021.150786.
[56] Moshref-Javadi M, Edris H, Shafyei A, Salimi-Jazi H. Diffusion behavior of hydrogen through thermally sprayed coating of 316L stainless steel. Int J Hydrogen Energy 2017;42:6409–19. https://doi.org/10.1016/j.ijhydene.2016.11.026.
[57] Sagiroun MI, Xinrong C. Zirconium-based cladding coating technique for oxidation, corrosion and embrittlement reduction at high-temperature: an overview. IOP conference series: materials science and engineering. IOP Publishing; 2019, 012008. https://doi.org/10.1088/1757-899X/649/1/012008.
[58] Zhou P, Yu B, Hou Y, Duan G, Yang L, Zhang B, et al. Revisiting the cracking of chemical conversion coating on magnesium alloys. Corros Sci 2021;178:109069. https://doi.org/10.1016/j.corsci.2020.109069.
[59] Reda Y, El-Shamy A, Eessaa AK. Effect of hydrogen embrittlement on the microstructures of electroplated steel alloy 4130. Ain Shams Eng J 2018;9:2973–82. https://doi.org/10.1016/j.asej.2018.08.004.
[60] Wang L, Zhu C, Liang C, Feng Y, Gong B, Wang X, et al. Preparation and characterization of Al2O3/Y2O3 multilayer coatings as tritium permeation barrier. Mater Res Express 2019;6:106403. https://doi.org/10.1088/2053-1591/ab3498.
[61] Addach H, Berçot P, Rezrazi M, Takadoum J. Study of the electrochemical permeation of hydrogen in iron. Corros Sci 2009;51:263–7. https://doi.org/10.1016/j.corsci.2008.10.024.
[62] International A. ASTM International, ASTM F2078-22. Standard terminology relating to hydrogen embrittlement testing. ASTM; 2022.
[63] International A. ASTM International, ASTM G193-12d. Standard terminology and acronyms relating to corrosion. ASTM; 2012.
[64] Campari A, Ustolin F, Alvaro A, Paltrinieri N. A review on hydrogen embrittlement and risk-based inspection of hydrogen technologies. Int J Hydrogen Energy 2023;48:35316–46. https://doi.org/10.1016/j.ijhydene.2023.05.293.
[65] Tohme E. A contribution to the understanding of hydrogen diffusion and embrittlement in metallic materials based on SKPFM measurements and mechanical testing. Université de Lyon; 2019.
[66] LaFleur C, Hecht E, Ehrhart B, Ronevich J, San Marchi C. Safety of hydrogen for large-scale energy deployment in a decarbonized economy. Hydrogen economy. Elsevier; 2023. p. 511–35.
[67] Wang Z, Wang Y, Afshan S, Hjalmarsson J. A review of metallic tanks for H2 storage with a view to application in future green shipping. Int J Hydrogen Energy 2021;46:6151–79. https://doi.org/10.1016/j.ijhydene.2020.11.168.
[68] Qin X. Hydrogen embrittlement and corrosion behavior of low temperature carburized austenitic stainless steel: chalmers university of technology. Gothenburg, Sweden: Department of Industrial and Materials Science; 2023.
[69] Das T, Legrand E, Brahimi SV, Song J, Yue S. Evaluation of material susceptibility to hydrogen embrittlement (HE): an approach based on experimental and finite element (FE) analyses. Eng Fract Mech 2020;224:106714. https://doi.org/10.1016/j.engfracmech.2019.106714.
[70] Ogawa Y, Okazaki S, Takakuwa O, Matsunaga H. The roles of internal and external hydrogen in the deformation and fracture processes at the fatigue crack tip zone of metastable austenitic stainless steels. Scr Mater 2018;157:95–9. https://doi.org/10.1016/j.scriptamat.2018.08.003.
[71] San Marchi C, Michler T, Nibur K, Somerday B. On the physical differences between tensile testing of type 304 and 316 austenitic stainless steels with internal hydrogen and in external hydrogen. Int J Hydrogen Energy 2010;35:9736–45. https://doi.org/10.1016/j.ijhydene.2010.06.018.
[72] Jia G, Lei M, Li M, Xu W, Li R, Lu Y, Cai M. Hydrogen embrittlement in hydrogen-blended natural gas transportation systems: a review. Int J Hydrogen Energy 2023;48:32137–57. https://doi.org/10.1016/j.ijhydene.2023.04.266.
[73] Li X, Yin J, Zhang J, Wang Y, Song X, Zhang Y, Ren X. Hydrogen embrittlement and failure mechanisms of multi-principal element alloys: a review. J Mater Sci Technol 2022;122:20–32. https://doi.org/10.1016/j.jmst.2022.01.008.
[74] Louthan M. Hydrogen embrittlement of metals: a primer for the failure analyst. J Fail Anal Prev 2008;8:289–307. https://doi.org/10.1007/s11668-008-9133-x.
[75] Patanwar YK, Kim H-M, Deb D, Gujjala YK. Underground storage of hydrogen in lined rock caverns: an overview of key components and hydrogen embrittlement challenges. Int J Hydrogen Energy 2024;50:116–33. https://doi.org/10.1016/j.ijhydene.2023.08.342.
[76] Gabetta G, Cioffi P, Bruschi R. Engineering thoughts on hydrogen embrittlement. Procedia Struct Integr 2018;9:250–6. https://doi.org/10.1016/j.prostr.2018.06.038.
[77] Takasugi T, Izumi O. Factors affecting the intergranular hydrogen embrittlement of Co3Ti. Acta Metall 1986;34:607–18. https://doi.org/10.1016/0001-6160(86)90176-8.

[78] Alvaro A, Wan D, Olden V, Barnoush A. Hydrogen enhanced fatigue crack growth rates in a ferritic Fe-3 wt% Si alloy and a X70 pipeline steel. Eng Fract Mech 2019; 219:106641. https://doi.org/10.1016/j.engfracmech.2019.106641.
[79] Nanninga N, Levy Y, Drexler ES, Condon R, Stevenson A, Slifka AJ. Comparison of hydrogen embrittlement in three pipeline steels in high pressure gaseous hydrogen environments. Corros Sci 2012;59:1–9. https://doi.org/10.1016/j.corsci.2012.01.028.
[80] Slifka AJ, Drexler ES, Amaro RL, Hayden LE, Stalheim DG, Lauria DS, Hrabe NW. Fatigue measurement of pipeline steels for the application of transporting gaseous hydrogen. J Pressure Vessel Technol 2018;140:011407. https://doi.org/10.1115/1.4038594.
[81] Stalheim D, Boggess T, San Marchi C, Jansto S, Somerday B, Muralidharan G, Sofronis P. Microstructure and mechanical property performance of commercial grade API pipeline steels in high pressure gaseous hydrogen. Int Pipelin Conf 2010. p. 529-537.https://doi.org/10.1115/IPC2010-31301.
[82] Amaro RL, White RM, Looney CP, Drexler ES, Slifka AJ. Development of a model for hydrogen-assisted fatigue crack growth of pipeline steel. J Pressure Vessel Technol 2018;140:021403. https://doi.org/10.1115/1.4038824.
[83] Chou S-L, Tsai W-T. Effect of grain size on the hydrogen-assisted cracking in duplex stainless steels. Mater Sci Eng 1999;270:219–24. https://doi.org/10.1016/S0921-5093(99)00174-4.
[84] Claeys L, De Graeve I, Depover T, Verbeken K. Hydrogen-assisted cracking in 2205 duplex stainless steel: initiation, propagation and interaction with deformation-induced martensite. Mater Sci Eng 2020;797:140079. https://doi.org/10.1016/j.msea.2020.140079.
[85] Young M, Chan S, Tsay L, Shin C-S. Hydrogen-enhanced cracking of 2205 duplex stainless steel welds. Mater Chem Phys 2005;91:21–7. https://doi.org/10.1016/j.matchemphys.2004.10.042.
[86] Khosravi A, Song J, Mousseau N. Understanding the influence of hydrogen on BCC iron grain boundaries using the kinetic activation relaxation technique (k-ART). J Phys: Materials 2025. https://doi.org/10.1088/2515-7639/ada994.
[87] Jo JW, Seo HJ, Jung B-I, Choi S, Lee CS. Effect of bainite fraction on hydrogen embrittlement of bainite/martensite steel. Mater Sci Eng 2021;814:141226. https://doi.org/10.1016/j.msea.2021.141226.
[88] Michler T, Naumann J. Microstructural aspects upon hydrogen environment embrittlement of various bcc steels. Int J Hydrogen Energy 2010;35:821–32. https://doi.org/10.1016/j.ijhydene.2009.10.092.
[89] Olden V, Thaulow C, Johnsen R. Modelling of hydrogen diffusion and hydrogen induced cracking in supermartensitic and duplex stainless steels. Mater Des 2008; 29:1934–48. https://doi.org/10.1016/j.matdes.2008.04.026.
[90] Sobol O, Straub F, Wirth T, Holzlechner G, Boellinghaus T, Unger W. Real time imaging of deuterium in a duplex stainless steel microstructure by time-of-flight SIMS. Sci Rep 2016;6:19929. https://doi.org/10.1038/srep19929.
[91] Park GT, Koh SU, Jung HG, Kim KY. Effect of microstructure on the hydrogen trapping efficiency and hydrogen induced cracking of linepipe steel. Corros Sci 2008;50:1865–71. https://doi.org/10.1016/j.corsci.2008.03.007.
[92] López-Suárez A. Influence of surface roughness on consecutively hydrogen absorption cycles in Ti–6Al–4V alloy. Int J Hydrogen Energy 2010;35:10404–11. https://doi.org/10.1016/j.ijhydene.2010.07.163.
[93] Leng Z, Zhang S, Wang W, Gu H, Yin J, Wang Z, Liu Y. Study on the influence of surface integrity on hydrogen permeation resistance of hydrogen production reactor materials. Appl Sci 2023;13:10461. https://doi.org/10.3390/app131810461.
[94] Oriani R. Hydrogen embrittlement of steels. Annu Rev Mater Sci 1978;8:327–57.
[95] Young Jr G, Scully J. The diffusion and trapping of hydrogen in high purity aluminum. Acta Mater 1998;46:6337–49. https://doi.org/10.1016/S1359-6454(98)00333-4.
[96] Kiuchi K, McLellan R. The solubility and diffusivity of hydrogen in well-annealed and deformed iron. Perspectives in hydrogen in metals. Elsevier; 1986. p. 29–52.
[97] de Souza Brandolt C, Noronha LC, Hidalgo GEN, Takimi AS, Schroeder RM, de Fraga Malfatti C. Niobium coating applied by HVOF as protection against hydrogen embrittlement of API 5CT P110 steel. Surf Coating Technol 2017;322: 10–8. https://doi.org/10.1016/j.surfcoat.2017.05.017.
[98] Li Q, Ghadiani H, Jalilvand V, Alam T, Farhat Z, Islam MA. Hydrogen impact: a review on diffusibility, embrittlement mechanisms, and characterization. Materials 2024;17:965. https://doi.org/10.3390/ma17040965.
[99] Gangloff RP, Somerday BP. Gaseous hydrogen embrittlement of materials in energy technologies: the problem, its characterisation and effects on particular alloy classes. Elsevier; 2012.
[100] Kussmaul K, Deimel P, Fischer H, Sattler E. Fracture mechanical behaviour of the steel 15 MnNi 6 3 in argon and in high pressure hydrogen gas with admixtures of oxygen. Int J Hydrogen Energy 1998;23:577–82. https://doi.org/10.1016/S0360-3199(97)00104-3.
[101] Shang J, Chen W, Zheng J, Hua Z, Zhang L, Zhou C, Gu C. Enhanced hydrogen embrittlement of low-carbon steel to natural gas/hydrogen mixtures. Scr Mater 2020;189:67–71. https://doi.org/10.1016/j.scriptamat.2020.08.011.
[102] Somerday BP, Sofronis P, Nibur KA, San Marchi C, Kirchheim R. Elucidating the variables affecting accelerated fatigue crack growth of steels in hydrogen gas with low oxygen concentrations. Acta Mater 2013;61:6153–70. https://doi.org/10.1016/j.actamat.2013.07.001.
[103] Laureys A, Depraetere R, Cauwels M, Depover T, Hertelé S, Verbeken K. Use of existing steel pipeline infrastructure for gaseous hydrogen storage and transport: a review of factors affecting hydrogen induced degradation. J Nat Gas Sci Eng 2022;101:104534. https://doi.org/10.1016/j.jngse.2022.104534.
[104] Matsuoka S, Takakuwa O, Okazaki S, Yoshikawa M, Yamabe J, Matsunaga H. Peculiar temperature dependence of hydrogen-enhanced fatigue crack growth of low-carbon steel in gaseous hydrogen. Scr Mater 2018;154:101–5. https://doi.org/10.1016/j.scriptamat.2018.05.035.
[105] Li H, Niu R, Li W, Lu H, Cairney J, Chen Y-S. Hydrogen in pipeline steels: recent advances in characterization and embrittlement mitigation. J Nat Gas Sci Eng 2022;105:104709. https://doi.org/10.1016/j.jngse.2022.104709.
[106] San Marchi C, Somerday B. Effects of high-pressure gaseous hydrogen on structural metals. SAE Trans 2007:94–109.
[107] An T, Peng H, Bai P, Zheng S, Wen X, Zhang L. Influence of hydrogen pressure on fatigue properties of X80 pipeline steel. Int J Hydrogen Energy 2017;42: 15669–78. https://doi.org/10.1016/j.ijhydene.2017.05.047.
[108] Briottet L, Moro I, Lemoine P. Quantifying the hydrogen embrittlement of pipeline steels for safety considerations. Int J Hydrogen Energy 2012;37: 17616–23. https://doi.org/10.1016/j.ijhydene.2012.05.143.
[109] Faucon LE, Boot T, Riemslag T, Scott SP, Liu P, Popovich V. Hydrogen-accelerated fatigue of API X60 pipeline steel and its weld. Metals 2023;13:563. https://doi.org/10.3390/met13030563.
[110] Raja V, Padekar BS. Role of chlorides on pitting and hydrogen embrittlement of Mg–Mn wrought alloy. Corros Sci 2013;75:176–83. https://doi.org/10.1016/j.corsci.2013.05.030.
[111] Kawashima A, Hashimoto K, Shimodaira S. Hydrogen electrode reaction and hydrogen embrittlement of mild steel in hydrogen sulfide solutions. Corrosion 1976;32:321–31. https://doi.org/10.5006/0010-9312-32.8.321.
[112] Claeys L, Laureys A, De Waele W, Schweicher J, Depover T, Verbeken K. Gaseous inhibitors: a comprehensive overview on mitigating hydrogen embrittlement in pipeline steels. Int J Hydrogen Energy 2024. https://doi.org/10.1016/j.ijhydene.2024.08.018.
[113] Giannini L, Razavi N, Alvaro A, Paltrinieri N. Embrittlement, degradation, and loss prevention of hydrogen pipelines. MRS Bull 2024;49:464–77. https://doi.org/10.1557/s43577-024-00695-9.
[114] Bryan W, Dodge B. Diffusivity of hydrogen in pure iron. AIChE J 1963;9:223–8. https://doi.org/10.1002/aic.690090217.
[115] Giannis S, Maxwell T, Omoniyi F, Veerabhadrappa M. Hydrog Gas Permeabil Polym Compos–Test Set-up Dev 2022.
[116] Laadel N-E, El Mansori M, Kang N, Marlin S, Boussant-Roux Y. Permeation barriers for hydrogen embrittlement prevention in metals–a review on mechanisms, materials suitability and efficiency. Int J Hydrogen Energy 2022;47: 32707–31.
[117] International A. ASTM D1434-23. Standard Test Method for Determining Gas Permeability Characteristics of Plastic Film and Sheeting 2023.
[118] International A. ASTM G148-97. Standard practice for evaluation of hydrogen uptake. Permeation, and Transport in Metals by an Electrochemical Technique 2018.
[119] Zhang Z, Chattot R, Bonorand L, Jetsrisuparb K, Buchmueller Y, Wokaun A, Gubler L. Mass spectrometry to quantify and compare the gas barrier properties of radiation grafted membranes and Nafion®. J Membr Sci 2014;472:55–66. https://doi.org/10.1016/j.memsci.2014.08.020.
[120] Fraga S, Monteleone M, Lanč M, Esposito E, Fuoco A, Giorno L, et al. A novel time lag method for the analysis of mixed gas diffusion in polymeric membranes by on-line mass spectrometry: method development and validation. J Membr Sci 2018; 561:39–58. https://doi.org/10.1016/j.memsci.2018.04.029.
[121] Ouyang Y, Yu G, Ou A, Hu L, Xu W. Double electrolyte sensor for monitoring hydrogen permeation rate in steels. Corros Sci 2011;53:2247–52. https://doi.org/10.1016/j.corsci.2011.03.002.
[122] Ouyang Y, Wang X, Yu G, Song Z, Zhang X. Performance of amperometric and potentiometric hydrogen sensors. J Mater Sci Technol 2014;30:1160–5. https://doi.org/10.1016/j.jmst.2014.07.001.
[123] Dan A, Bijalwan PK, Pathak AS, Bhagat AN. A review on physical vapor deposition-based metallic coatings on steel as an alternative to conventional galvanized coatings. J Coating Technol Res 2022;19:403–38. https://doi.org/10.1007/s11998-021-00564-z.
[124] Liu L, Ruan Q, Xiao S, Meng X, Huang C, Wu Y, et al. Fabrication and hydrogen permeation resistance of dense CrN coatings. Surf Coating Technol 2022;437: 128326. https://doi.org/10.1016/j.surfcoat.2022.128326.
[125] He D, Lei Y, Zhang C, Li S, Liu X, Zhang H, et al. Deuterium permeation of Al2O3/Cr2O3 composite film on 316L stainless steel. Int J Hydrogen Energy 2015;40: 2899–903. https://doi.org/10.1016/j.ijhydene.2014.12.058.
[126] Levchuk D, Koch F, Maier H, Bolt H. Gas-driven deuterium permeation through Al2O3 coated samples. Phys Scripta 2004;2004:119.
[127] Faraji G, Kim HS, Kashi HT. Severe plastic deformation: methods, processing and properties. Elsevier; 2018.
[128] Pahade VS, Chavan PS, Baisane VP. A review paper on vapour deposition coating. Int J Eng Appl Sci 2016;3:257640.
[129] Creighton J, Ho P. Introduction to chemical vapor deposition (CVD). ASM international; 2001. p. 407.
[130] Dobrzanski L, Pakula D, Staszuk M. Chemical vapor deposition in manufacturing. In: Nee A, editor. Handbook of manufacturing engineering and technology. London: Springer London; 2013. p. 1–41.
[131] Cruz JN, Altalhi T. Green Sustain Proc Chem Environ Eng Sci: Recent Adv Nanocarr 2023.
[132] Kuzminykh Y, Dabirian A, Reinke M, Hoffmann P. High vacuum chemical vapour deposition of oxides:: a review of technique development and precursor selection. Surf Coating Technol 2013;230:13–21. https://doi.org/10.1016/j.surfcoat.2013.06.059.
[133] Tamura M, Eguchi T. Nanostructured thin films for hydrogen-permeation barrier. J Vac Sci Technol A 2015;33. https://doi.org/10.1116/1.4919736.

[134] Qadir D, Sharif R, Nasir R, Awad A, Mannan HA. A review on coatings through thermal spraying. Chem Pap 2024;78:71–91. https://doi.org/10.1007/s11696-023-03089-4.
[135] Li Y, Huard M, Wong K, Wang X, Adane KF. Gap analysis of coating and liner for hydrogen pipeline. International Pipeline Conference: American Society of Mechanical Engineers; 2024, V003T05A25. https://doi.org/10.1115/IPC2024-133821.
[136] Morimoto T, Kumai T. Prevention of hydrogen embrittlement using ultra rapid cooling thermal spraying Gun. ISIJ Int 2017;57:1461–7. https://doi.org/10.2355/isijinternational.ISIJINT-2017-060.
[137] Wang Y, Bai Y, Liu K, Wang J, Kang Y, Li J, et al. Microstructural evolution of plasma sprayed submicron-/nano-zirconia-based thermal barrier coatings. Appl Surf Sci 2016;363:101–12. https://doi.org/10.1016/j.apsusc.2015.12.010.
[138] Hatano Y, Zhang K, Hashizume K. Fabrication of ZrO2 coatings on ferritic steel by wet-chemical methods as a tritium permeation barrier. Phys Scripta 2011;2011:014044. https://doi.org/10.1088/0031-8949/2011/T145/014044.
[139] Kaczmarczyk N, Szczurek J, Babiarczuk B, Gronowicz P, Paszkowski M, Kowalski M, et al. Thin film quality of sol–gel SiO2 coatings prepared on Ti6Al4V depending on their composition and titanium substrate preparation. J Mater Sci 2025:1–31. https://doi.org/10.1007/s10853-025-11273-y.
[140] Almeida RM, Gonçalves MC. Sol–Gel process and products. Encycloped Glass Sci Technol Histor Cult 2021;2:969–79. https://doi.org/10.1002/9781118801017.ch8.2.
[141] Hench LL, West JK. The sol-gel process. Chem Rev 1990;90:33–72. https://doi.org/10.1021/cr00099a003.
[142] Wang T, Pu J, Bo C, Jian L. Sol–gel prepared Al2O3 coatings for the application as tritium permeation barrier. Fusion Eng Des 2010;85:1068–72. https://doi.org/10.1016/j.fusengdes.2010.01.021.
[143] Yao Z, Suzuki A, Levchuk D, Chikada T, Tanaka T, Muroga T, Terai T. Hydrogen permeation through steel coated with erbium oxide by sol–gel method. J Nucl Mater 2009;386:700–2. https://doi.org/10.1016/j.jnucmat.2008.12.286.
[144] Zhang K, Hatano Y. Sealing of pores in sol–gel-derived tritium permeation barrier coating by electrochemical technique. J Nucl Mater 2011;417:1229–32. https://doi.org/10.1016/j.jnucmat.2010.12.276.
[145] Johnson RW, Hultqvist A, Bent SF. A brief review of atomic layer deposition: from fundamentals to applications. Mater Today 2014;17:236–46. https://doi.org/10.1016/j.mattod.2014.04.026.
[146] George SM. Atomic layer deposition: an overview. Chem Rev 2010;110:111–31. https://doi.org/10.1021/cr900056b.
[147] Bull SK. Atomic layer deposition of environmental barrier coatings for preventing hydrogen ingress. University of Colorado at Boulder; 2021.
[148] Zhang M, Zhao R, Ling Y, Wang R, Zhou Q, Wang J, et al. Preparation of Cr2O3/Al2O3 bipolar oxides as hydrogen permeation barriers by selective oxide removal on SS and atomic layer deposition. Int J Hydrogen Energy 2019;44:12277–87. https://doi.org/10.1016/j.ijhydene.2019.03.086.
[149] Liu Q, Cao Y, Chen S, Xu X, Yao M, Fang J, et al. Hot-dip galvanizing process and the influence of metallic elements on composite coatings. J Compos Sci 2024;8:160. https://doi.org/10.3390/jcs8050160.
[150] Serra E, Glasbrenner H, Perujo A. Hot-dip aluminium deposit as a permeation barrier for MANET steel. Fusion Eng Des 1998;41:149–55. https://doi.org/10.1016/S0920-3796(98)00224-5.
[151] Zhang DL, Li Y. Hydrogen permeation characterization of hot-dip galvanized steel in simulated marine atmospheric environment. Adv Mater Res 2009;79:1051–4. https://doi.org/10.4028/www.scientific.net/AMR.79-82.1051.
[152] Ben Dhieb F, Tabatabaei SH, Mighri F, Ajji A. Comparison of crosslinking efficiency in dip and roll-deposited coatings on their oxygen barrier. ACS Omega 2019;4:15772–9. https://doi.org/10.1021/acsomega.9b00950.
[153] Yuan S, Sun Y, Yang C, Zhang Y, Cong C, Yuan Y, et al. A novel dual-functional epoxy-based composite coating with exceptional anti-corrosion and enhanced hydrogen gas barrier properties. Chem Eng J 2022;449:137876. https://doi.org/10.1016/j.cej.2022.137876.
[154] Sharun V, Rajasekaran M, Kumar SS, Tripathi V, Sharma R, Puthilibai G, et al. Study on developments in protection coating techniques for steel. Adv Mater Sci Eng 2022;2022. https://doi.org/10.1155/2022/2843043.
[155] Fujiwara H, Ono H, Ohyama K, Kasai M, Kaneko F, Nishimura S. Hydrogen permeation under high pressure conditions and the destruction of exposed polyethylene-property of polymeric materials for high-pressure hydrogen devices (2). Int J Hydrogen Energy 2021;46:11832–48. https://doi.org/10.1016/j.ijhydene.2020.12.223.
[156] Kane M. Permeability, solubility, and interaction of hydrogen in polymers-An assessment of materials for hydrogen transport. Savannah River Site (SRS), Aiken, SC (United States) 2008.
[157] Khare A, Vishwakarma M, Ahmed S. Combating hydrogen embrittlement with graphene based coatings. Int J Adv Res Eng Technol 2019;10:234–51. https://doi.org/10.34218/IJARET.10.6.2019.027.
[158] Nemanič V. Hydrogen permeation barriers: basic requirements, materials selection, deposition methods, and quality evaluation. Nuclear Mater Energy 2019;19:451–7. https://doi.org/10.1016/j.nme.2019.04.001.
[159] Xiao S, Meng X, Shi K, Liu L, Wu H, Lian W, et al. Hydrogen permeation barriers and preparation techniques: a review. J Vac Sci Technol A 2022;40. https://doi.org/10.1116/6.0002178.
[160] Xiang X, Wang X, Zhang G, Tang T, Lai X. Preparation technique and alloying effect of aluminide coatings as tritium permeation barriers: a review. Int J Hydrogen Energy 2015;40:3697–707. https://doi.org/10.1016/j.ijhydene.2015.01.052.
[161] Presuel-Moreno F, Jakab M, Tailleart N, Goldman M, Scully J. Corrosion-resistant metallic coatings. Mater Today 2008;11:14–23. https://doi.org/10.1016/S1369-7021(08)70203-7.
[162] Tardif H, Marquis H. Protection of steel from hydrogen by surface coatings. Can Metall Q 1962;1:153–71. https://doi.org/10.1179/cmq.1962.1.2.153.
[163] Nemanič V, Kovač J, Žumer M, Zavašnik J. Impact of surface oxide on hydrogen permeability of chromium membranes. Int J Hydrogen Energy 2023;48:9723–33. https://doi.org/10.1016/j.ijhydene.2022.11.267.
[164] Williams D, Riahi A, Carcea A, Giallonardo J, Keech P, Persaud S, et al. Hydrogen embrittlement and strain rate sensitivity of electrodeposited copper: part I–the effect of hydrogen content. npj Mater Degrad 2024;8:79. https://doi.org/10.1038/s41529-024-00498-y.
[165] Frauenfelder R. Solution and diffusion of hydrogen in tungsten. J Vac Sci Technol 1969;6:388–97.
[166] Bhadeshia HKDH. Prevention of hydrogen embrittlement in steels. ISIJ Int 2016;56:24–36. https://doi.org/10.2355/isijinternational.ISIJINT-2015-430.
[167] Jones RH, Thomas GJ. Materials for the hydrogen economy. CRC Press; 2007.
[168] Hillier E, Robinson M. Hydrogen embrittlement of high strength steel electroplated with zinc–cobalt alloys. Corros Sci 2004;46:715–27. https://doi.org/10.1016/S0010-938X(03)00180-X.
[169] REB Res Consult. Accessed: May 13, 2025. [Online]. Available: https://www.rebresearch.com/H2perm2.htm.2011.
[170] Hollenberg G, Simonen E, Kalinin G, Terlain A. Tritium/hydrogen barrier development. Fusion Eng Des 1995;28:190–208. https://doi.org/10.1016/0920-3796(95)90039-X.
[171] Yamabe J, Awane T, Matsuoka S. Elucidating the hydrogen-entry-obstruction mechanism of a newly developed aluminum-based coating in high-pressure gaseous hydrogen. Int J Hydrogen Energy 2015;40:10329–39. https://doi.org/10.1016/j.ijhydene.2015.06.023.
[172] Kim KH, Park HC, Lee J, Cho E, Lee SM. Vanadium alloy membranes for high hydrogen permeability and suppressed hydrogen embrittlement. Scr Mater 2013;68:905–8. https://doi.org/10.1016/j.scriptamat.2013.02.028.
[173] Liu L, Gong H. Hydrogen solubility and diffusivity at Σ3 grain boundary of PdCu. RSC Adv 2021;11:13644–52. https://doi.org/10.1039/D0RA10133H.
[174] Abramov E, Riehm M, Thompson D, Smeltzer W. Deuterium permeation and diffusion in high-purity beryllium. J Nucl Mater 1990;175:90–5. https://doi.org/10.1016/0022-3115(90)90274-Q.
[175] Araujo L, de Almeida L, dos Santos D. Hydrogen embrittlement of a hard chromium plated cylinder assembly. Eng Fail Anal 2019;103:259–65. https://doi.org/10.1016/j.engfailanal.2019.04.052.
[176] Ganchenkova M, Borodin VA, Nieminen RM. Hydrogen in beryllium: solubility, transport, and trapping. Phys Rev B Condens Matter 2009;79:134101. https://doi.org/10.1103/PhysRevB.79.134101.
[177] Xu Y, Hirooka Y, Ashikawa N, Nagasaka T. Hydrogen isotopes transport in sputter-deposited tungsten coatings. Fusion Eng Des 2017;125:239–44. https://doi.org/10.1016/j.fusengdes.2017.07.021.
[178] Vargas F, Latorre G, Uribe I. Behavior of thermal spray coatings against hydrogen attack. CT F Ciencia, Tecnol, Futuro 2003;2:65–73.
[179] Ćwiek J. Prevention methods against hydrogen degradation of steel. J Achiev Mater Manufact Eng 2010;43:214–21.
[180] Kyo Y, Yadav AP, Nishikata A, Tsuru T. Hydrogen entry behaviour of hot-dip Al–Mg–Si coated steel. Corros Sci 2011;53:3866–71. https://doi.org/10.1016/j.corsci.2011.07.027.
[181] Han S, Li H, Wang S, Jiang L, Liu X. Influence of silicon on hot-dip aluminizing process and subsequent oxidation for preparing hydrogen/tritium permeation barrier. Int J Hydrogen Energy 2010;35:2689–93. https://doi.org/10.1016/j.ijhydene.2009.04.033.
[182] Tamura M, Takizawa H. TiAlN/TiMoN coatings as hydrogen barriers. J Mater Sci Eng 2019;9(1–2):1–7. https://doi.org/10.17265/2161-6213/2019.1-2.001.
[183] Tamura M. Hydrogen permeation of multi-layered-coatings. Adv Mater Res 2019;1152:9–18. https://doi.org/10.4028/www.scientific.net/AMR.1152.9.
[184] Matějíček J, Veverka J, Nemanič V, Cvrček L, Lukáč F, Havránek V, Illková K. Characterization of less common nitrides as potential permeation barriers. Fusion Eng Des 2019;139:74–80. https://doi.org/10.1016/j.fusengdes.2018.12.056.
[185] McGuiness PJ, Čekada M, Nemanič V, Zajec B, Rečnik A. Hydrogen permeation through TiAlN-coated Eurofer'97 steel. Surf Coating Technol 2011;205:2709–13. https://doi.org/10.1016/j.surfcoat.2010.08.133.
[186] Nemanič V, McGuiness PJ, Daneu N, Zajec B, Siketić Z, Waldhauser W. Hydrogen permeation through silicon nitride films. J Alloys Compd 2012;539:184–9. https://doi.org/10.1016/j.jallcom.2012.05.110.
[187] Forcey K, Perujo A, Reiter F, Lolli-Ceroni P. The formation of tritium permeation barriers by CVD. J Nucl Mater 1993;200:417–20. https://doi.org/10.1016/0022-3115(93)90319-T.
[188] Ueda M, Kurokawa H, Kawamura K, Maruyama T, Oyama Y. Hydrogen permeation measurement of iron and its oxide membranes by using A dew point hygrometer. Proceedings of the proceedings—electrochemical society. 2004. p. 3–8. Honolulu, HI, USA.
[189] Yunyi W, Li S, He D, Liu X, Wang S, Jiang L. Influence of annealing atmosphere on the deuterium permeation of Y2O3 coatings. Int J Hydrogen Energy 2016;41:10374–9. https://doi.org/10.1016/j.ijhydene.2015.12.004.
[190] Lee D, Oyama ST. Gas permeation characteristics of a hydrogen selective supported silica membrane. J Membr Sci 2002;210:291–306. https://doi.org/10.1016/S0376-7388(02)00389-7.
[191] Checchetto R, Bonelli M, Gratton L, Miotello A, Sabbioni A, Guzman L, et al. Analysis of the hydrogen permeation properties of TiN-TiC bilayers deposited on

martensitic stainless steel. Surf Coating Technol 1996;83:40–4. https://doi.org/10.1016/0257-8972(96)02851-4.
[192] Yamabe J, Matsuoka S, Murakami Y. Surface coating with a high resistance to hydrogen entry under high-pressure hydrogen-gas environment. Int J Hydrogen Energy 2013;38:10141–54. https://doi.org/10.1016/j.ijhydene.2013.05.152.
[193] Chen P, Wallace R. Deuterium transport through device structures. J Appl Phys 1999;86:2237–44. https://doi.org/10.1063/1.371036.
[194] Lee L-H. The chemistry and physics of solid adhesion. Fundamentals of adhesion. 1991. p. 1–86. https://doi.org/10.1007/978-1-4899-2073-7_1.
[195] Toth L. Transition metal carbides and nitrides. Elsevier; 2014.
[196] Yang L, Wirth B. First-principles study of hydrogen behavior near W/WC interfaces. J Appl Phys 2020;127. https://doi.org/10.1063/1.5141761.
[197] Ooi S, Yan P, Vegter R. Black oxide coating and its effectiveness on prevention of hydrogen uptake. Mater Sci Technol 2019;35:12–25. https://doi.org/10.1080/02670836.2018.1530425.
[198] Alberta Innovates, "$20 million in hydrogen funding awarded by the Hydrogen Centre of Excellence." Accessed: December 21, 2024. [Online]. Available: https://albertainnovates.ca/news/20-million-in-hydrogen-funding-awarded-by-the-hydrogen-centre-of-excellence/.
[199] Lingnau DG, Cochrane J. Vitreous coating application by induction heating and integration with induction kinetic weld joining. Google Patents; 2023.
[200] Mittra J, Kavalur A, Kumbhar N, Majumdar S, Das N, Arya A. Effectiveness of pulsed laser deposited ZrO2 surface film over autoclaved oxide film on a Zr alloy for hydrogen barrier application. Surf Coating Technol 2020;404:126548. https://doi.org/10.1016/j.surfcoat.2020.126548.
[201] Levchuk D, Bolt H, Döbeli M, Eggenberger S, Widrig B, Ramm J. Al–Cr–O thin films as an efficient hydrogen barrier. Surf Coating Technol 2008;202:5043–7. https://doi.org/10.1016/j.surfcoat.2008.05.012.
[202] Holbrook J, Cialone H, Collings E, Drauglis E, Scott P, Mayfield M. 5- control of hydrogen embrittlement of metals by chemical inhibitors and coatings. Gaseous hydrogen embrittlement of materials in energy technologies. Elsevier; 2012. p. 129–53.
[203] Xie JZ, Murarka SP, Guo XS, Lanford WA. Stability of hydrogen in silicon nitride films deposited by low-pressure and plasma enhanced chemical vapor deposition techniques. J Vac Sci Technol B Microelectron Process Phenom 1989;7:150–2. https://doi.org/10.1116/1.584707.
[204] Wang P, Liu J, Wang Y, Shi B. Investigation of SiC films deposited onto stainless steel and their retarding effects on tritium permeation. Surf Coating Technol 2000;128:99–104. https://doi.org/10.1016/S0257-8972(00)00614-9.
[205] Levchuk D, Koch F, Maier H, Bolt H. Deuterium permeation through Eurofer and α-alumina coated Eurofer. J Nucl Mater 2004;328:103–6.
[206] Kermetico. Ceramic lined pipe wear resistant piping fitting tungsten carbide coating. https://kermetico.com/applications/ceramic-lined-pipe-fitting. [Accessed 22 December 2024].
[207] Nemanič V, Zajec B, Dellasega D, Passoni M. Hydrogen permeation through disordered nanostructured tungsten films. J Nucl Mater 2012;429:92–8. https://doi.org/10.1016/j.jnucmat.2012.05.031.
[208] Wang Y, Liu D, Feng S, Zhang Y, Ouyang T, Suo J. Preparation of tritium permeation barrier consisting of titanium by the pack cementation method. Surf Coating Technol 2016;307:271–7. https://doi.org/10.1016/j.surfcoat.2016.08.082.
[209] Zhu L, Zheng L, Xie H, Liu D-G, Xu Q, Luo L-M, Wu Y-C. Design and properties of FeAl/Al2O3/TiO2 composite tritium-resistant coating prepared through pack cementation and sol–gel method. Mater Today Commun 2021;26:101848. https://doi.org/10.1016/j.mtcomm.2020.101848.
[210] Feng S, Wang Y, Zhang C, Luo C, Xu J, Suo J. Preparation of Al2O3/Cr2O3 tritium permeation barrier with combination of pack cementation and sol–gel methods. Fusion Eng Des 2018;131:1–7. https://doi.org/10.1016/j.fusengdes.2018.03.069.
[211] Park J, Jung M. Hydrogen permeation of SiC-CeO 2 composite membrane by dip-coating process. J Korean Ceram Soc 2013;50:485–8. https://doi.org/10.4191/kcers.2013.50.6.485.
[212] Sperling LH. Introduction to physical polymer science. John Wiley & Sons; 2015.
[213] Grulke EA, Immergut E, Brandrup J. Polymer handbook. John Wiley & Sons; 1999.
[214] Zhang X, Zhai L, Li H, Qi G, Gao X, Yang W. Molecular simulation study on the hydrogen permeation behavior and mechanism of common polymers. Polymers 2024;16:953. https://doi.org/10.3390/polym16070953.
[215] Takeuchi K, Kuo A-T, Hirai T, Miyajima T, Urata S, Terazono S, et al. Hydrogen permeation in hydrated perfluorosulfonic acid polymer membranes: effect of polymer crystallinity and equivalent weight. J Phys Chem C 2019;123:20628–38. https://doi.org/10.1021/acs.jpcc.9b05502.
[216] Orme CJ, Stone ML, Benson MT, Peterson ES. Testing of polymer membranes for the selective permeability of hydrogen. Separ Sci Technol 2003;38:3225–38. https://doi.org/10.1081/SS-120022595.
[217] Jain N, Singh VK, Chauhan S. A review on mechanical and water absorption properties of polyvinyl alcohol based composites/films. J Mech Behav Mater 2017;26:213–22. https://doi.org/10.1515/jmbm-2017-0027.
[218] Saha S, Son W, Kim NH, Lee JH. Fabrication of impermeable dense architecture containing covalently stitched graphene oxide/boron nitride hybrid nanofiller reinforced semi-interpenetrating network for hydrogen gas barrier applications. J Mater Chem A 2022;10:4376–91. https://doi.org/10.1039/D1TA09486F.
[219] Lin H, Kai T, Freeman BD, Kalakkunnath S, Kalika DS. The effect of cross-linking on gas permeability in cross-linked poly (ethylene glycol diacrylate). Macromolecules 2005;38:8381–93. https://doi.org/10.1021/ma0510136.
[220] Deckers F, Rasim K, Schröder C. Molecular dynamics simulation of polypropylene: diffusion and sorption of H2O, H2O2, H2, O2 and determination of the glass transition temperature. J Polym Res 2022;29:463. https://doi.org/10.1007/s10965-022-03304-y.
[221] Jung JK, Lee JH, Jeon SK, Tak NH, Chung NK, Baek UB, et al. Correlations between H2 permeation and physical/mechanical properties in ethylene propylene diene monomer polymers blended with carbon black and silica fillers. Int J Mol Sci 2023;24:2865. https://doi.org/10.3390/ijms24032865.
[222] Jung JK, Baek UB, Lee SH, Choi MC, Bae JW. Hydrogen gas permeation in peroxide-crosslinked ethylene propylene diene monomer polymer composites with carbon black and silica fillers. J Polym Sci 2023;61:460–71. https://doi.org/10.1002/pol.20220494.
[223] Yamabe J, Nishimura S. Influence of fillers on hydrogen penetration properties and blister fracture of rubber composites for O-ring exposed to high-pressure hydrogen gas. Int J Hydrogen Energy 2009;34:1977–89. https://doi.org/10.1016/j.ijhydene.2008.11.105.
[224] San Marchi CW, Somerday BP. Technical reference for hydrogen compatibility of materials. Sandia National Laboratories (SNL); 2012. SANDIA REPORT, SAND2012-7321.
[225] Kanesugi H, Ohyama K, Fujiwara H, Nishimura S. High-pressure hydrogen permeability model for crystalline polymers. Int J Hydrogen Energy 2023;48:723–39. https://doi.org/10.1016/j.ijhydene.2022.09.205.
[226] Lee J-H, Kim Y-W, Jung J-K. Investigation of the gas permeation properties using the volumetric analysis technique for polyethylene materials enriched with pure gases under high pressure: H2, He, N2, O2 and Ar. Polymers 2023;15:4019. https://doi.org/10.3390/polym15194019.
[227] Yasuda H, Rosengren K. Isobaric measurement of gas permeability of polymers. J Appl Polym Sci 1970;14:2839–77. https://doi.org/10.1002/app.1970.070141117.
[228] Jung JK, Kim IG, Chung KS, Kim Y-I, Kim DH. Determination of permeation properties of hydrogen gas in sealing rubbers using thermal desorption analysis gas chromatography. Sci Rep 2021;11:17092. https://doi.org/10.1038/s41598-021-96266-y.
[229] Andrady A, Sefcik M. Transport of hydrogen and carbon monoxide in highly crosslinked poly (propylene glycol) networks. J Polym Sci Polym Phys Ed 1984;22:237–43. https://doi.org/10.1002/pol.1984.180220208.
[230] Bhide B, Stern S. Permeability of silicone polymers to hydrogen. J Appl Polym Sci 1991;42:2397–403. https://doi.org/10.1002/app.1991.070420904.
[231] Srinivasan R, Auvil S, Burban P. Elucidating the mechanism (s) of gas transport in poly [1-(trimethylsilyl)-1-propyne](PTMSP) membranes. J Membr Sci 1994;86:67–86. https://doi.org/10.1016/0376-7388(93)E0128-7.
[232] Kim DW, Kim H, Jin ML, Ellison CJ. Impermeable gas barrier coating by facilitated diffusion of ethylenediamine through graphene oxide liquid crystals. Carbon 2019;148:28–35. https://doi.org/10.1016/j.carbon.2019.03.039.
[233] Menon NC, Kruizenga AM, Nissen A, San Marchi CW. Behavior of polymers in high pressure hydrogen environments as applicable to the Hydrogen infrastructure. Sandia national lab. Livermore, CA (United States): SNL-CA); 2016. https://doi.org/10.1115/PVP2016-63713.
[234] Kargari A, Shamsabadi AA, Babaheidari MB. Influence of coating conditions on the H2 separation performance from H2/CH4 gas mixtures by the PDMS/PEI composite membrane. Int J Hydrogen Energy 2014;39:6588–97. https://doi.org/10.1016/j.ijhydene.2014.02.009.
[235] Prewitz M, Gaber M, Müller R, Marotztke C, Holtappels K. Polymer coated glass capillaries and structures for high-pressure hydrogen storage: permeability and hydrogen tightness. Int J Hydrogen Energy 2018;43:5637–44. https://doi.org/10.1016/j.ijhydene.2017.12.092.
[236] Monson L, Moon SI, Extrand C. Permeation resistance of poly (ether ether ketone) to hydrogen, nitrogen, and oxygen gases. J Appl Polym Sci 2013;127:1637–42. https://doi.org/10.1002/app.37517.
[237] Dagdag O, Kim H. Recent advances in the hydrogen gas barrier performance of polymer liners and composites for type IV hydrogen storage tanks: fabrication, properties, and molecular modeling. Polymers 2025;17:1231. https://doi.org/10.3390/polym17091231.
[238] Calabrese L, Mastronardo E, Piperopoulos E, Scionti G, De Antonellis S, Freni A, Milone C. Effect of alternating humidity and dryness on the durability of adsorbent sheets used in opencycle adsorption processes. Polym Degrad Stabil 2025;234:111201. https://doi.org/10.1016/j.polymdegradstab.2025.111201.
[239] Reduction of hydrogen permeation. https://www.ifam.fraunhofer.de/en/technologies/hydrogen-permeation-barrier-coatings.html?utm_source=chatgpt.com. [Accessed 21 August 2025].
[240] Zhao J, Ding G, Feng P, Wu C. High-pressure hydrogen effects on thermoplastics: a comprehensive review of permeation, decompression failure, and mechanical properties. Adv Ind Eng Polym Res 2025. https://doi.org/10.1016/j.aiepr.2025.05.001.
[241] Li Y, Huard M, Wong K, Wang X, Adane K. Coatings and liners for hydrogen service pipelines. Toronto, ON, Canada: Canadian Standards Association; 2024.
[242] Shin HK, Ha SK. A review on the cost analysis of hydrogen gas storage tanks for fuel cell vehicles. Energies 2023;16:5233. https://doi.org/10.3390/en16135233.
[243] Yuan S, Sun Y, Cong C, Liu Y, Lin D, Pei L, et al. A bi-layer orientated and functionalized graphene-based composite coating with unique hydrogen gas barrier and long-term anti-corrosion performance. Carbon 2023;205:54–68. https://doi.org/10.1016/j.carbon.2023.01.027.
[244] Shi K, Meng X, Xiao S, Chen G, Wu H, Zhou C, et al. MXene coatings: novel hydrogen permeation barriers for pipe steels. Nanomaterials 2021;11:2737. https://doi.org/10.3390/nano11102737.
[245] Zhou P, Li W, Zhu X, Li Y, Jin X, Chen J. Graphene containing composite coatings as a protective coatings against hydrogen embrittlement in quenching &

partitioning high strength steel. J Electrochem Soc 2016;163:D160. https://doi.org/10.1149/2.0551605jes.
[246] Zhu Y, Liu G, Cui Z, Yang H, Liu F, Jiang B, Chen L. Effect and mechanism of ionic liquid-polymer composite coating on enhancing hydrogen embrittlement resistance of X80 pipeline steel for hydrogen blended natural gas transportation. Int J Hydrogen Energy 2024;80:1305–16. https://doi.org/10.1016/j.ijhydene.2024.07.091.
[247] Yang Y-H, Haile M, Park YT, Malek FA, Grunlan JC. Super gas barrier of all-polymer multilayer thin films. Macromolecules 2011;44:1450–9. https://doi.org/10.1021/ma1026127.
[248] Bandyopadhyay P, Park WB, Layek RK, Uddin ME, Kim NH, Kim H-G, Lee JH. Hexylamine functionalized reduced graphene oxide/polyurethane nanocomposite-coated nylon for enhanced hydrogen gas barrier film. J Membr Sci 2016;500:106–14. https://doi.org/10.1016/j.memsci.2015.11.029.
[249] Li P, Chen K, Zhao L, Zhang H, Sun H, Yang X, et al. Preparation of modified graphene oxide/polyethyleneimine film with enhanced hydrogen barrier properties by reactive layer-by-layer self-assembly. Compos B Eng 2019;166:663–72. https://doi.org/10.1016/j.compositesb.2019.02.058.
[250] Liu W, Xue L, Di J, Zhou Q, Zhang H, Li H, Yan Y. An efficient graphene oxide reinforced aluminum phosphate/Cr2O3 double coating as an enhanced tritium permeation barrier. Surf Coating Technol 2021;405:126699. https://doi.org/10.1016/j.surfcoat.2020.126699.
[251] Bahlakeh G, Ghaffari M, Saeb MR, Ramezanzadeh B, De Proft F, Terryn H. A close-up of the effect of iron oxide type on the interfacial interaction between epoxy and carbon steel: combined molecular dynamics simulations and quantum mechanics. J Phys Chem C 2016;120:11014–26. https://doi.org/10.1021/acs.jpcc.6b03133.
[252] Interf Hydrog Barr CoatAccessed: August. 21, 2025.[online]. Available: https://www.mpie.de/5042800/interfaces_hydrogen_barrier_coatings?utm_source.
[253] Moazzam P, Luciano G, Razmjou A, Akbari E, Ul'yanov PG, Mahanty S. Effect of molecular-scale surface energy alteration of aluminium on its corrosion resistance behaviour. Colloids Surf A Physicochem Eng Asp 2019;562:26–33. https://doi.org/10.1016/j.colsurfa.2018.10.046.
[254] Luo Y, Liu S, Yang Y, Chen G, Cai L, Lyu S, et al. Superior interface adhesion and protective mechanism of room-temperature-curable polymer composite coating on engineering substrates with lower roughness. Polym Test 2024;134:108430. https://doi.org/10.1016/j.polymertesting.2024.108430.
[255] Terrones M, Martín O, González M, Pozuelo J, Serrano B, Cabanelas JC, et al. Interphases in graphene polymer-based nanocomposites: achievements and challenges. Adv Mater 2011;23:5302–10. https://doi.org/10.1002/adma.201102036.
[256] Bunch JS, Verbridge SS, Alden JS, Van Der Zande AM, Parpia JM, Craighead HG, McEuen PL. Impermeable atomic membranes from graphene sheets. Nano Lett 2008;8:2458–62. https://doi.org/10.1021/nl801457b.
[257] Compton OC, Kim S, Pierre C, Torkelson JM, Nguyen ST. Crumpled graphene nanosheets as highly effective barrier property enhancers. Adv Mater 2010;22:4759–63. https://doi.org/10.1002/adma.201000960.
[258] Sadasivuni KK, Saiter A, Gautier N, Thomas S, Grohens Y. Effect of molecular interactions on the performance of poly (isobutylene-co-isoprene)/graphene and clay nanocomposites. Colloid Polym Sci 2013;291:1729–40. https://doi.org/10.1007/s00396-013-2908-y.
[259] Ji X, Cui L, Xu Y, Liu J. Non-covalent interactions for synthesis of new graphene based composites. Compos Sci Technol 2015;106:25–31. https://doi.org/10.1016/j.compscitech.2014.10.018.
[260] Huang H, Sheng X, Tian Y, Zhang L, Chen Y, Zhang X. Two-dimensional nanomaterials for anticorrosive polymeric coatings: a review. Ind Eng Chem Res 2020;59:15424–46. https://doi.org/10.1021/acs.iecr.0c02876.
[261] Yang G-h, Bao D-d, Liu H, Zhang D-q, Wang N, Li H-t. Functionalization of graphene and applications of the derivatives. J Inorg Organomet Polym Mater 2017;27:1129–41. https://doi.org/10.1007/s10904-017-0597-6.
[262] Seo OB, Saha S, Kim NH, Lee JH. Preparation of functionalized MXene-stitched-graphene oxide/poly (ethylene-co-acrylic acid) nanocomposite with enhanced hydrogen gas barrier properties. J Membr Sci 2021;640:119839. https://doi.org/10.1016/j.memsci.2021.119839.
[263] Anagnostopoulos G, Sygellou L, Paterakis G, Polyzos I, Aggelopoulos CA, Galiotis C. Enhancing the adhesion of graphene to polymer substrates by controlled defect formation. Nanotechnology 2018;30:015704. https://doi.org/10.1088/1361-6528/aae683.
[264] Hu L, Wei G, Yin R, Hong M, Cheng T, Zhang D, et al. Significant hydrogen isotopes permeation resistance via nitride nano-multilayer coating. Int J Hydrogen Energy 2020;45:19583–9. https://doi.org/10.1016/j.ijhydene.2020.05.123.
[265] Kim J, Yao X, Somjit V, Kim SY, Li J, Yildiz B, Tasan CC. Multilayer alumina/aluminum coatings for damage-resistant hydrogen permeation barrier. Int J Hydrogen Energy 2025;106:226–30. https://doi.org/10.1016/j.ijhydene.2025.01.300.
[266] Shastry T, Basdogan Y, Wang Z-G, Kumar SK, Carbone MR. Machine learning-based discovery of molecular descriptors that control polymer gas permeation. J Membr Sci 2024;697:122563. https://doi.org/10.1016/j.memsci.2024.122563.
[267] Lu GM, Witman M, Agarwal S, Stavila V, Trinkle DR. Explainable machine learning for hydrogen diffusion in metals and random binary alloys. Phys Rev Mater 2023;7:105402. https://doi.org/10.1103/PhysRevMaterials.7.105402.
[268] Sun C, Yuan Y, Xu M, Li X, Li M, Zhou C. A high-throughput molecular dynamics study with a machine-learning method on predicting diffusion coefficient of hydrogen in α-iron grain boundaries. Mater Today Commun 2025;44:111997. https://doi.org/10.1016/j.mtcomm.2025.111997.
[269] Bhattacharyya A, Saha S, Jena S, Nguyen HT, Tran DT, Kim NH, Lee JH. Epoxy-based vitrimeric semi-interpenetrating network/MXene nanocomposites for hydrogen gas barrier applications. Nanoscale 2025;17:5755–69. https://doi.org/10.1039/D4NR04702H.
[270] Frias-Cacho X, Castro M, Nguyen D-D, Grolleau A-M, Feller J-F. A review of In-Service coating health monitoring technologies: towards "Smart" neural-like networks for condition-based preventive maintenance. Coatings 2022;12:565. https://doi.org/10.3390/coatings12050565.
[271] Sugawara Y, Sato T. Real-time and highly responsive hydrogen mapping in pure Fe using TiO2 thin films. Int J Hydrogen Energy 2024;72:237–46. https://doi.org/10.1016/j.ijhydene.2024.05.376.
[272] Abedini S, Chan FMACP, Dong C, Davies IJ. Failure analysis of a functionally graded multilayer coated stainless steel pipe for hydrogen storage. Discov Mechan Eng 2024;3:28. https://doi.org/10.1007/s44245-024-00064-5.
[273] Tzeng P, Lugo EL, Mai GD, Wilhite BA, Grunlan JC. Super hydrogen and helium barrier with polyelectolyte nanobrick wall thin film. Macromol Rapid Commun 2015;36:96–101. https://doi.org/10.1002/marc.201400559.
[274] Kang H, Bae J, Lee J, Yun Y, Jeon S, Chung N, et al. The synergistic effect of carbon black/carbon nanotube hybrid fillers on the physical and mechanical properties of EPDM composites after exposure to high-pressure hydrogen gas. Polymers 2024;16:1065. https://doi.org/10.3390/polym16081065.
[275] International A. ASTM D3985-24. S. tandard Test Method for Oxygen Gas Transmission Rate Through Plastic Film and Sheeting Using a Coulometric Sensor 2024.